TENSILE TESTING AND STABILIZATION/CARBONIZATION STUDIES OF POLYACRYLONITRILE/CARBON NANOTUBE COMPOSITE FIBERS

A Thesis
Presented to
The Academic Faculty

by

Kevin Mark Lyons

In Partial Fulfillment
of the Requirements for the Degree
Masters of Science in the
School of Materials Science and Engineering

Georgia Institute of Technology
December 2012

TENSILE TESTING AND STABILIZATION/CARBONIZATION STUDIES OF POLYACRYLONITRILE CARBON NANOTUBE COMPOSITE FIBERS

Approved by:

Dr. Satish Kumar, Advisor
School of Materials Science and Engineering
Georgia Institute of Technology

Dr. Anselm Griffin
School of Materials Science and Engineering
Georgia Institute of Technology

Dr. Chuck Zhang
School of Materials Science and Engineering
Georgia Institute of Technology

Dr. Han Gi Chae
School of Industrial and Systems Engineering
Georgia Institute of Technology

Date Approved: November 6, 2012

ACKNOWLEDGEMENTS

I would first like to thank my advisor, Dr. Satish Kumar, for the opportunity to conduct research in such a unique and exciting field of study. I am especially grateful for his guidance, knowledge, and support during my time at Georgia Institute of Technology. The valuable lessons I learned under his tutelage will remain with me throughout my professional and personal life.

I would also like to thank Dr. Han Gi Chae, Dr. Chuck Zhang, and Dr. Anselm Griffin for their service as my committee members as well as their input in regards to my thesis work.

Dr. Han Gi Chae deserves special thanks for the many valuable discussions he and I had in terms of theoretical and practical research topics. The constant dedication and hard work he displays is something I will always admire.

I would also like to acknowledge Dr. Yaodong Liu for his help with regard to reaction kinetics and characterization techniques (especially FTIR), Mr. Bradley Newcomb for his assistance with precursor fiber characterization (e.g., - Raman) and general discussions, Mr. An-Ting Chien for assistance with XRD, and Mr. Kenneth McDonald for his help with tensile testing. Many thanks also go to all remaining group members for their advice, support, and friendship.

Finally, I would like to express a special appreciation to my parents for raising me in such a way that has instilled hard work, determination, and curiosity as characteristics I carry with me everyday. Their patience, support, and understanding throughout my studies are also greatly appreciated.

TABLE OF CONTENTS

LIST OF TABLES

LIST OF FIGURES

SUMMARY

The need for lighter and stronger materials drives the demand for carbon fiber production. Polyacrylonitrile (PAN)-based carbon fibers have exceptional mechanical properties that make them a practical option for composite materials. This study focuses on the testing and processing of composite PAN/carbon nanotube (CNT) carbon fibers. Achieving moderate improvements in tensile strength of current high strength carbon fibers will have a significant impact on expanding their use in a number of industries.

The first chapter focuses on a brief history of carbon fibers as well as the process required for making PAN-based carbon fiber. Emphasis is given to the structural changes thought to occur during the thermal processing of PAN precursor fibers. Important results from previous PAN/CNT composite carbon fiber research are reviewed. Finally, the Weibull modulus method for quantifying the distribution of defects within a material is presented.

The second chapter focuses on the tensile testing of both precursor and carbon fibers. Effect of testing parameters such as gauge length, strain rate, pre-stress, and assumed linear density are discussed in an effort to determine testing protocols for reliable mechanical property determination. Compliance correction for precursor and carbon fibers has also been studied on two very different tensile testing instruments. The results from single filament tensile tests are also compared to the strand testing method used by industry as a way to validate the single filament testing method.

Chapter 3 involves stabilization and carbonization studies of a sheath-core PAN precursor fiber. Characterization tools (e.g., - Fourier Transform Infrared Spectroscopy (FTIR), wide angle X-ray diffraction (WAXD), differential scanning calorimetry (DSC),

scanning electron microscopy (SEM)) were used to determine the chemical and physical structure of stabilized fibers in an attempt to find signatures indicative of the optimal stabilized structure (resulting in highest tensile strength carbon fibers). A term (M_{cyc}) that quantifies the non-isothermal extent of reaction has been developed from DSC reaction kinetics results to aid in the optimization process.

Studies on the carbonization of islands-in-sea (INS) precursor fibers are presented in Chapter 4. This INS technology allows for small diameter (< 1μm) carbon fibers to be produced. The resulting carbon fibers were tested using both single filament tests (involving MEMS-based device at University of Illinois at Urbana-Champaign) as well as bundle tests. Comparison of test methods as well as a brief characterization of the structure and morphology of INS carbon fibers is discussed.

Chapter 5 presents the important conclusions of this study and introduces recommendations for future works.

CHAPTER 1
INTRODUCTION

1.1 Carbon Fibers

1.1.1 Importance

Commercially available carbon fibers are in high demand due to their impressive mechanical properties and low density. This unique combination of mechanical and physical properties results in a specific strength that is eleven times greater than that of AISI 1060 steel. These properties make carbon fibers well suited for high strength structural applications. Aerospace, automotive, industrial, and sports equipment are a few of the industries in which carbon fibers are currently being utilized. Boeing's new 787 Dreamliner is now made from over 50% carbon fiber reinforced composites and has experienced an average savings of 20% associated with fuel consumption, maintenance, and operation. According to the Federal Aviation Administration (FAA), Delta Airlines spent a combined 5.3 billion dollars in these categories in 2010. Therefore, with complete integration of Boeing's new carbon fiber composite based 787, Delta can save 1 billion dollars per year. However, despite this incredible potential, the strength of current commercially available carbon fibers is only ~5-7% of the theoretical tensile strength of the carbon-carbon bond. Making even modest improvements to the mechanical properties of high strength carbon fiber will lead to widespread adoption in the applications mentioned above and a far greater impact in energy savings worldwide.

1.1.2 History

The first documented mention of carbon fiber was in a patent by Thomas Edison on November 10th 1879[1] which outlined the use of carbon filaments for the purpose of incandescent light bulbs. More robust metallic filaments (such as tungsten) replaced these carbon materials in the early 1900s. It was not until the mid 1900s until another significant application for this material was discovered: high strength carbon fibers.

Rayon was the first precursor to be commercialized yielding high strength carbon fiber in 1959.[2] There were a number of successful attempts at commercializing rayon-based carbon fibers in the United States, which is the reason for it becoming an early precursor candidate. However, around the same time (1961), Shindo had demonstrated a carbon fiber derived from a PAN precursor having triple the modulus of rayon based carbon fibers[3,4]. Eventually, PAN overtook rayon as the precursor of choice due to the superior combination of properties that were achieved from PAN precursors.[2]

Pitch is another precursor material for carbon fiber. Pitch is a general term that refers to the tarry substance that is the result of a number of processes. Some example processes are: 1) petroleum refining, 2) destructive distillation of coal, and 3) pyrolysis of PVC[5]. The advantage of pitch-based carbon fibers manifests itself in the form of higher modulus values due to the increase in order and formation of graphitic structure. In addition to the increase in modulus, the structure of pitch-based carbon fibers also leads to higher density (compared to PAN and rayon-based carbon fibers) and improved thermal and electrical conductivity. While the pitch-based carbon fiber possesses the aforementioned advantages over PAN-based carbon fiber, its compressive strength is inferior to that of

PAN-based carbon fiber. Therefore, for composites in structural applications, PAN-based carbon fiber is the predominant material of choice.

1.1.3 Properties of Commercial Carbon Fibers

As previously mentioned, the properties of carbon fibers are very desirable due to their unique combination of high strength and lightweight characteristics. As a benchmark for what current carbon fiber technology has achieved, the properties of some of the major commercial carbon fibers are listed in Table 1.1.[6]

Table 1.1 Current properties of PAN-based* and pitch-based† commercial carbon fibers[#].[6]

Fiber	Tensile Strength [GPa]	Tensile Modulus [GPa]	Elongation to Break [%]	Density,ρ [g/cm^3]	Thermal Conductivity [W/mK]	Electrical Conductivity [S/m]
Hexcel Magnamite* ®						
AS4	4.27	228	1.87	1.79	-	6.5×10^4
AS4C	4.34	231	1.88	1.78	-	-
IM4	4.79	276	1.74	1.78	-	-
IM8	5.58	304	1.84	1.79	-	-
PV-42/850	5.76	292	1.97	1.79	-	-
Cytec Thornel* ®						
T300	3.75	231	1.4	1.76	8	5.56×10^4
T650/35	4.28	255	1.7	1.77	14	6.67×10^4
Torya Torayca* ®						
T300	3.53	230	1.5	1.76	-	-
T700SC	4.90	230	2.1	1.80	-	-
M35JB	4.70	343	1.4	1.75	-	-
M50JB	4.12	475	0.9	1.88	-	-
M55J	4.02	540	0.8	1.91	-	-
M30SC	5.49	294	1.9	1.73	-	-
Cytec Thornel† ®						
P-25	1.38	159	0.9	1.90	22	7.69×10^4
P-55S	1.90	379	0.5	1.90	120	1.18×10^5
P-100S	2.41	758	0.3	2.16	520	4.00×10^5
P-120S	2.41	827	0.3	2.17	640	4.55×10^5
K-800X	2.34	896	-	2.20	900-1,000	6.67-8.33 (10^5)
K1100	3.10	965	-	2.20	900-1,100	7.69-9.09 (10^5)

#Property data obtained from the data sheets of the respective manufacturer (e.g., - Hexcel, Cytec, and Toray).

1.2 Processing of PAN-based Carbon Fibers

In this section, a brief overview of the steps involved in carbon fiber production will be presented. Each processing step will then be discussed in more detail with an emphasis on how each step impacts the evolution of the carbon fiber structure.

1.2.1 Process Overview

The process of converting a polyacrylonitrile (PAN) precursor fiber into a carbon fiber involves three distinct stages: 1) oxidative stabilization, 2) carbonization, and 3) graphitization. Stabilization and carbonization are required for creating a carbon fiber, while graphitization involves processing at ultra-high temperatures (> 2000 ^{o}C) to obtain a highly ordered structure, resulting in high tensile modulus.

1.2.1.1 Oxidative Stabilization

The stabilization of the precursor fiber is the most critical and least understood aspect of carbon fiber manufacturing. During stabilization, the PAN precursor is subjected to thermal treatments in the range of 200ºC to 400ºC in an oxygen-containing environment. During stabilization, the polymer molecules undergo a series of chemical reactions that transforms the polymer chain into a more rigid and thermally resistant ladder structure. Upon achieving this ladder structure, the stabilized fiber can then be subjected to the higher temperature treatments (e.g., – carbonization/graphitization).

1.2.1.2 Carbonization

Carbonization is performed in an inert atmosphere and typically in the temperature range of 900 to 1600ºC. During this process, neighboring ladder structures cross-link

with each other and form a turbostratic graphitic structure. During carbonization, non-carbon elements are released in the form of H_2, NH_3, HCN, N_2, etc.[7]

1.2.1.3 Graphitization

Similar to carbonization, graphitization also occurs in an inert environment but at much higher temperatures (1800ºC to 3000ºC). During this process, the orientation and spacing of turbostratic structure becomes more graphite-like. As a result, the stiffness of the fiber is also increased during this stage.

1.2.2 Structure Evolution: Polyacrylonitrile to Carbon Fiber

This section discusses the morphology changes of polyacrylonitrile (PAN) as it is subjected to the number of processes that are necessary for creating a high strength carbon fiber. Figure 1.1 shows some of the reactions that are thought to occur during stabilization (left) and carbonization (right).

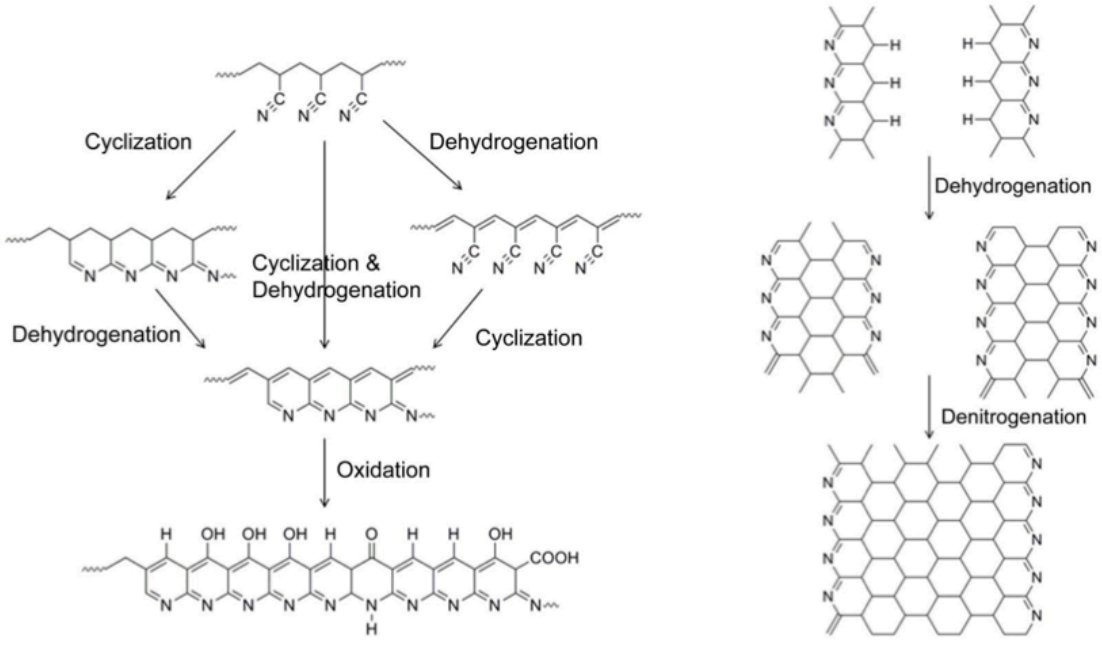

Figure 1.1 Chemical reactions during the stabilization and carbonization stages of carbon fiber production.[8,9]

1.2.2.1 Oxidative Stabilization

As briefly discussed in section 1.2.1.1, oxidative stabilization transforms the PAN molecules into a more rigid ladder structure. Due to the complexity of different reactions simultaneously taking place during stabilization, the actual sequence of structural changes is not well defined.

There have been a number of works focused on characterizing the proposed structure of stabilized PAN.[10,11,12,13,14,15] The commonly accepted form of stabilized PAN is derived from Morita et al. in which they proposed the following structure fractions based on XPS and NMR data.

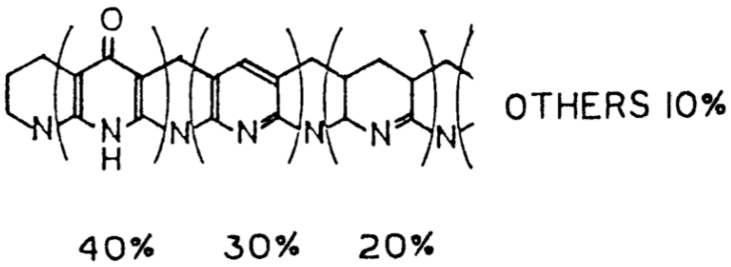

Figure 1.2 Relative proportions of stabilized constituents as proposed by Morita et. al[14].

The main reactions required to form the above structure include cyclization, oxidation, dehydrogenation, and intermolecular cross-linking (illustrated in Figure 1.1). In 1950, Houtz was the first to discover the changes in color that occur during the degradation of PAN.[16] The conclusions made by Houtz were slightly modified in subsequent studies to conclude a partially cyclized aromatic structure.[17,18,19]

Berlin et al. conducted experiments of dilute solutions of PAN and DMF to create negligible chain-to-chain interactions during heating. The IR spectra results indicate that

there is evidence of carbon-carbon double bonds yet no change in the nitrile-group band even after 90 hours of treatment in boiling DMF (~150ºC).[20] As a result, the authors suggested a dehydrogenation reaction scheme where a double bond is formed along the backbone of the polymer chain while leaving the nitrile group unreacted. The authors used an oxygen containing medium (DMF) for the experiment, and as a result concluded that dehydrogenation precedes both cyclization and oxidation reactions in an environment where chain-to-chain interactions can be neglected. Since this study neglects chain interactions, the conclusion cannot be directly applied to PAN fibers. However, there are many other studies that indicate dehydrogenation as one of the major reactions taking place during the stabilization of PAN fibers.[14,21,22]

The reactions discussed previously do not account for the experimental observations that stabilized fibers contain between 8 – 15% oxygen.[12,23] As such, a number of oxygen containing chemical species have been proposed to be included in the final structure of stabilized PAN.[24,25,10] Watt et al. studied the oxygen uptake of two PAN copolymers with one having 0.4 mol% of an acidic constituent (which acts as an initiator to the ladder structure formation). The authors concluded that the cyclization reaction was a prerequisite for oxidation reactions to occur since the oxygen uptake was greater in the acid containing co-monomer PAN fiber.[12]

1.2.2.2 Inter-molecular Cross-linking Reaction

The azomethine cross-linking mechanism was debated by Schurz,[26] Grassie,[17] and Takata[27] for many years. The result of which was an agreement in the possibility of the reaction occurring, possibly with an abnormal/defect structure as a required prerequisite.[28,29,30] Another reaction scheme proposed by Olivé et al.[31] gives an

alternative route for PAN to achieve cross-linking. The authors claimed that while the intra-molecular nitrile interaction is repulsive leading to its helical conformation, the inter-molecular interaction between nitrile groups of neighboring chains is attractive and leads to cross-linking reaction.[13] Since inter-molecular interaction is more energetically favorable (due to the high energy associated with the planar zig-zag conformation required for cyclization), it is reasonable to conclude that cross-linking will take place to a higher degree than the cyclization reaction.

1.2.2.3 Carbonization/Graphitization

A fully stabilized fiber is capable of being exposed to the tension and elevated temperatures required for carbonization (900 – 1600 ºC) and graphitization (2000 – 3000 ºC). Depending on the precursor and heat treatment temperature, the structure of carbon fibers will have varying fractions of near perfect graphite (Figure 1.3a, top) and turbostratic (Figure 1.3a, bottom) structures. Applying a sufficient tension during these processes ensures better alignment of the basal planes ((002) plane) with respect to the fiber axis, which is beneficial for achieving high modulus. For PAN, the conversion to a well-ordered graphitic structure is known to be limited due to the preferred orientation of the ladder polymer chains. Pitch-based carbon fiber has no preferred orientation in its precursor material, which is one reason why it is able to achieve higher modulus carbon fibers.

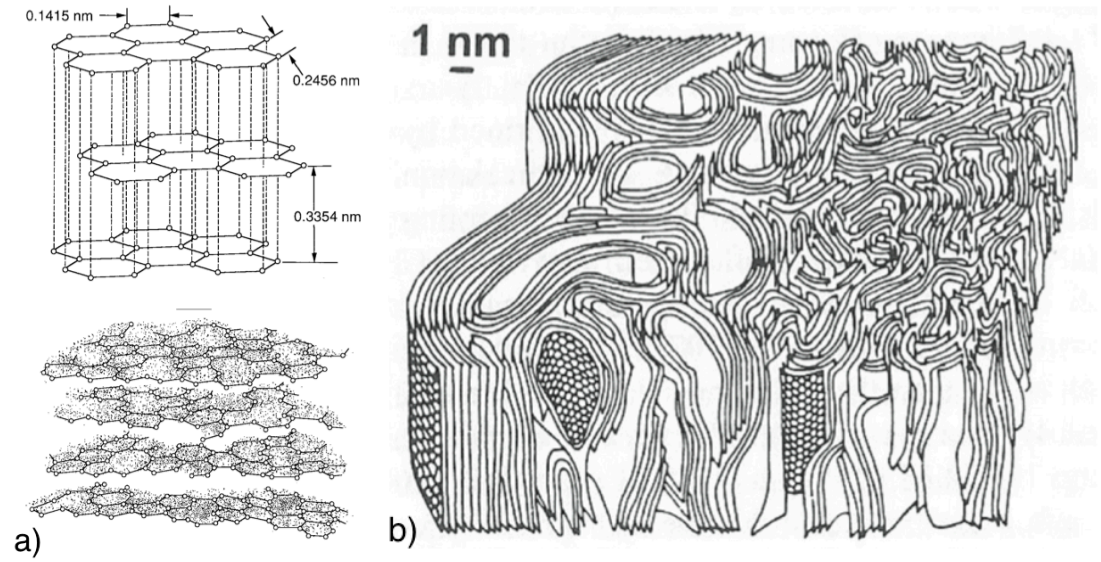

Figure 1.3 a) The differences between graphite and turbostratic structures and b) proposed structure of PAN-based carbon fiber.[32,33]

At higher processing temperatures, the structure of carbon fibers becomes more ordered. During this refinement process, non-carbon elements are removed from the fiber in the form of gaseous byproducts.[6,34,35]

The properties of carbon fibers are a direct result of the internal structure (e.g., - perfection, purity, and order). Important structural parameters that are crucial to understanding the resultant properties are the crystallite sizes shown in Figure 1.4 (L_c and L_a) and Herman's orientation parameter (Equation 1.1a,b). The layer plane lengths parallel ($L_{a\|}$) and perpendicular ($L_{a\perp}$) to the fiber axis are calculated from the peak widths of the meridional and equatorial scans of the (10) plane, respectively.[36]

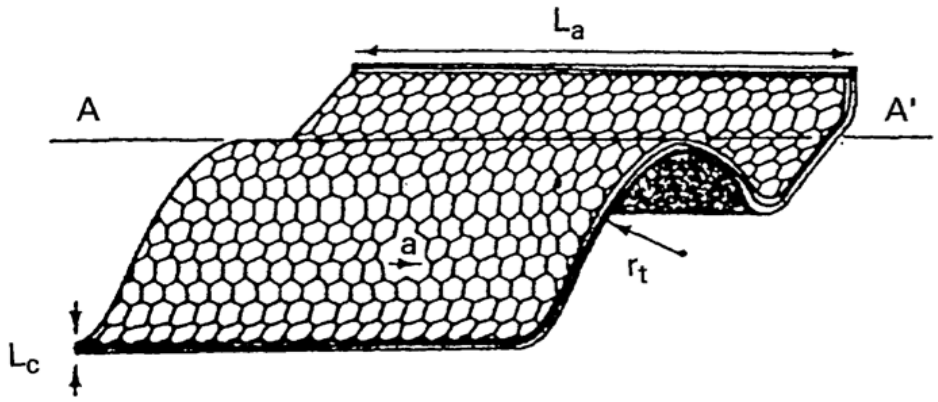

Figure 1.4 Structural parameters describing crystallite sizes in PAN carbon fibers (AA' is fiber axis).[37]

$$f_c = \frac{1}{2}(3\langle cos^2\phi\rangle - 1) \tag{1.1a}$$

$$\langle cos^2\phi\rangle = \frac{\int_{-\pi/2}^{\pi/2}\left(I(\phi)\sin(\phi)\,cos^2(\phi)\right)d\phi}{\int_{-\pi/2}^{\pi/2}(I(\phi)\sin(\phi))d\phi} \tag{1.1b}$$

Where, I is the intensity of diffraction and ϕ is the reference angle describing the position around the diffraction ring.

While there are some unresolved issues whether it is a linear[36,38] or non-linear[39,40,41] relationship for PAN-based carbon fibers, the crystal size in the lateral direction (L_c) increases with higher processing temperatures during carbonization/graphitization. Similarly, the remaining crystallite dimensions ($L_{a\parallel}$ and $L_{a\perp}$) have also shown an analogous trend.[39,40,41,42] Rennhofer et al., studied the dependence of temperature and applied stress on the carbon fiber structure with in situ X-ray diffraction.[43] Interestingly, there seems to be a threshold of stress ($20 < \sigma_{th} < 100$ MPa, σ_{th} is the stress applied to fiber during carbonization) at high temperatures after which there is an increase in the orientation of the fiber. Previous studies[44] have confirmed an increase in the overall alignment (i.e., - orientation) of the carbon fiber structure with higher processing

temperature. Therefore, in general, increasing the processing temperature during carbonization/graphitization will result in a structure consisting of larger and more ordered crystallites.

1.3 PAN/CNT-based Composite Carbon Fibers

Carbon nanotubes (CNTs) have been shown to have exceptional mechanical, electrical, and thermal properties. Due to their unique characteristics, CNTs are considered to have potential in a number of applications (e.g., - structural reinforcement, enhancing electrical conductivity). Carbon nanotubes are available in single walled (SWNT), double walled (DWNT), and multi walled (MWNT) although the control over producing a particular type of CNT needs further refinement. CNTs have exhibited impressive mechanical properties with experimental tensile strengths in the range of 15-60 GPa and tensile modulus values of ~1 TPa.[45,46,47] With these exceptional mechanical properties, CNTs have the potential to significantly influence the behavior of a composite material provided a suitable matrix is chosen. It has been demonstrated that PAN experiences good interaction with CNTs as discussed in the following sections.

1.3.1 Effect of CNT on PAN Precursor Fiber

Various PAN/CNT composite fibers have been processed and shown to have improved structural, chemical, and electrical properties.[48,49,50,51] PAN/CNT fibers showed an increase in the glass transition temperature (T_g) indicating that the chain mobility is being restricted by the presence of CNTs (Figure 1.5a).[52] This restriction of mobility is a direct result of the attractive interaction between the PAN chains and the CNTs. Thermal shrinkage behavior also showed a similar effect of CNT on PAN matrix (Figure 1.5b).

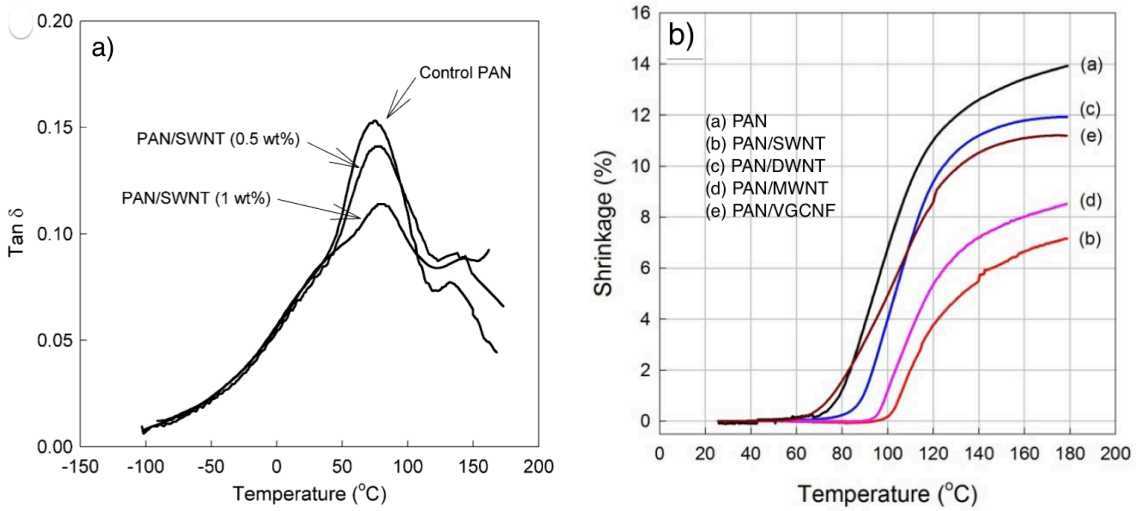

Figure 1.5 a) Dynamic mechanical analysis[8] and b) thermal shrinkage measurmements for various PAN and PAN/CNT fibers[49]. Tan(δ) peak temperature of PAN/CNT fiber shifted to higher temperature with increasing CNT content and amplitude suppression was observed due to the presence of CNTs (a). The PAN/SWNT fiber delayed the onset of thermal shrinkage indicating highest level/extent of interaction.

From wide-angle X-ray diffraction (WAXD), the inclusion of CNTs in a PAN matrix has shown to increase the orientation and crystal size of the precursor fibers.[49] Furthermore, the meridional peak position of PAN has been deconvoluted into two peaks at 2θ = 36º and 40º, and attributed to the planar zig-zag and helical conformations respectively.[53] The presence of CNTs has also shown a shift to lower 2θ values indicating that the CNTs preferentially orient the PAN molecules in a planar zig-zag conformation.[52] The shift from helical to planar zig-zag conformations is beneficial to the production of carbon fibers because helical conformations are considered to cause chain scission during thermal treatments.[54]

Significantly improved mechanical properties result from the interaction between PAN molecules and CNTs. When SWNT, DWNT, and MWNTs are used as a filler material, the tensile strength has shown a 37%, 41%, and 84% improvement respectively. Similarly, for tensile modulus, an increase of 74%, 24%, and 38% has been observed (for

SWNT, DWNT, and MWNT respectively).[49] The superior improvement in tensile strength for MWNTs is attributed to the fact that the MWNTs are significantly longer. The SWNTs are thought to have the largest impact on tensile modulus due to the fact that they are expected to be more reactive than DWNTs/MWNTs (due to the bond strain that results from high curvature).[55]

1.3.2 Effect of CNT on Stabilized and Carbonized Fibers

Chae et al.[54] have observed that the PAN/CNT fiber evolved less heat when compared to the PAN fiber in differential scanning calorimetry (DSC) experiments; the results suggest that the CNT has an effect on 36% of the PAN molecules. The authors claimed that the PAN in the vicinity of the CNT has higher thermal stability and thus, may require longer stabilization time to achieve the same level of stabilization.

During stabilization, FTIR results show that the chemical structure of PAN is also affected by the presence of CNTs.[54] Figure 1.6 shows the de-convoluted peak fitting of the nitrile band of PAN and PAN/SWNT fibers subjected to three different stabilization conditions. From the figure, it is apparent that when comparing PAN to PAN/SWNT fibers there are significant differences in the nitrile band especially when a 0.006 N/tex and 0.025 N/tex stress is applied to the fiber (conditions b and c respectively). These differences indicate that the presence of SWNTs in the PAN matrix results in more conjugated nitrile groups and less β-amino nitrile groups. Since the β-amino nitrile groups are a result of cyclization termination and/or chain scission and act as defect sites, reducing this fraction will only be beneficial to the overall fiber structure.

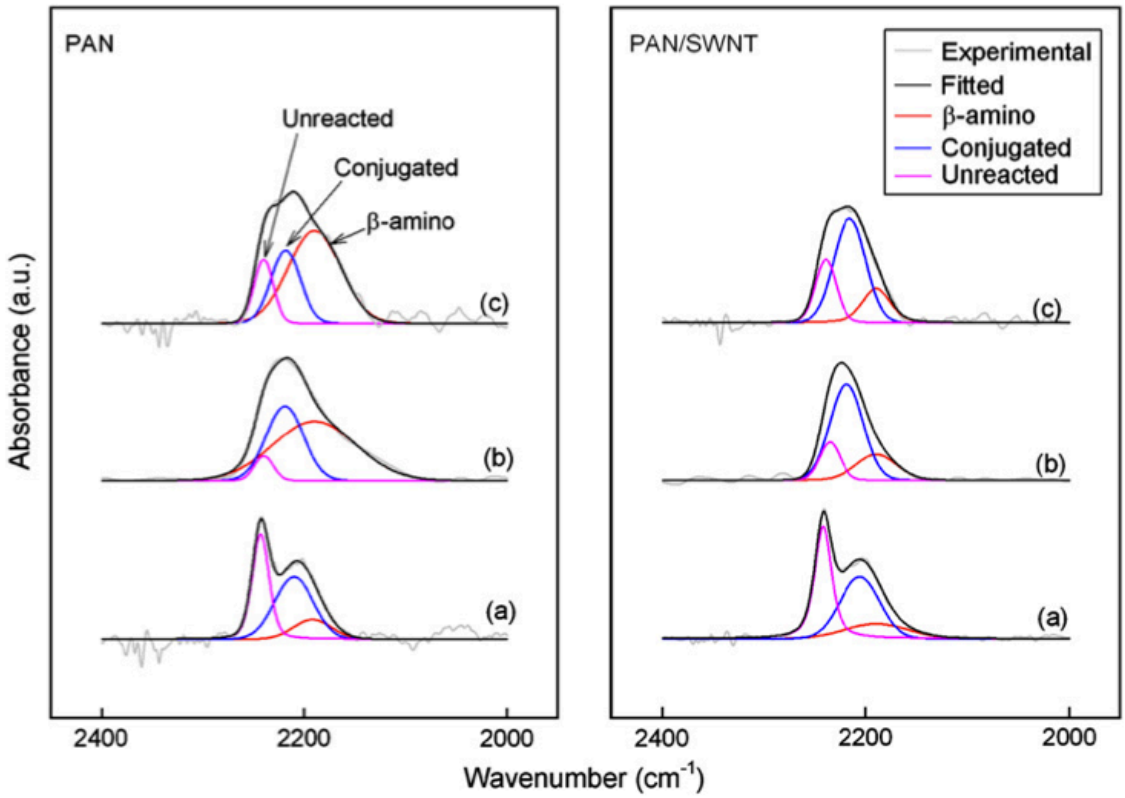

Figure 1.6 FTIR spectra of the stabilized PAN and PAN/CNT fibers.[54] Peak de-convolution was achieved based on three different nitrile group structures. The presence of CNTs causes most conjugated nitrile and less β-amino nitrile. Stabilized (a) in TGA (no pre-stress) at 285°C for 30min, (b) in furnace under 0.006 cN/tex pre-stress, and (c) in furnace under 0.025 cN/tex pre-stress

Raman and WAXD analysis also provide evidence of the PAN/CNT interaction resulting in a highly oriented and graphitic structure formation in the stabilized and carbonized fibers. [54,56] Figure 1.7 shows the azimuthal WAXD scan for the stabilized (Figure 1.7a) and carbonized (Figure 1.7b) fibers. The best peak fit of the data was achieved using two separate peaks, which suggests two separate phases present in the fibers. Furthermore, it can be concluded that one of the phases is highly oriented looking at the full-width at half maximum (FWHM) of each peak. The Raman spectra of the carbonized PAN/SWNT fibers (Figure 1.8b) also indicate an additional phase, which is not present in the control PAN fibers. From the G-band (~1580cm^{-1}) intensity the

PAN/SWNT fiber shows graphitic signatures (not present in the PAN-based fibers). Therefore, WAXD and Raman data provide evidence in support of an extra phase that is both highly ordered (WAXD) and graphitic (Raman) in nature.

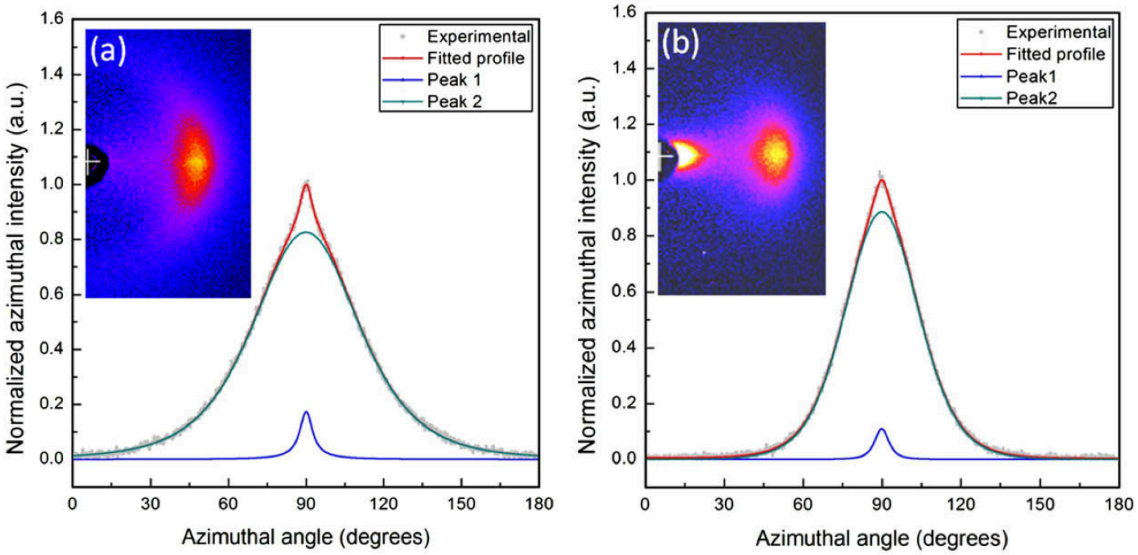

Figure 1.7 WAXD diffraction patterns of a) the stabilized and b) the carbonized PAN/CNT fiber. Highly ordered phase was observed both in the stabilized and the carbonized fibers.[56]

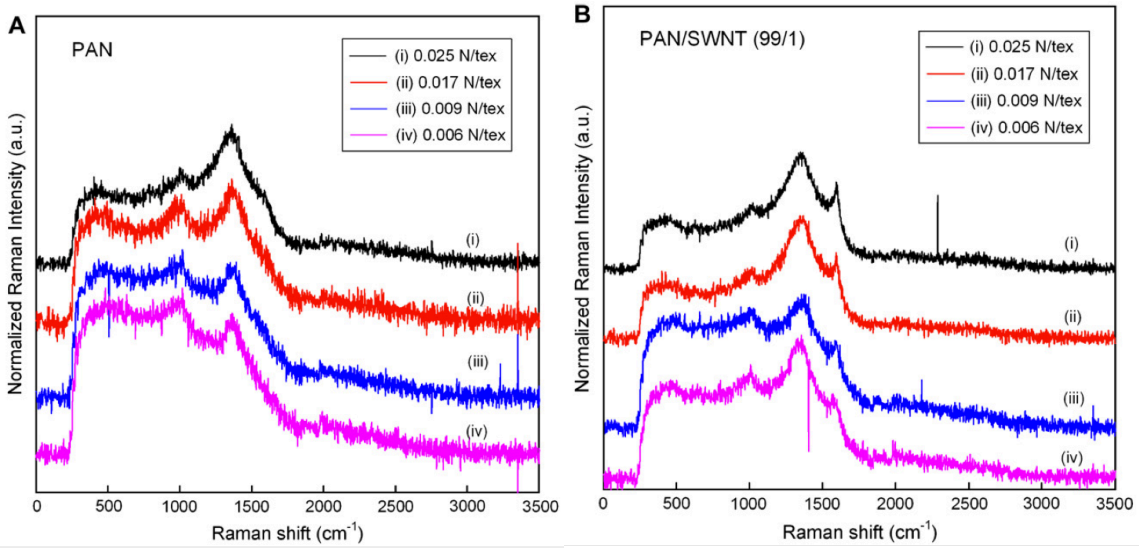

Figure 1.8 Raman spectra for carbonized a) PAN and b) PAN/SWNT carbon fibers. Presence of G-band intensity (~1580cm^{-1}) in the case of PAN/SWNT indicates graphitic structure development, whereas no G-band evolution was observed in the control carbon fiber.[54]

1.4 Carbon Fiber Testing and Analysis

In industry, the production of carbon fibers occurs on a large enough scale that tow testing (i.e., - strand testing) of the material becomes advantageous. There are standard testing protocols to follow when conducting muti-filament tensile tests (e.g., - ASTM D4018 and SACMA - SRM 16). Single filament testing can be a viable alternative to tow testing as long as proper testing conditions are followed. Typically, this involves first investigating the effect of testing parameters (e.g., - gauge length) of a known sample to determine under what conditions single filament testing agrees well with tow testing.

The Weibull modulus is a parameter that is used to indirectly quantify the distribution of defects within a material using its distribution of failure strengths. The probability of failure in a uniform specimen (under constant tension) can be described via the Weibull cumulative distribution function (CDF) (Equation 1.2, Figure 1.9).

$$P_f(\sigma) = 1 - e^{-\left(\frac{\sigma-\sigma_u}{\sigma_o}\right)^m} \tag{1.2}$$

Where, P_f is the probability of failure CDF, σ is the stress applied to the material, σ_u is the stress threshold at which failure does not occur (i.e., - failure does not occur at $\sigma < \sigma_u$), σ_o is the scale factor, and m is the shape factor of the Weibull distribution.

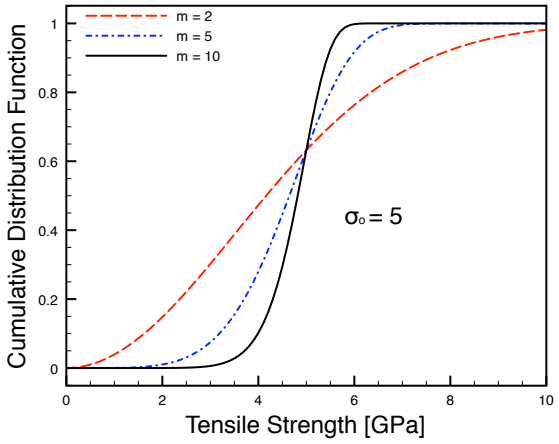

Figure 1.9 Cumulative distribution function for a variety of shape parameters (m) with constant scale parameter (σ_o = 5).

The term σ_u represents the stress at which failure will not occur. Commonly, this parameter is set to a conservative value of zero. The values of m and σ_o for a given data set are determined through two main methods: 1) linear regression and/or 2) maximum likelihood estimation (MLE).

The linear regression method involves ranking the tensile strength values (σ_i) from lowest to highest and assigning them a rank (and corresponding probability of failure). In this method, a high (observed) strength value (σ_H) is assigned a high probability of failure ($P_f \sim 99\%$), meaning that if σ_H was applied to a random fiber, the probability of survival at σ_H of that fiber would be ~1%. It has been shown that the choice of the failure probability estimator has a significant effect on the bias of the result; this is one of the main disadvantages of the linear regression method. Once the probabilities are determined, Equation 1.2 can be rearranged such that the slope of the curve of ln(ln(1/(1-P_f))) vs. ln(σ) is the Weibull modulus (m).

$$\ln\left(\ln\left(\frac{1}{1-P_f}\right)\right) = m\ln\sigma - m\ln\sigma_o \tag{1.3}$$

Despite being a simple and straightforward method, the linear regression approach has many disadvantages. Estimation bias (which depends on the failure probability estimator), wider confidence intervals (not desirable for design), and the tendency to overemphasize low strength values are all major concerns with the linear regression method. The majority of standards (ASTM, Japanese Industrial Standards Organization, European Committee for Standardization, and the International Standards Organization – ISO) recommend the maximum likelihood estimation (MLE) method for Weibull modulus determination.[57,58] The MLE method does not depend on a failure probability

estimator, but rather determines the statistical parameters (e.g., - m and σ_o) that best describe the population in question. The likelihood function is defined as the product of outcomes of the probability density function (Equation 1.4a,b).

$$L(\theta) = \prod_{i=1}^{N} P(\sigma_i) \tag{1.4a}$$

$$L(\theta) = \prod_{i=1}^{N} \left\{ \left(\frac{m}{\sigma_o}\right) \left(\frac{\sigma_i}{\sigma_o}\right)^{m-1} e^{-\left(\frac{\sigma}{\sigma_o}\right)^m} \right\} \tag{1.4b}$$

Where, $L(\theta)$ is the likelihood function, $P(\sigma_i)$ is the Weibull probability density function (PDF), N is the total number of observed tensile strength values, and the remaining variables are defined in Equation 1.2 (page 30).

Given the observed strength values (σ_i) and reasonable starting estimates for the statistical parameters, the optimal values of m and σ_o will be determined through an iterative process.

1.5 Objectives of this Thesis

PAN/CNT-based carbon fibers offer an exciting new opportunity in the advanced materials industry. The development of new materials requires those involved to be meticulous and diligent in accurately characterizing the properties of the material. This becomes especially critical when the material in question begins to push the boundaries of current state-of-the-art. The objectives of this study are:

- To develop protocols for single filament tensile testing of both precursor and carbon fibers to ensure accurate property determination and compare to the strand testing results.

- To optimize the stabilization conditions for sheath-core composite precursor fiber using various characterization tools such as Fourier Transformed Infrared (FTIR) spectroscopy, Differential Scanning Calorimetry (DSC) kinetics study, and Wide Angle X-ray Diffraction (WAXD) analysis.
- To obtain small diameter carbon fiber via islands-in-a-sea bi-component spinning technology for high tensile strength.

CHAPTER 2
FIBER TESTING AND ANALYSIS

2.1 Introduction

The importance of carbon fibers as a structural reinforcement material cannot be overemphasized. In addition to their impressive mechanical properties, carbon fibers (typical density 1.8 g/cm^3) are also lighter than even the lightweight metals such as Aluminum (2.7 g/cm^3).[59] While various novel approaches have been developed for further advancement in carbon fiber research (e.g., - lower cost precursors[60], composite carbon fibers[48,49,54], advanced processing[61]), the testing procedures of these new fibers need to be validated. However, due to significant differences in manufacturing scale, implementing the industrial test methods in a research setting may not be practical. Therefore, protocols need to be developed to ensure accurate measurement of carbon fiber properties from single filament tests.

Carbon fiber manufacturers test their material through a strand testing (i.e., - tow testing) procedure. ASTM D4018 and SACMA (SRM 16) test methods provide standards for testing the properties of continuous multifilament carbon fiber tows. An alternative testing method is the single filament test. This method has certain advantages over strand testing, yet oftentimes does not agree well with strand testing results. When comparing tensile strength values of single filament testing to the industrially reported values, the single filament results are 0.3 to 0.7 GPa lower.[62] Even when both test methods are performed by the same group, the single filament average tensile strengths are approximately 0.5 GPa lower than what is obtained by strand testing.[63] Therefore, for

projects where the accuracy of the mechanical properties are of the utmost importance, detailed single filament testing protocols need to be developed to ensure reliable results.

Determining the Weibull modulus can aid in the understanding, design, and execution of a particular application especially if proper data analysis is performed. The Weibull distribution originates from empirical observations from Weibull et al. in 1951. Dr. Weibull states: "The only merit of this distribution function is to be found in the fact that it is the simplest mathematical expression of the appropriate form. Experience has shown that, in many cases, it fits the observations better than other known distribution functions." [64] In terms of Weibull analysis, a material is assumed to have a distribution of defects (D_i) each of which are assigned a characteristic strength (σ_i). That is to say, if a material only has type D_7 defects present, then its tensile strength will be σ_7. Since each defect (D_i) in the distribution is assumed to cause macroscopic failure, the ultimate tensile strength of a brittle material is then dependent solely on the lowest characteristic strength (or correspondingly, the largest defect).[65]

For materials in which multiple failure mechanisms (i.e., - multiple defect distributions) are thought to exist, modified Weibull models have been proposed to accurately describe this behavior.[66] The importance of the Weibull modulus is its application in terms of design of brittle materials. Since inaccurately predicting brittle material behavior can have serious consequences, proper analysis of the tensile property data needs to be employed. There are two main methods for determining the Weibull modulus: linear regression (LR) and maximum likelihood estimation (MLE) (discussed in more detail in Chapter 1). Bergman et al. conducted studies to determine the estimation bias in calculating the Weibull modulus based on the failure probability estimators (P_f)

chosen (for the LR method). The conclusion being that $P_f = \frac{i-0.5}{n}$ results in the least bias estimation provided the sample size is greater than 20 specimens (where i is the rank of the observed tensile strength value: lowest tensile strength assigned $i = 1$).[67] Similar work was conducted on larger sample sizes in addition to investigating two and three-parameter models.[68] A good reference for an explanation of the advantages of the MLE method is given by Quinn et al.[57] Fundamentally, the Weibull modulus should not have any dependence on external factors (e.g., - time, environment, gauge length), however, there have been a number of experimental works that suggest otherwise in the case of gauge length.[68,69,70]

2.2 Experimental

2.2.1 Precursor Fiber Preparation

2.2.1.1 Materials

Two different polymers were used in the current study: 1) PAN-co-MAA (96/4; 453 kg/mol) and 2) PAN-co-MAA (96/4; 513 kg/mol). All polymers were obtained from Japan Exlan Company. Carbon nanotubes (CNTs) were obtained from Continental Carbon Nanotechnoligies Inc. (CCNI) with 1 wt% catalytic impurity (Lot Number: XO122UA). Dimethylformamide (DMF) was obtained from Sigma Aldrich and used as received. Precursor fibers (18S1D4, 25S2D3, and 29S1D2) were spun on a multi-filament spinning system (Hills, Inc.) and collected after gelation and drawing. Experimental precursors (Experimental #1 and Experimental #2) were obtained and used as received for testing.

Carbon fiber was produced from Experimental Fiber #1 on a continuous carbonization line under conditions that yielded the best mechanical properties. Carbon fibers (T300, T650, and IM7) were obtained and used either as received or after an acetone treatment to remove the sizing material.

2.2.1.2 Solution Preparation, Spinning, and Drawing

The details of the solution preparation, spinning, and drawing procedures are listed in Table 2.1. For the control fiber (25S2D3), the solution was made in a one step process of dissolving PAN in DMF and mixing for about 6 hours. For the composite fibers, the spinning solutions were made from three separate components: 1) dilute PAN/DMF solution 2) CNT/DMF dispersions and 3) fresh PAN/DMF solution. The CNT/DMF dispersions were added to the dilute PAN solution and excess DMF was removed by vacuum distillation. This preliminary PAN/CNT/DMF solution was then added to the fresh PAN solution and mixed for 3 hours prior to spinning.

For spinning, the prepared solutions were spun on a multi-filament spinning line at the conditions specified in Table 2.1. The temperatures listed are those of the solution tank, spin head, and spinneret jacket respectively. The air gap is the distance between the spinneret and the coagulation bath. The spin draw ratio (SDR) is defined as the ratio of the take-up speed to the jetting speed of the polymer (from the spinneret). The drawing process was done in four stages; cold drawing (room temperature - CDR), the first hot drawing (110 °C - HDR1), and the second hot drawing (185 °C - HDR2). After the primary drawing stages were completed, the fibers were minimally drawn (HDR3) and concurrently dried at 110 °C as listed in Table 2.1.

Table 2.1 Solution preparation, spinning, and drawing conditions of precursor fiber samples.

	18S1D4	**25S2D3**	**29S1D2**
Solution			
Polymer molecular weight	453 kg/mol	513 kg/mol	513 kg/mol
Co-monomer / content	Methacrylic acid / 4 wt%	Methacrylic acid / 4 wt%	Methacrylic acid / 4 wt%
CNT concentration for dispersion [mg/L]	30	-	20
Solid concentration for final PAN/CNT solution [g/dL]	11	10.5	10.5
CNT Concentration with respect to polymer	0.5 wt%	-	1.0 wt%
Spinning			
Spinneret	40 hole / 200 μm	100 hole / 200 μm	100 hole / 200 μm
Temperatures [°C]*	75 / 85 / 95		
Coagulation Bath	100% methanol (-50°C)		
Air Gap [mm]	12.7	12.7	19.0
SDR	3		
Gelation time	44 hours (-40°C methanol)		
CDR / HDR1 / HDR2 / HDR3	1.00 / 2.50 / 4.20 / 1.05	1.10 / 2.30 / 3.20 / 1.03	1.10 / 2.18 / 3.46 / 1.10

*The temperatures listed are those of the solution tank, spin head, and spinneret jacket respectively.

2.2.2 Tensile Testing of Fibers

2.2.2.1 Precursor Fibers

Various testing parameters such as linear density measurement, strain rate, gauge length, and compliance correction were investigated for the precursor fibers. In the case of gauge length dependence, the prepared precursors were compared to the results from two Experimental fibers.

Linear density measurements were conducted using a vibroscope, which relates the resonant frequency of a single filament to its diameter (in microns) through Equation 2.1.

$$d = 1\times10^{6}\sqrt{10\left(\frac{T}{L^{2}f^{2}\rho\pi}\right)} \tag{2.1}$$

where, T = tension (cN), L = length (mm), f = resonant frequency (Hz), and ρ = material density (g/cm^3).

The assumed linear density and pre-stress inputs were varied independently of one another from 0.4 – 1.8 dtex and 0.4 – 3.0 cN/tex respectively. These ranges were determined from the limitations of the machine; linear density data could be collected at conditions outside these ranges. While varying the assumed linear density, the pre-stress was held constant at 1 cN/tex. While varying the pre-stress values, the assumed linear density was held constant at the expected linear density of the material (1.11 dtex). For each set of conditions, 10 specimens were tested at a gauge length of 25.4 mm and a strain rate of 1.0 %/s (i.e., - a cross-head speed of 0.254 mm/s).

Gauge length dependence testing was performed at 50.8, 25.4, 12.7, and 6 mm gauge lengths at a constant strain rate of 0.1 %/s. Three cleanroom fibers (18S1D4–0.5 wt% CNT, 25S2D3, and 29S1D2–1.0 wt% CNT) and two Experimental fibers were subjected

to the aforementioned conditions. Tests were performed with an assumed linear density that was expected for each fiber and a pre-stress of 1 cN/tex. At least 20 specimens were tested for each gauge length. Strain rate effects were also investigated by testing 25S2D3 and 29S2D2 (1 wt% CNT) at strain rates of 0.5, 1.0, 2.0, 3.0, 4.0, 6.0, and 8.0 %/s at a gauge length of 25.4 mm. At least 20 specimens were tested at each condition.

Compliance correction was done on 25S2D3 and 29S1D2 (1 wt% CNT) on both the Favimat single filament tensile tester (Measured Solutions Inc.) and the RSA III Solids Analyzer (TA Instruments Inc.). For each tensile testing machine, at least 10 specimens were tested at each gauge length (50.8, 25.4, 12.7, and 6 mm).

2.2.2.2 Carbon Fibers

The experimental carbon fibers were processed using continuous carbonization, and tested using both single filament testing and strand testing methods. Unless otherwise noted, single filament tests were conducted at a gauge length of 25.4 mm and at a strain rate of 0.1 %/s (e.g., - for 25.4mm gauge length a strain rate of 0.025 mm/s was used). For single filament testing, individual filaments were isolated from the processed carbon fiber tow and tested using a single filament tensile tester (Favimat, Measured Solutions, Inc). For strand testing, the standard procedure (SACMA SRM16 method) was used for specimen preparation and testing. The commercial carbon fibers (T300, T650, and IM7) were also tested using single filament testing condition and compared to the data reported by the manufacturers. [71,72,73]

Developing the testing protocols for carbon fibers involved investigating the effects of gauge length, strain rate, and linear density measurement conditions. To investigate the effect of gauge length, tensile tests were conducted at 1, 3, 6, 12.7, 25.4, and 50.8 mm

gauge lengths. The strain rate was held constant at 1 %/s by varying the cross-head speed for the different gauge length conditions. At least 25 single filaments were tested at each condition and 50 filaments were typically tested at the two largest gauge lengths (25.4 and 50.8 mm). The specimens were either used as received (i.e., - with sizing) or subjected to an acetone treatment for 5 min (prior to fiber separation from the tow) to remove the sizing material. To investigate the strain rate effects, tests were conducted at strain rates of 0.1, 0.2, 0.4, 0.6, 0.8, and 1.0 %/s at a constant gauge length of 25.4 mm and 50 single filaments were tested at each condition. The applied tension during the linear density measurement (by inbuilt vibroscope in the Favimat test system) was also investigated by varying both the assumed linear density and pre-stress value. For each condition, a total of 10 single filaments were tested. Compliance correction was done based on the gauge length dependence testing results. In addition, to investigate the effect of compliance of different testing machines, both the Favimat single filament tester and RSA III Solids Analyzer were used. For testing by RSA III, fibers were mounted on paper templates[2] and the RSA III tests were conducted at gauge lengths of 6, 12.7, 25.4, and 50.8 mm at the strain rate of 0.1 %/s. The Weibull modulus was calculated by both linear regression (LR) and maximum likelihood estimation (MLE) methods for T300, T650, and IM7 at different gauge lengths.

2.3 Results and Discussion

2.3.1 Determination of Testing Procedure – Precursor Fiber

2.3.1.1 Linear Density Measurement

The linear density measurement of precursor fibers by vibroscope showed little dependence on pre-factors (assumed linear density and pre-stress). Despite varying both assumed linear density and pre-stress values over a wide range, the acceptable values for a reasonably accurate linear density measurement are 0.8 – 1.8 dtex (Figure 2.1a) and 0.4 – 1.6 cN/tex (Figure 2.1b) for assumed linear density and pre-stress, respectively. It should be noted that overestimating the linear density of the material is preferred. For a material with a nominal LD of 1.11 dtex, the maximum allowable overestimate (+62.2%) is much more than the allowable underestimate (-28.0%). Therefore, overestimating is a more conservative method to obtain accurate linear density.

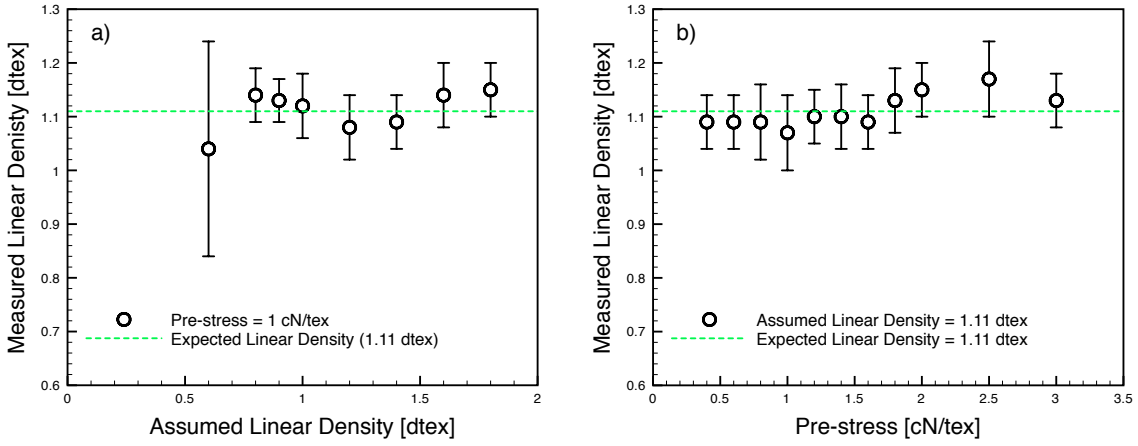

Figure 2.1 Linear density measurement by vibroscope by varying a) assumed linear density and b) pre-stress of Experimental fiber #1.

2.3.1.2 Effect of Gauge Length

Since precursors do not behave as brittle materials, the effect of gauge length on their mechanical properties will be much less when compared to carbon fibers (Section

2.3.2.2). Figure 2.2 shows the tensile strength results as a function of gauge length for cleanroom processed precursor fibers and Experimental fibers processed in ambient conditions. In the case of Experimental fibers, there is a slight dependence on gauge length (lower tensile strength at large gauge length). However, the cleanroom processed precursor fibers exhibited no dependence or higher strength at larger gauge length. While this latter trend is fundamentally incorrect, the observations remain (data well within error of each other). The difference in gauge length trends between the two fibers (i.e., - cleanroom vs. ambient processed) may be attributed to the reduction in airborne particle incorporation into the cleanroom fibers due to the processing conditions.

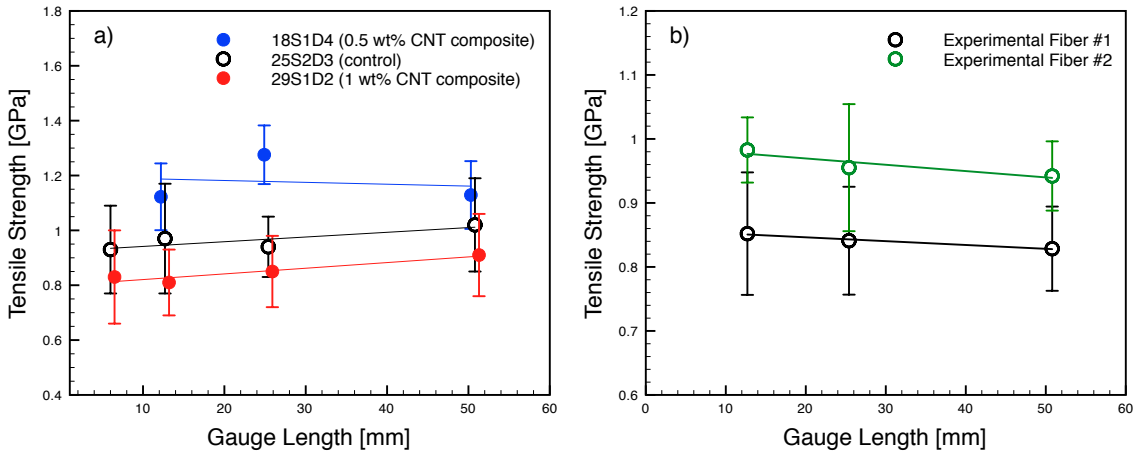

Figure 2.2 Tensile strength of various precursor fibers as a function of gauge length: a) processed under cleanroom environment and b) processed under ambient condition.

2.3.1.3 Effect of Strain Rate

It is well known that polymers exhibit viscoelastic behavior. Therefore, the tensile properties of a polymeric fiber are strongly dependent on the strain rate. This can be explained using Maxwell's model of viscoelasticity (Equation 2.1). Assuming an infinitely fast strain rate $\left(\frac{d\varepsilon(t)}{dt} \to \infty\right)$, the viscous component $\left(\sigma_d = \eta \cdot \frac{d\varepsilon(t)}{dt};\ \text{where } \eta \text{ is the viscosity of the material}\right)$ behaves as a solid body with

infinite stiffness. In this case, the compliance of the material would depend solely on the elastic component ($\sigma_s = E \cdot \varepsilon$; where E is the Young's Modulus and ε is the strain), resulting in the maximum possible modulus value. Therefore, as the strain rate approaches infinity, we expect to obtain higher tensile modulus values (approaching the limit as defined by the storage modulus of the material).

$$\sigma_T = \sigma_s + \sigma_d \quad (2.1a)$$

$$\sigma_T = E \cdot \varepsilon + \eta \cdot \frac{d\varepsilon(t)}{dt} \quad (2.1b)$$

However, despite this theory, the results of the strain rate dependence tests (Figure 2.3a) were not in good agreement. Tensile modulus values increased until the strain rate reached 2 %/s and then exhibited a steep decrease at higher strain rates. The decrease in tensile modulus was unexpected and can be explained from Figure 2.3b, which shows the stress-strain curve for the 25S2D3 precursor fiber at various strain rates. When tests were conducted at 0.5 %/s, there was a well-defined linear elastic region, whereas, at higher strain rates (e.g., - 4 and 8 %/s), the linear elastic region appeared only after a significant initiation period. This initiation period presumably involves a significant amount of movement between the precursor sample and the hydraulic rubber-faced grips. Once the grips secure the sample to a reasonable degree, a linear-elastic region is observed (Figure 2.3b). However, this 'reasonable degree' of securing does not yield accurate modulus measurement due to the persistence of movement between the sample and grips. This movement has presumably reduced when compared to the initiation period, but is not negligible in the linear elastic region at strain rates above 2 %/s.

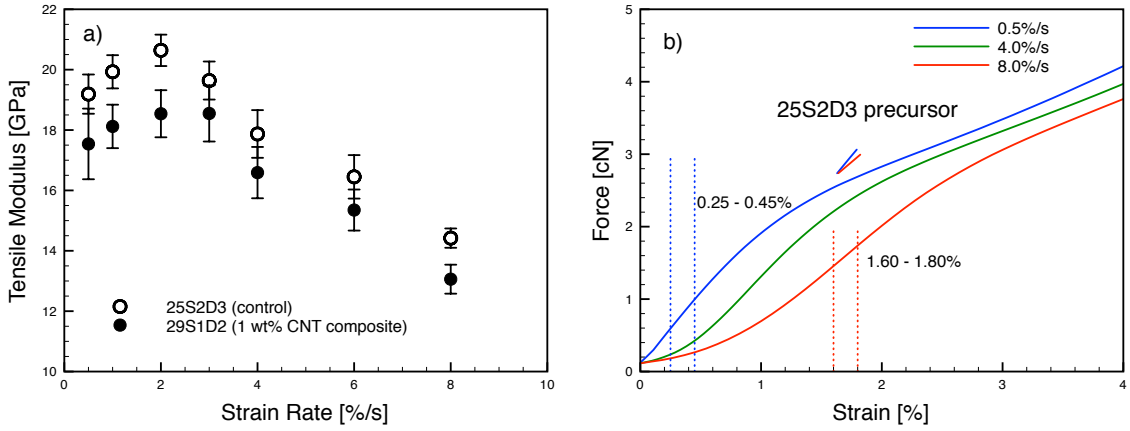

Figure 2.3 a) Tensile modulus as a function of strain rate for PAN and PAN/CNT precursor fibers and b) typical force-strain curves for 25S2D3 precursor fiber at various strain rates.

2.3.2 Determination of Testing Procedure – Carbon Fiber

2.3.2.1 Linear density measurement

A vibroscope was also used to measure the linear density of carbon fibers and the effect of various parameters was investigated in this section. The tension (T) applied to the fiber is determined by changing two variables: 1) assumed linear density (units: dtex) and 2) pre-stress (units: cN/tex). The commercial carbon fiber (T300) was used for the experiments with a known linear density of 0.677 dtex based on the reported diameter of 7 μm and the reported density of 1.76 g/cm^3.[71]

The effect of assumed linear density was investigated while holding the pre-stress at a constant value of 1 cN/tex. The measured linear density was reasonably accurate when the assumed linear density was in the range of 0.5 to 1.2 dtex (Figure 2.4a). The actual linear density of T300 (0.677 dtex) is on the lower-end of this range, which leads to the conclusion that a pre-stress value of 1 cN/tex may be slightly lower than what should be used. The pre-stress dependence on linear density measurement was also investigated by

holding the assumed linear density constant at the expected value of 0.677 dtex. Figure 2.4b shows the linear density measurement results and it appears that, in order to obtain accurate linear density measurement (when assuming an accurate linear density), the allowable pre-stress range was very narrow (1.3 – 1.35 cN/tex) as compared to the range of assumed linear density.

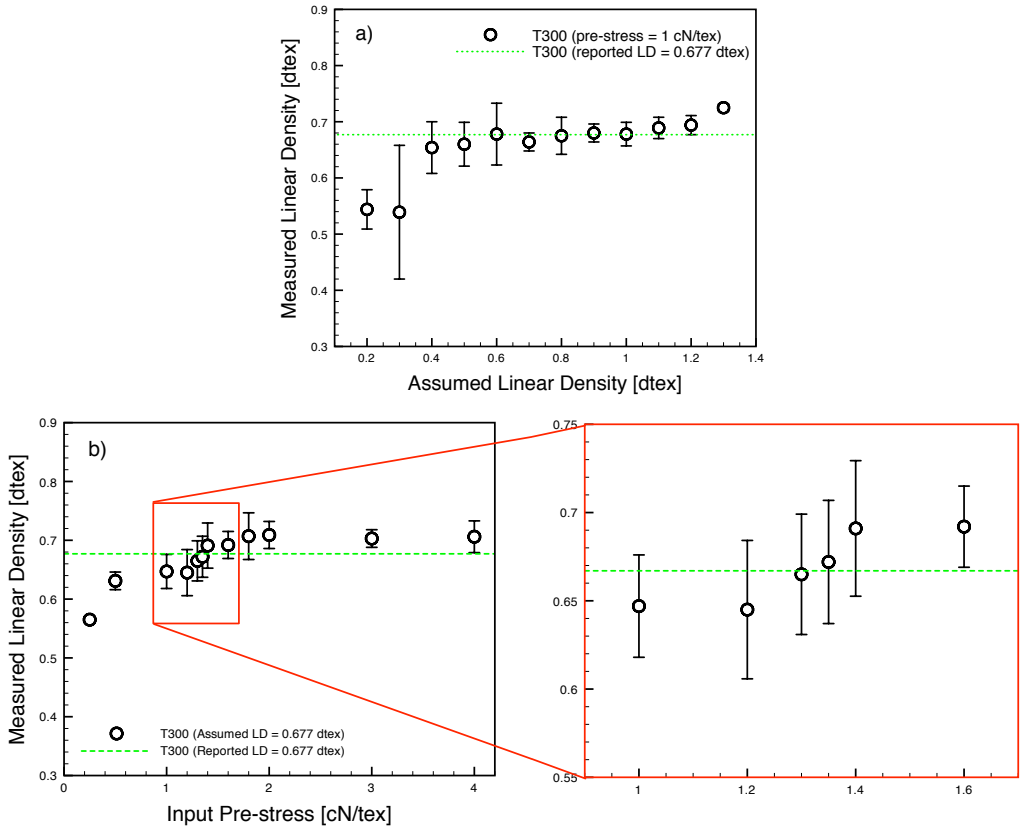

Figure 2.4 The T300 linear density measured by vibroscope as a function of a) assumed linear density and b) pre-stress. The assumed linear density exhibited relatively wide allowable range (0.7 – 1 dtex) whereas very narrow pre-stress range (1.3 – 1.35 cN/tex) was observed for accurate measurement.

Figure 2.5 shows the fiber diameters as measured by two different methods. The individual fiber diameter determined by vibroscope was re-examined by SEM. It should be noted that the pre-stress was 1 cN/tex and assumed linear density was 0.35 dtex. The fiber diameter measured by SEM was based on the effective cross-sectional area of fiber

and SEM was calibrated by certified standard. Based on SEM measurement, the average fiber diameter was 5.23 μm (Favimat Average = 5.05 μm). This also shows the importance of proper test parameter inputs. Most large diameter filaments were underestimated using the expected linear density input and a pre-stress value of 1 cN/tex. This result indicates that either 1) the assumed linear density was underestimated or 2) the pre-stress value was insufficient. Therefore, accurate determination of the nominal (assumed) linear density will be an important parameter in order for accurate linear density measurements.

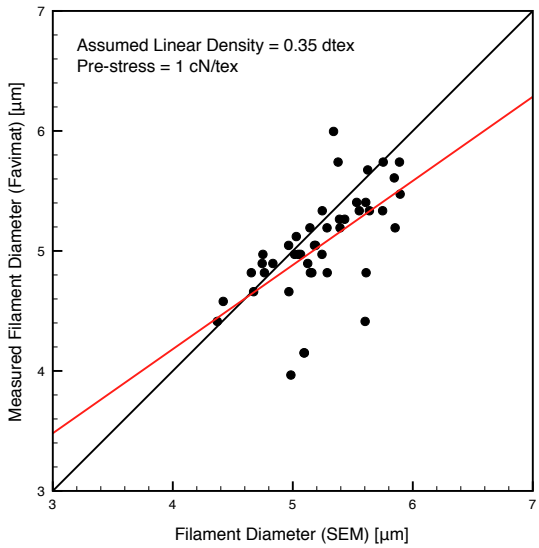

Figure 2.5 Measured diameter (calculated from linear density; ρ=1.7g/cm^3) as a function of filament diameter as determined from SEM images for 25S2D2 control fiber.

2.3.2.2 Effect of Gauge Length

Figure 2.6 shows the tensile strength as a function of gauge length for various commercial carbon fibers, showing that tensile strength of all the fibers increased with decreasing gauge length. As discussed earlier, the tensile strength of carbon fiber is strongly dependent on the frequency of defects/imperfections along the fiber axis. For IM7, tensile strength tested at 1 mm gauge length was approximately 8 GPa. Single

filament testing at a gauge length between 1 – 2 inches results in data that agrees well with the industry reported tensile strength values. It should be noted that the manufacturer reported values were based on the standardized tow testing (SACMA strand method). Figure 2.6 also shows the effect of sizing on the average tensile strength as measured from single filament tests, and shows little effect on the tensile strength.

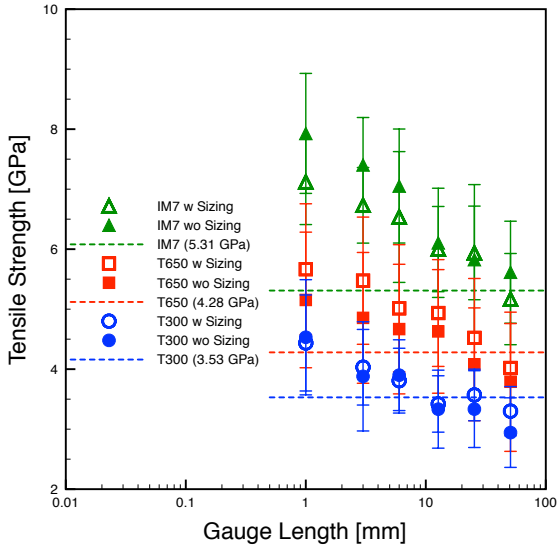

Figure 2.6 Tensile strength vs. gauge length for single filament tests using Favimat for various commercial carbon fibers. For comparison, results of strand tests reported by the manufacturers are also included.

2.3.2.3 Effect of Strain Rate

Unlike the precursor fiber, carbon fibers are elastic materials and it is expected that they will have little or no dependence on the testing strain rate. Figure 2.7 shows the strain rate dependence of tensile strength and modulus for T300. Tests were performed at a gauge length of 25.4 mm and linear density (LD) was determined prior to the tensile test (assumed LD = 0.70 dtex; pre-stress = 1.2 cN/tex). The results show no strength or modulus on strain rate, as explained. It should also be noted that the tensile modulus data

is not corrected for compliance. Compliance correction for carbon fibers will be discussed in Section 2.3.3.2.

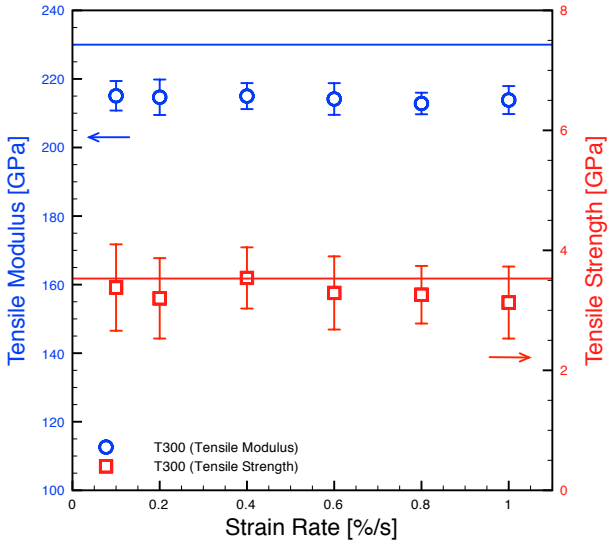

Figure 2.7 Tensile modulus and strength as a function of strain rate for commercial carbon fiber (T300). The lines (blue and red) represent the manufacturer reported data.

2.3.3 Compliance Correction

Compliance correction eliminates external compliance effects by extrapolating the tensile modulus of a material to infinite gauge length. At an infinite gauge length, any minor compliance that originates from external sources (e.g., - testing equipment, sample preparation) can be neglected. This relationship is shown in Equation 2.2.

$$E = \frac{stress}{strain} = \frac{\sigma}{\Delta L_T / L_o} = \frac{\sigma}{(\Delta L_s + \Delta L_{ext}) / L_o} = \frac{\sigma \cdot L_o}{\Delta L_s + \Delta L_{ext}}; \quad \text{as } L_o \to \infty, \Delta L_{ext} \ll \Delta L_s \tag{2.2}$$

where, E is the elastic modulus, σ is the stress applied to the sample, ΔL_T is the total change in length from all factors, ΔL_S is the change in length of the sample; ΔL_{ext} is the change in length from external sources; and L_o is the original length of the test specimen (i.e., - gauge length).

Therefore, the compliance corrected modulus can be determined by plotting the modulus results as a function of inverse gauge length (1/GL). Assigning a linear fit to the data will result in the y-intercept being the compliance corrected modulus value (y-intercept being at 1/GL = 0, which is equivalent to GL = ∞).

2.3.3.1 Precursor Fibers

The compliance corrected moduli of precursor fibers (both control and composite) are in very good agreement regardless of the tensile testing machine. For the control precursor sample, the tensile modulus value obtained from the RSA III and Favimat were 22.9 GPa and 21.4 GPa respectively. For the composite precursor, tensile modulus values of 19.4 GPa and 21.1 GPa were measured (for RSA III and Favimat).

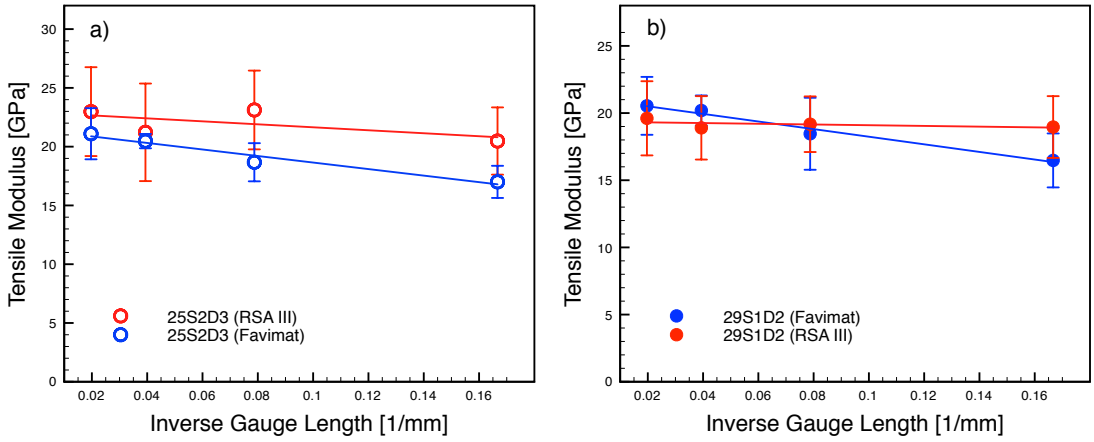

Figure 2.8 Tensile modulus vs. inverse gauge length of various precursor fibers: a) 25S2D3 and b) 29S1D2 for compliance correction from both the Favimat and RSA III tensile testers.

2.3.3.2 Carbon Fibers

Compliance corrected tensile modulus values were obtained by single filament testing for several commercial carbon fibers (T300, T650, and IM7) and the results have been

compared with the industry reported values based on multifilament tows. Figure 2.9 shows that the compliance corrected modulus for all industrial carbon fibers is within ~5% of the industry reported modulus value.

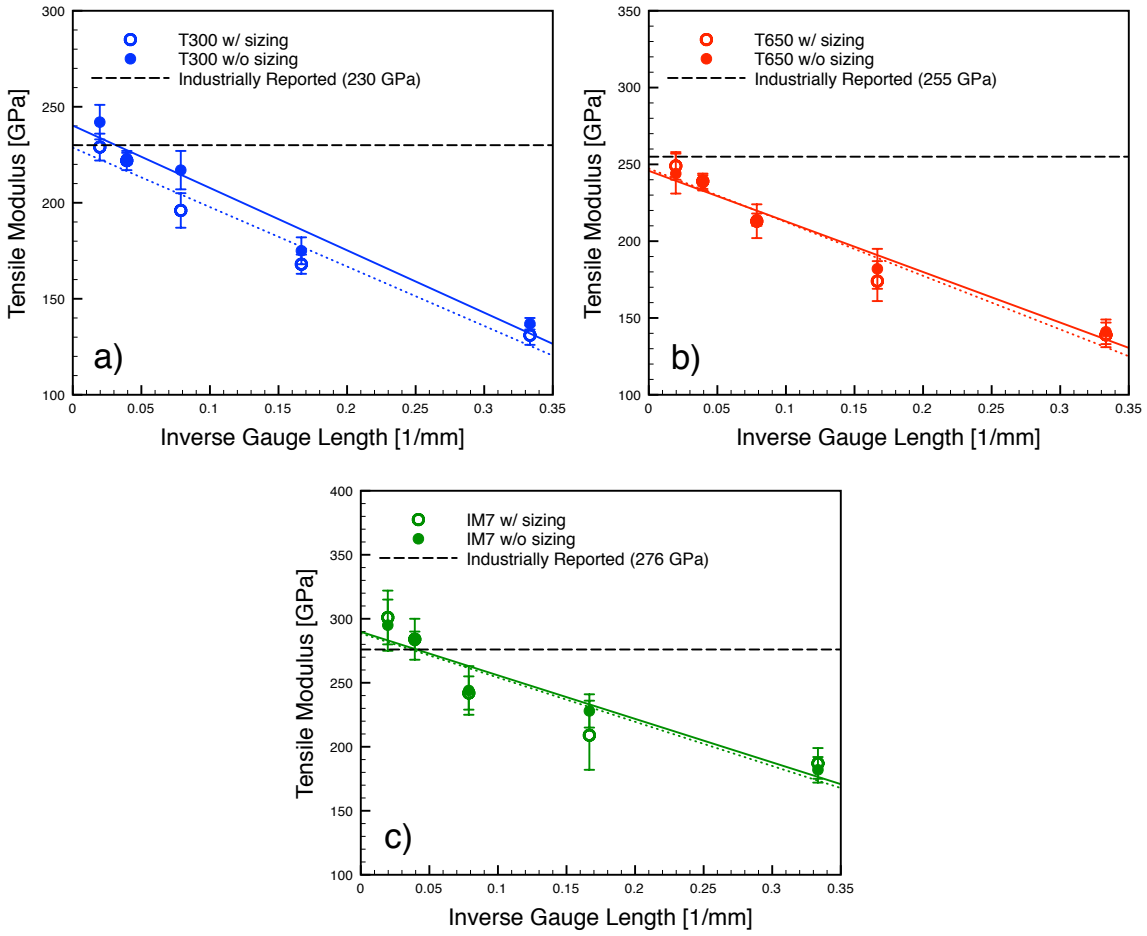

Figure 2.9 Tensile modulus as a function of inverse gauge length on the Favimat single filament tester for a) T300 b) T650 and c) IM7 carbon fibers. For comparison, tensile modulus values measured on multifilament tows as per standard test methods and as reported by the manufacturers are also included in the Figures.

In order to investigate the difference in compliance of carbon fiber on different testing equipment, single filament tests were also conducted on an RSA III solids analyzer. For testing on RSA III, fibers were mounted on paper templates using Loctite super glue. A comparison of the RSA III and Favimat tensile modulus data shows that the

Favimat is significantly more compliant than the RSA III (Figure 2.10). However test data in Figure 2.10 shows that with appropriate compliance correction, accurate moduli can be obtained by single filament tests using either equipment.

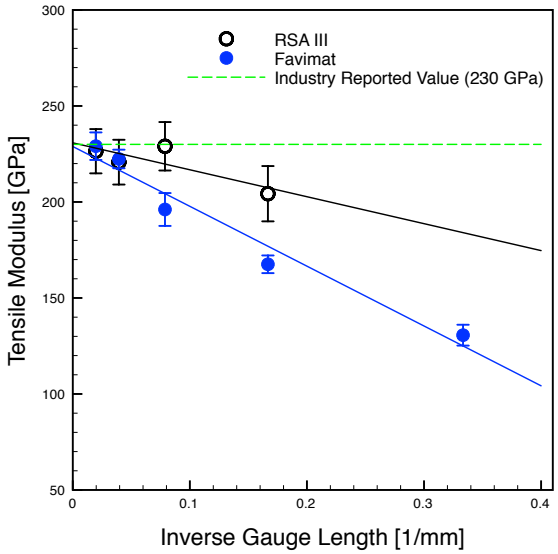

Figure 2.10 Tensile modulus as a function of inverse gauge length for T300 based on single filament testing using RSA III and Favimat. The compliance corrected modulus values based on the Favimat (229 GPa) and the RSA (231 GPa) tests are comparable to each other as well as to the industrially reported value (230 GPa) based on the multifilament tests.

2.3.4 Weibull Modulus Analysis

As discussed in Chapter 1, calculating the Weibull modulus for a set of tensile strength observations can be a very valuable exercise to deduce information about the distribution of defects in a material. The two most popular methods for calculating the Weibull modulus are 1) linear regression (LR) and 2) maximum likelihood estimation (MLE). As stated in Chapter 1, the MLE method is preferred for a number of reasons. The results in Figure 2.11 show the differences in Weibull modulus that is the result of the analysis method only (i.e., - the LR and MLE methods are performed on the sample set of data and significant differences in Weibull modulus are observed).

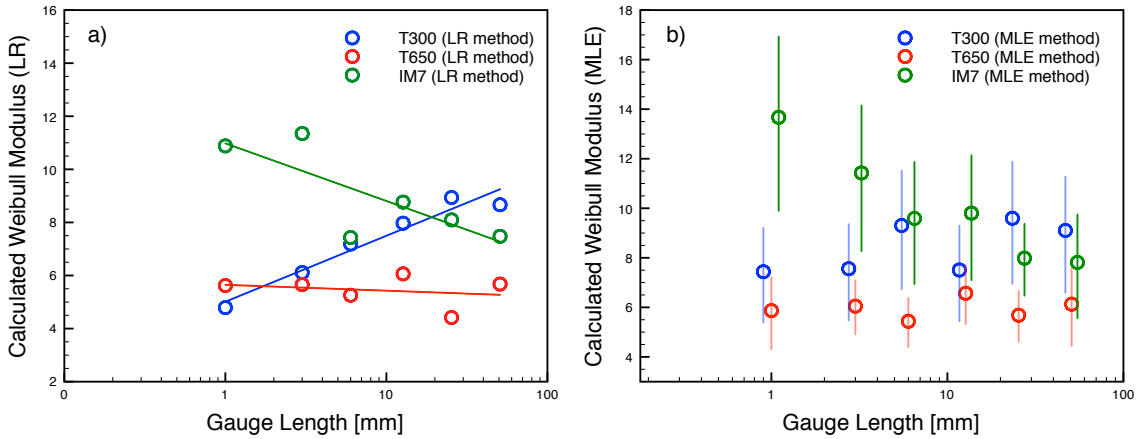

Figure 2.11 Weibull modulus data as a function of gauge length for various commercial carbon fibers calculated from a) linear regression and b) maximum likelihood estimation methods.

The LR results appear to indicate that there is a gauge length dependence on the calculated Weibull modulus, which changes trends when testing low to high-grade carbon fiber. After analyzing the data via the MLE method (with 90% confidence intervals included) the T300 trend was eliminated yet the trend with IM7 remained. This trend with IM7 can be explained by the fact that testing at smaller gauge lengths (and constant test number) results in a shorter 'sampling length' when compared to larger gauge length tests (e.g., - 50 tests at 1 mm and 25.4 mm result in a sampling length of 50 mm and 1270 mm respectively). The probability of randomly selecting a sampling length that contains a critical defect is much less in the case of small gauge length tests. Testing these small sections will result in a very tight distribution of strength values since the presence of critical defects has been avoided through sampling such a small length of fiber. This tight distribution of strength values will then result in a high Weibull modulus.

2.3.5 Single Filament vs. Strand Testing Results

The single filament testing results were compared with strand (tow) testing method as shown in Table 2.2. The strand testing tensile strength results (4.98 GPa) were higher than that obtained through single filament testing (4.72 ± 0.35 GPa). This may be due to fiber damage during the process of isolating single filaments from the tow. The average tensile modulus value obtained via single filament tests is comparable to the strand testing results because tensile modulus is not dependent on the defect structure. It should be noted that the modulus from the single filament testing reported in Table 2.2 has not been corrected for compliance.

Table 2.2. Mechanical testing results between single filament and strand testing methods.

	Single Filament Testing	Strand Testing
Density [g/cm^3]	1.76*	1.70†
Tensile Strength [GPa]	4.72 ± 0.35	4.98
Tensile Modulus [GPa]	264 ± 7#	270
Weibull Modulus	7.0	-

*Density obtained through pycnometer method.
†Density obtained through liquid displacement method.
#Value has not been corrected for compliance.

2.4 Conclusions

Various testing parameters were investigated to obtain valid tensile properties for precursor fibers and carbon fibers. The precursor fibers did not show a strong dependence on either of the vibroscope inputs (assumed linear density and pre-stress). The strain-rate effects on precursor fibers showed an unexpected trend that was attributed to the insufficient gripping mechanism at very high strain rates. Conditions for obtaining reliable mechanical properties by single filament testing as compared to strand testing for carbon fibers include: 1 – 2 inch gauge length, pre-stress of 1.3 – 1.35 cN/tex, and an accurate assumed linear density of the material. The strand testing results indicate

agreement with what was determined through single filament testing methods. The compliance corrected modulus for both precursor and carbon fibers were confirmed through both the Favimat and RSA III testing systems (agreement within 10%). The Weibull modulus trend has been found to significantly depend on the analysis method; the method of maximum likelihood estimation is preferred.

CHAPTER 3
STABILIZATION AND CARBONIZATION OF PAN/CNT SHEATH-CORE FIBERS

3.1 Introduction

Processing high-strength carbon fibers requires an understanding of the structural and chemical changes occurring during stabilization and carbonization. Stabilization is widely regarded as the most complex and least understood step in the production of carbon fibers. The reason for this is that there are a number of chemical reactions taking place simultaneously during this step. Figure 1.1 shows a schematic of the major chemical reactions that are thought to occur during the stabilization process.[8] Cyclization, dehydrogenation, oxidation, and chemical cross-linking are the major chemical reactions taking place. It is absolutely crucial to gather information about these reactions as the properties of the carbon fiber are thought to ultimately depend on the stabilization conditions.

Many studies have been devoted to quantifying the extent of stabilization through XRD[74], DSC[75] and FTIR[76] methods. The reaction kinetics is another important aspect to investigate during stabilization. There have been a number of works involved in determining the reaction kinetics of polyacrylonitrile films and fibers. Fitzer and Mueller investigated the kinetic behavior of homo-polymer and copolymer (5% methyl acrylate) through differential scanning calorimetry (DSC); in nitrogen atmosphere, they determined the activation energy of the homo-polymer sample to be more than that of the copolymer.[21] Collins et al. attempted to develop an empirical relationship for the heat evolution of both homo-polymer and copolymer films in a nitrogen atmosphere.[77] There

have been a number of other studies aimed toward quantifying the kinetic parameters of stabilization reactions. Ouyang et al. concluded from DSC studies in air that the activation energy of stabilization reactions of PAN-co-IA (1.5 mol%) is reduced by ~20 kJ/mol for cyclization and ~6 kJ/mol for the oxidation reaction when compared to PAN homo-polymer.[78] Bajaj et al. observed a much greater decrease in the activation energy when studying PAN-co-IA (2% IA) in an air atmosphere as compared to a homo-polymer sample; the reduction in activation energy was over 50 kJ/mol.[79] Bahrami et al. studied the effect of co-monomer on the observed activation energy. They studied acrylic acid (AA), methacrylic acid (MAA), and itaconic acid (IA) co-monomers and observed activation energies in an air atmosphere to be 184.8 kJ/mol, 123.3 kJ/mol, and 109.1 kJ/mol respectively.[80] While there still remain some differences in terms of absolute values, all studies are in agreement that co-monomers initiate the reaction at lower temperatures and exhibit lower activation energies. It has also been shown that the kinetic parameters of the stabilization reactions (i.e., - cyclization, oxidation, and cross-linking) can be determined through atmosphere-controlled DSC experiments.[81] If an optimal extent of reaction can be derived from the reaction kinetics, then it can be used as a benchmark for subsequent trials.

This study is focused on optimization of stabilization and determining the reaction kinetic parameters (i.e., activation energy and pre-exponential factor) of a 250 kg/mol homo-polymer precursor fiber. The kinetic results were used in conjunction with a temperature dependent Arrhenius rate constant (k) in an effort to calculate the extent of reaction for cyclization. This procedure can be used regardless of polymer characteristics

(e.g., - physical and chemical) to reveal optimal processing parameters for the best carbon fiber properties.

3.2 Precursor Fiber Preparation

This section describes the details of fiber preparation and characterization that was performed on the most promising PAN/CNT sheath-core precursor (and resulting carbon fiber). It should be noted that two additional precursor fibers (Fiber B and Fiber C) were also spun and subjected to preliminary carbonization trials as well as limited characterization. The details of Fibers B and C can be found in Appendix D. For the remainder of this section, only Fiber A will be discussed.

3.2.1 Materials

A polyacrylonitrile (PAN) polymer used in this study was a 250 kg/mol homo-polymer. The polymer was obtained from Japan Exlan Company. Poly(methyl methacrylate) (PMMA) 350 kg/mol was used as received. The carbon nanotubes (CNTs) used in the composite solution were obtained from Continental Carbon Nanotechnology Inc. (CCNI) (Lot No. XO122UA, catalytic impurity – 1 wt%). Dimethylformamide (DMF) was used as a solvent for both the PAN and PMMA solutions as well as for the CNT dispersion.

3.2.2 Spinning Dope Preparation and Fiber Spinning

For core component, PAN/CNT solutions were prepared separately from the sheath component. PAN was dissolved in DMF at a concentration of 15 g/100mL. CNT dispersions were prepared separately in 300mL of DMF and sonicated for 24 hours. The CNT dispersions were added to the PAN solution and excess DMF was removed by

vacuum distillation at 90 ^{o}C. The CNT addition and DMF distillation step was iterated to achieve a CNT concentration of 0.75 wt% with respect to the weight of the polymer. For the sheath component, PMMA (350 kg/mol) was prepared at a concentration of 30g/100mL DMF.

Sheath-core bi-component fiber spinning was performed on a single-hole spinning system with a spinneret diameter of 200 μm. The spinneret temperature was kept at 100°C and the distance between the spinneret and the coagulation bath (i.e., - the air gap) was maintained at 2 inches during spinning. The coagulation bath was 100% methanol and was maintained at about -50°C. The as spun fiber was collected at a spin draw ratio (SDR) of 3 and was stored in -50°C methanol for 5 days for further gelation after spinning was completed. A two-stage post-spin draw was conducted after the gelation period. The first stage was in air (cold drawing) and the second stage used a hot glycerol bath at 170°C (hot drawing). The drawing conditions of Fiber A are shown Table 3.1. The sheath component was removed during the cold drawing by soaking fibers in a nitromethane bath.

3.2.3 Characterization

The mechanical properties of single filaments were tested on either the Favimat single filament tensile tester (Measured Solutions Inc.) or the RSA III Solids Analyzer (TA Instruments). For RSA III, all tests were conducted at 6 mm gauge length and at a strain rate of 0.1 %/s. When testing on the Favimat, 10-20 specimens were tested at 25.4 mm gauge length to determine the linear density of the material and then, at least 30 specimens were tested at 6 mm gauge length and 0.1%/s strain rate (for mechanical property reporting). Differential scanning calorimetry (DSC) was used to determine the

peak temperatures of stabilization as well as the kinetics of stabilization reactions. Raman spectra (Holoprobe Research 785 Raman microscope – Kaiser Optical system) were collected to determine CNT orientation. WAXD patterns were collected by Rigaku micromax-002 (CuK_{α} radiation) using a Rigaku R-axis IV++ detector. The collected 2D patterns were analyzed using Area Max v2 and peak fitting was performed using JADE 9.1.5. Infrared spectra (IR) were collected using an infrared microscope (Spectrum One, Perkin Elmer) with a resolution of 2 cm^{-1} and 256 scans. Peak fitting software (PeakFit v4.12) was used to fit the nitrile band. Surface and cross-sectional morphologies were determined using the Zeiss Ultra 60 FE-SEM.

3.2.4 Results and Discussion

The processing parameters along with structural and mechanical properties of the PAN precursor fiber are listed in Table 3.1. Fiber A exhibits high strength (1.06 GPa) and a reasonably high tensile modulus (19.8 GPa). WAXD analysis also shows high orientation of PAN molecules and CNTs.

Table 3.1 Structural and mechanical properties of PAN/CNT sheath-core precursor fiber (Fiber A).

	Fiber A
CNT Loading (wt%)	0.75
Polymer Description	250K homo-polymer
Draw Ratios (SDR/CDR/ HDR/TDR)*	3.00 / 1.19 / 7.06 / 25.20
Diameter [µm]†	6.71 ± 0.2
Tensile Strength [GPa]	1.06 ± 0.1
Tensile Modulus [GPa]	19.8 ± 0.7
Elongation at [%]	9.5 ± 1.2
d-spacing$_{110}$ [Å]‡	5.247
Meridional Peak Pos.	39.05°
Crystallinity [%]#	66%
Crystal Size [nm]&	10.3
f_{PAN}**	0.91
f_{CNT}††	0.93

*SDR, CDR, HDR, and TDR stand for spin draw ratio, cold draw ratio, hot draw ratio, and total draw ratio, respectively; †Favimat vibroscope linear density measurement (assumed bulk density: 1.18 g/cc) ‡Bragg equation using the (110) peak position of the equatorial scan (XRD); #Peak fitting methods from integrated scan (XRD); &Scherrer equation of (110) peak from equatorial scan; **Herman's orientation parameter from azimuthal scan of ~17° peak; ††Determined from curve fitting methods of Raman data.[82,83]

3.3 Stabilization and Carbonization Studies

3.3.1 Preliminary Carbonizations (Fiber A)

To determine the appropriate stabilization temperatures in an oxidizing atmosphere, DSC experiment was conducted in air. Figure 3.1 shows the DSC exotherms of the 250 kg/mol homo-polymer sample. The reaction initiates at ~240°C and reaches a maximum rate of reaction at 310°C. Since controlling the heat evolution from within the fiber is critical to its ultimate potential as a carbon fiber, temperature profiles were chosen with the majority of time at the lower temperature (T_1).

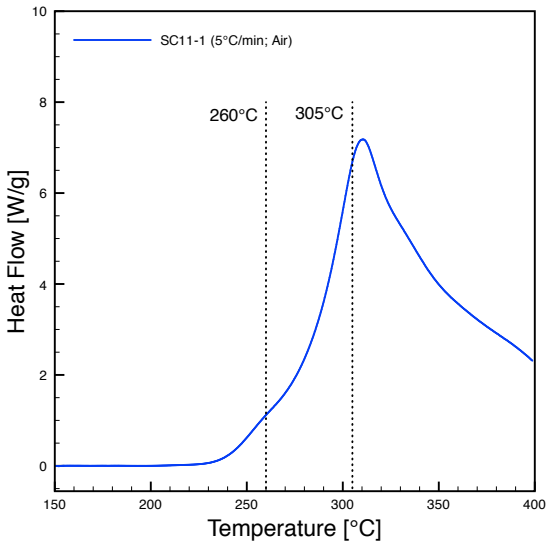

Figure 3.1 DSC heat flow curve for PAN/CNT sheath-core composite fiber (Fiber A) in air atmosphere. The dotted lines at 260 and 305 ^{o}C represent the temperatures used for stabilization.

The first set of carbonization trials revealed a strong dependence on the applied pre-stress to the fiber (Table 3.2). As the pre-stress was increased from 27.3 to 34.7 MPa, a corresponding increase in tensile modulus was observed (276 to 365 GPa). This initial result was promising as a modulus of 365 GPa was achieved without compliance correction (based on Figure 2.10, a modulus of ~405 GPa is expected after compliance correction). Figure 3.2 shows the individual filament test results for C-1.3 displaying a majority of very high tensile strength and modulus values. The maximum values for tensile strength and modulus that were observed in C-1.3 were 6.5 GPa and 392 GPa (uncorrected) respectively.

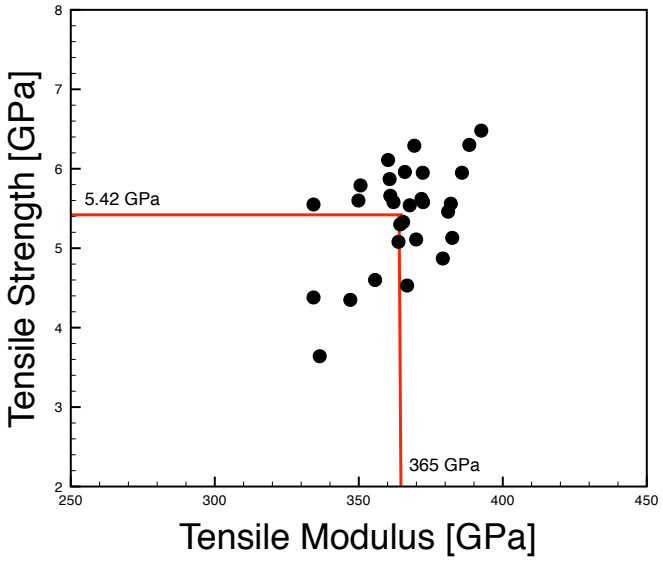

Figure 3.2 Single filament tensile results on C-1.3 from RSA III. Highest tensile strength and modulus occurred at 6.5 GPa and 392 GPa respectively.

Figure 3.3 shows the surface and cross-sectional morphologies of two carbonized sheath-core fibers. The samples were each subjected to a two-stage stabilization at 260°C and 305°C for various times. It is obvious that the stabilization conditions have an effect on the resultant carbon fiber properties (both mechanical and morphological). The well-stabilized sample (100/10 min; Figure 3.3c,d) has a very clean surface. In contrast to this, the poorly stabilized sample (50/30 min; Figure 3.3a,b) has a number of surface features that will limit the ultimate strength of the carbon fiber. Presumably, these detrimental surface features are a result of improper stabilization conditions prior to high-temperature treatment. The cross-sections of both fibers show well-dispersed CNT fibrils within the carbon fiber matrix.

Table 3.2 Preliminary carbonization trials for Fiber A showing a strong dependence on the pre-stress that was applied to the fiber during thermal treatments.

Trial No.	Pre-stress [MPa]	Stabilization Time [min]		Tensile strength* [GPa]	Tensile modulus* [GPa]	Strain to failure* [GPa]
		260°C	305°C			
C-1.1	27.3	100	10	3.47±0.84	276±31	1.25±0.27
C-1.2	29.4			4.16±0.77	296±21	1.39±0.22
C-1.3	34.7			5.42±0.66	365±15	1.47±0.16

* Tensile testing was done using RSAIII tensile tester at 6 mm gauge length. The strain rate was 0.1 %/s. Tensile modulus values are not corrected for compliance.

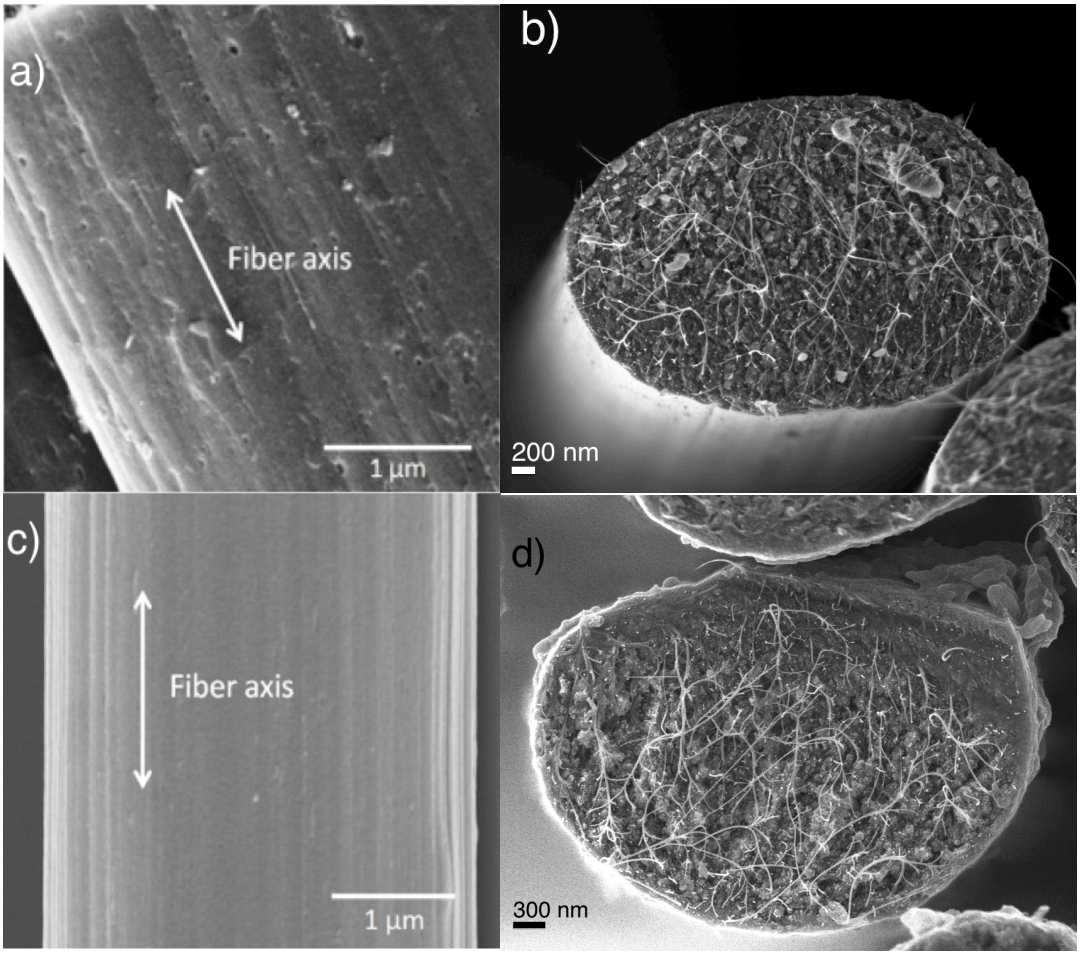

Figure 3.3 SEM images showing the difference in morphology between a poorly stabilized fiber (a) surface and b) cross-section (3.8 GPa/270 GPa) and a well-stabilized fiber (c) surface and d) cross-section (5.4 GPa/365 GPa). The mechanical properties are given as: tensile strength/tensile modulus.

In order to further improve the tensile properties of carbon fiber, a design of experiment (DOE) was devised, but as can be seen from Table 3.3, the mechanical

properties could not be improved with the given DOE. The advantage of the DOE is it yields maximum information about the effect of the investigated variables, especially interaction effects. The goal was to refine the stabilization conditions around the center point of 110min/10min to increase the carbon fiber tensile strength. However, the DOE did not result in any trials that exceeded the properties of C-1.3 (5.42 GPa). This may be due to the fact that the change in t_1 and t_2 was too large or the stabilization condition for C-1.3 was truly the best.

Table 3.3 Central composite design (CCD) of experiments for stabilization times t_1 and t_2 and the resulting carbon fiber properties.

Trial No.	Pre-stress [MPa]	Stabilization Time [min]		Diameter [mm]	Tensile strength* [GPa]	Tensile modulus* [GPa]	Strain to failure* [GPa]	Weibull Mod. (MLE)
		260°C	305°C					
C-2.1	33.2	124	3	3.57±0.34	4.03±0.42	243±12	1.77±0.18	12.2
C-2.2		124	17	3.36±0.18	3.88±0.41	248±13	1.65±0.14	10.1
C-2.3		96	3	3.40±0.11	4.35±0.87	261±19	1.75±0.26	6.3
C-2.4		96	17	3.46±0.18	4.02±0.79	237±15	1.75±0.27	6.0
C-2.5		130	10	3.42±0.09	4.65±0.62	242±12	1.97±0.22	8.9
C-2.6		90	10	3.45±0.25	4.28±0.79	241±15	1.84±0.32	4.0
C-2.7		110	0	3.52±0.10	4.82±0.76	249±12	2.00±0.30	8.2
C-2.8		110	20	3.42±0.09	4.10±0.57	250±20	1.71±0.16	8.0

* Tensile testing was done using Favimat tensile tester at 6 mm gauge length. The strain rate was 0.1 %/s. Modulus has not been corrected for compliance.

Since the preliminary results (C-1.3: 5.42 GPa in Table 3.2) were tested on a different tensile machine as compared to the DOE experimental results, this effect was also investigated. Taking the best sample from the Favimat results (C-2.7 in Table 3.3) and testing it on the RSA III yielded the resuls in Table 3.4. It can be seen that the RSAIII testing results exhibited higher tensile strength and modulus than those obtained from the Favimat. The tensile modulus value by RSAIII (323 GPa) was significantly (about 30%)

higher than the tensile modulus obtained by Favimat testing (249 GPa). This can be attributed to the difference in compliance between these testing instruments as discussed in Chapter 2. Considering the effect of testing equipment, the carbon fiber properties obtained in C-2.7 trial was very close to C-1.3 carbonization trial. The pre-stress for C-2.7 (33.2 MPa) was slightly lower than that of C-1.3 trial (34.7 MPa) (Table 3.2 and 3.3), which can be responsible for the lower modulus (and correspondingly lower strength). In addition, although the total residence time for stabilization was the same for both trials, the temperature profiles were slightly different. This suggests that the optimal processing window to obtain the best carbon fiber can be relatively narrow.

Table 3.4 Difference in mechanical properties resulting from testing instruments (6 mm).

Trial No.	Pre-stress [MPa]	Stabilization Time [min]		Tensile Tester	Tensile strength* [GPa]	Tensile modulus* [GPa]	Strain to failure* [GPa]	Weibull Mod.
		260°C	305°C					
C-2.7	33.2	110	0	**Favimat**	4.82±0.76	249±12	2.00±0.30	6.9
				RSA III	5.06±0.77	323±20	1.56±0.21	7.2

* Testing was done at 6 mm gauge length and strain rate was 0.1 %/s. Tensile modulus values are not corrected for compliance.

Figure 3.4a shows the plot of tensile strength vs. tensile modulus of the carbonized sample C-2.7 tested by Favimat, which displays the large spread of tensile strength values (coefficient of variation (CV) = 16%) that arises from the fiber defect structure. Contrary to this, the distribution of tensile modulus values (CV = 5%) is much tighter due to the well-controlled pre-stress condition. Figure 3.3b shows the tensile strength values as a function of fiber diameter, suggesting that the smaller diameter fibers have higher tensile strengths. As mentioned in the experimental section (Section 3.2.3), 10 specimens were used to obtain the average linear density of this particular sample (Figure 3.4b) and

Figure 3.4a shows the tensile property spread at 6 mm gauge length assuming the average linear density value determined previously.

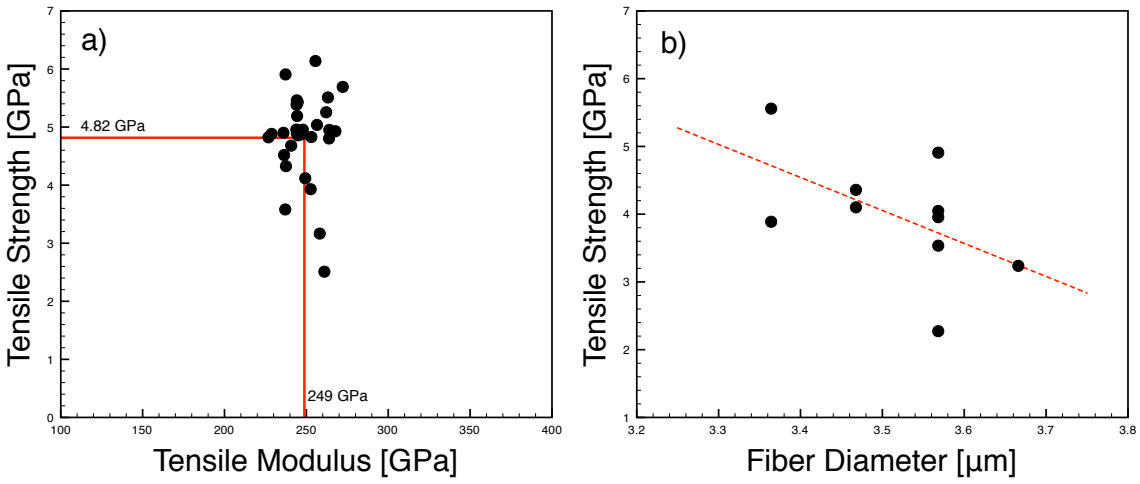

Figure 3.4 Tensile property relationships of C-2.7 sample: a) tensile strength vs. tensile modulus showing the spread of each (6 mm gauge length) and b) effect of fiber diameter on tensile strength (25.4 mm gauge length).

The Weibull moduli for commercial carbon fibers (T300, T650, and IM7) at 6 mm gauge length calculated by MLE method were 9.3, 5.9, and 9.6 respectively. Considering that C-2.7 has a lower Weibull modulus as compared to T300 (Figure 3.5b: m = 8.2), this indicates it possesses a wider defect distribution (undesireable). Despite this, Fiber A (C-2.7) still surpassed the tensile strength of T300 at 6 mm gauge length (C-2.7 (6mm): 4.82 GPa vs. T300 (6 mm): 3.90 GPa (Figure 2.6)).

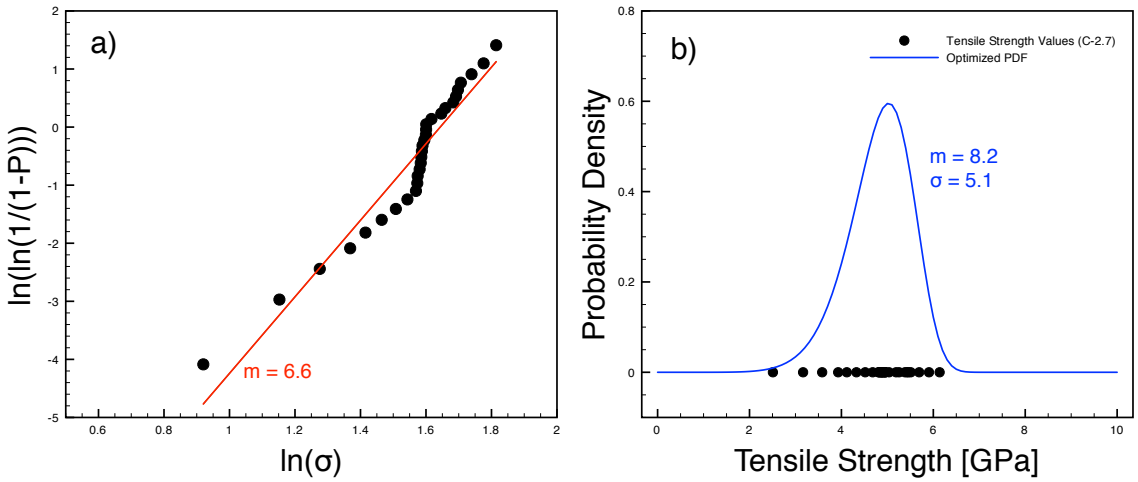

Figure 3.5 Determination of the Weibull modulus through a) linear regression and b) maximum likelihood estimation (MLE) methods.

3.3.2 Optimization of Stabilization

In the previous section, the optimization of stabilization and carbonization was achieved by varying stabilization conditions. However, the structural and chemical changes in stabilized fibers were not investigated. In the following sections, the ultimate carbon fiber properties were correlated to various characterization results such as DSC kinetics study, FTIR spectra analysis, and WAXD analysis.

3.3.2.1 Reaction Kinetics and Extent of Cyclization

An extent of cyclization (M_{cyc}) was developed from the reaction kinetic parameters. Differential scanning calorimetry (DSC) was used to determine these kinetic parameters by observing the changes in the exotherm peak temperature as a function of heating rate. The cyclization reaction was isolated by conducting the DSC scans in a nitrogen environment. This method has previously been reported.[81,84] Cyclization reaction can occur in an inert environment, but oxidation and cross-linking reactions require an oxygen-containing environment or the ladder structure as a pre-requisite. As a result, each reaction can be isolated by running a PAN precursor in a nitrogen environment

followed by a subsequent scan in air. The result of which is three separate exothermic peaks that correspond to the cyclization, oxidation/dehydrogenation, and cross-linking reactions. This behavior is illustrated in Figure 3.6b. The observed peak temperatures at the heating rates studied are shown in Table 3.5.

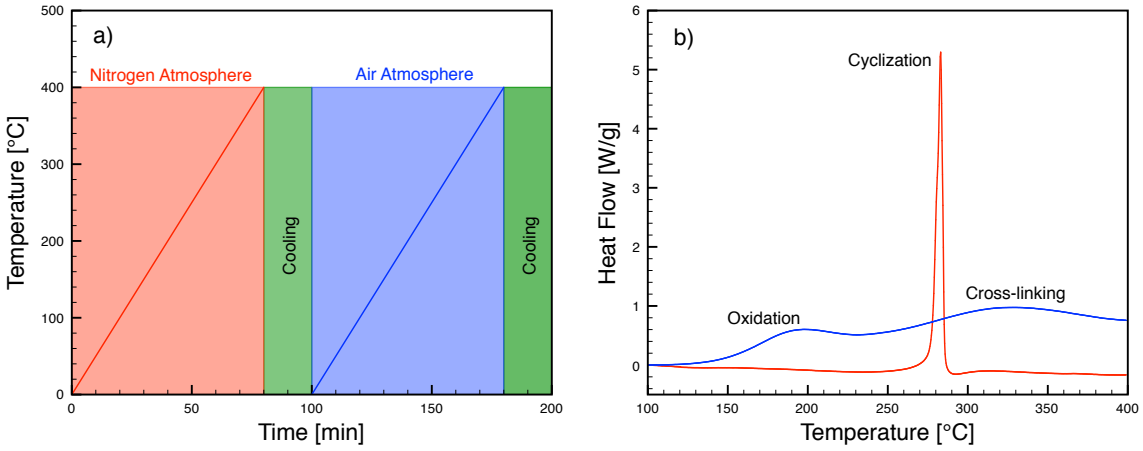

Figure 3.6 a) DSC temperature profile and b) heat flow curves under different environment (red line – under nitrogen and blue line – under air).

Table 3.5 Peak temperatures of DSC kinetics study for Fiber A.

	Fiber A		
	250K homo-polymer		
Heating Rate [°C/min]	in N2	rerun in Air	
	T_p	T_{p1}	T_{p2}
1	265.6	181.7	295.6
3	283.0	198.0	328.9
5	293.5	211.2	356.6
10	304.1	228.5	-
20	317.8	244.6	-

Two methods that are commonly used to determine the kinetic parameters from DSC curves were developed by Ozawa and Kissinger.[85,86] The Ozawa method used in this study follows the procedure outlined by ASTM E698-11. It is important to note that the ATSM method uses the 3-term Schlömilch approximation for the exponential integral

involved in the Ozawa analysis. Due to this approximation, five iterations were performed in estimating the kinetic parameters in order to reduce any errors to a negligible level. The relevant equations used in the analysis are given in Equation 3.1. The terms in Equation 3.1 are as follows: ϕ is the heating rate (°C/min), T_p is the observed peak temperature (K), E_a is the activation energy (J/mol), and R is the universal gas constant (8.3145 $\frac{J}{mol \cdot K}$). The order of reaction has been calculated to be 1.095,[86] but for simplicity a reaction order of one is assumed.

Kissinger	Ozawa	
$\frac{d\left(\ln\frac{\phi}{T_p^2}\right)}{d\left(\frac{1}{T_p}\right)} = -\frac{E_a}{R}$	$\frac{d(\log\phi)}{d\left(\frac{1}{T_p}\right)} = -2.19\frac{E_a}{R}$	(3.1)

Using Equation 3.1 and plotting either $\ln\left(\frac{\phi}{T_p^2}\right)$ or $\log\phi$ against $\left(\frac{1}{T_p}\right)$, the slope of the curve can be used to determine the activation energy (E_a) of the reaction. After the activation energies were calculated, the pre-exponential factor (A) in the Arrhenius equation was determined through the expression $A = \frac{\phi E_a}{RT_p^2} e^{E_a/RT_p}$.[87] The results of this analysis are shown in Table 3.6. The individual DSC curves that were used can be found in Appendix A.

Table 3.6 DSC kinetics analysis results for Fiber A precursor fiber.

		From Ozawa's Equation		From Kissinger's Equation	
		E_a (kJ/mol)	A (s^{-1})	E_a (kJ/mol)	A (s^{-1})
Fiber A precursor fiber	Cyclization	144.0	$5.0x10^{12}$	133.6	$2.0x10^{12}$
	Oxidation	86.1	$4.2x10^{8}$	72.0	$3.5x10^{7}$
	Cross-linking	74.8	$1.8x10^{5}$	61.1	$4.3x10^{4}$

Using the cyclization parameters from the reaction kinetics study, the Arrhenius rate constant (k) can be calculated for a given temperature (T). If the concentration of unreacted nitrile groups in the fiber (M) is normalized to 1, then the rate of change of a 1^{st}-order reaction is defined in Equation 3.2a. Integration of this equation for both isothermal and non-isothermal cases results in an equation that describes the extent of cyclization, M_{cyc} (details can be found in Appendix B).

Since cyclization is known to be a pre-requisite for oxidation and cross-linking reactions, the average of Ozawa and Kissinger results for its activation energy (E_a = 138.8 kJ/mol) and pre-factor ($A = 3.5x10^{12}$ s^{-1}) from the previous DSC kinetic study are used. For a given temperature profile, there are both isothermal and non-isothermal stages and this must be taken into account when calculating the extent of cyclization (M_{cyc}). This parameter allows for the comparison of multiple stabilization conditions for any given precursor regardless of temperatures or times.

Isothermal	**Non-Isothermal**	
$\frac{dM_{cyc}}{dt} = -kM_{cyc}$	$\frac{dM_{cyc}}{dt} = -k(t)M_{cyc}$	3.2a
$\int \frac{dM_{cyc}}{M_{cyc}} = -k\int dt$	$\int \frac{dM_{cyc}}{M_{cyc}} = -\int k(t)dt$	3.2b
$\ln M_{cyc} = -kt$	$\ln M_{cyc} = -A\int e^{-\frac{E_a}{RT(t)}}dt$	3.2c
$M_{cyc}(t) = e^{-kt}$	$M_{cyc}(t) = e^{-A\int e^{-\frac{E_a}{RT(t)}}dt}$	3.2d

Where, M_{cyc} is the fraction of unreacted nitrile groups, normalized to 1, k is the Arrhenius rate constant, t is time in seconds, E_a is the activation energy of reaction, A is the pre-exponential factor (i.e., - frequency factor), R is the universal gas constant, and T(t) represents the temperatures profile (Temperature as a function of time).

3.3.2.2 Characterization of Stabilization Reactions (FTIR, M_{cyc}, and XRD)

In addition to the DOE experiment in Section 3.3.1, the optimal stabilization conditions were investigated by various characterization methods in this section. The degree of stabilization was correlated with FTIR, WAXD, and M_{cyc} results and compared to the resulting carbon fiber properties. Stabilization and carbonization studies of PAN precursor fiber (Fiber A) were conducted in a tube furnace (MHI Inc.) by hanging the precursor fiber on a graphite platform as illustrated elsewhere[88]. The pre-stress values were held constant at 30.0 MPa. A two-stage stabilization was employed for these studies where the dwell times (t_1 and t_2) were varied at the temperature set points (T_1 and T_2). The temperatures were held at 260 ºC and 305 ºC for T_1 and T_2 respectively. Stabilization was performed under air atmosphere and the flow of air was controlled at a rate of 5 L/min. After completion of stabilization, the tube furnace was purged with Argon gas for ~30 min. After purging, the furnace was ramped to 1300 ºC at a rate of 5 ºC/min and held for 5 min while maintaining an inert atmosphere.

FTIR spectra were collected for fibers stabilized at 260 °C and 305 °C for various times t_1 and t_2. When n/a is reported for t_2, this means that the fiber was subjected to a 1-stage stabilization (did not ramp to T_2). Changes in the nitrile peak (~2244cm^{-1}) were monitored and quantified through deconvoluting the nitrile peak into its three constituents: 1) unreacted, 2) conjugated, and 3) β-amino nitrile. The relative fractions of the peak areas were taken as the relative fractions of each constituent in the stabilized fiber. The details of this method are discussed elsewhere.[8,81,84] Figure 3.7 shows three curve fitting results of the nitrile band under various stabilization conditions. From left to right (a to c), the stabilization time (t_1) at the first temperature (T_1=260 °C) was increased from 60 min to 80 min to 110 min, respectively. Corresponding to this change in stabilization time, a decrease in the unreacted nitrile fraction (green) and an increase in the conjugated nitrile fraction (blue) are observed. Interestingly, the fraction of β-amino nitrile (red) experiences a dramatic decrease from 80 min to 110 min (~17% to ~5% for b and c respectively), while the change between 60 min and 80 min is not as dramatic (~21% to ~17%). This may be an indication of the optimal stabilization conditions.

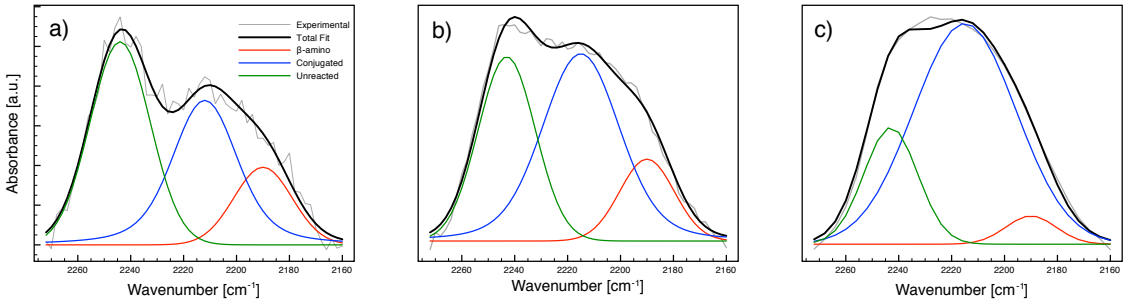

Figure 3.7 FTIR curve fitting results for a) 60/0min (S-3.8), b) 80/0min (S-3.5), and c) 110/0min (S-3.2).

The quantitative results of the peak deconvolution are presented in Table 3.7. Due to the subjective nature of peak fitting, three separate peak fits (under identical constraints) were conducted on each stabilized sample and the average value for area fraction is provided. It has been previously reported that the stabilization conditions that maximize Φ_c/Φ_β is a preliminary condition to produce the best carbon fibers.[89] Similar to the previous study, Figure 3.8 shows a decrease in Φ_c/Φ_β due to over-stabilization. It appears that an optimal extent of reaction exists at ~24% at which point the ratio, Φ_c/Φ_β, experienced its maximum values. The dashed line in Figure 3.8 is a 4th order polynomial fit of the data.

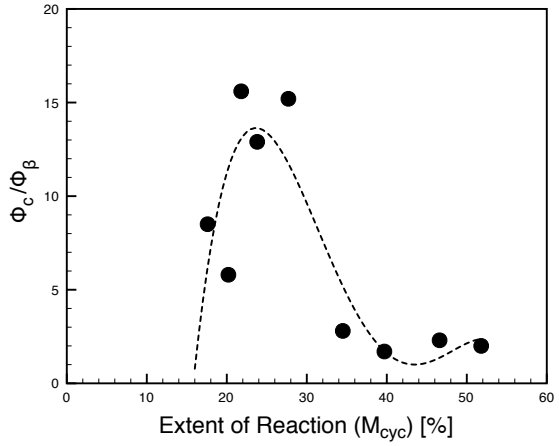

Figure 3.8 The correlation of FTIR peak deconvolution results (Φ_c/Φ_β) to the DSC kinetics analysis results (M_{cyc}) showing a maximum at M_{cyc} of ~24%.

Table 3.7 FTIR peak deconvolution results and tensile strength of the corresponding stabilized and carbonized fibers.

ID	Pre-stress [MPa]	Stabilization Time [min]		Mole Fraction [%]			$\frac{\phi_c}{\phi_\beta}$	Stab. Fiber Tensile Strength [GPa]	Carb. Fiber Tensile Strength* [GPa]
		260°C	305°C	Unreacted (Φ_u)	Conjugated (Φ_c)	β-amino (Φ_β)			
S-3.1	30	140	0	17.2±0.5%	77.8±1.2%	5.0±0.8%	15.6	0.26±0.01	n/a
S-3.2		110	0	20.6±0.2%	74.5±0.7%	4.9±0.6%	15.2	0.28±0.01	4.66±0.73
S-3.3		100	10	12.5±0.7%	81.2±1.6%	6.3±0.9%	12.9	0.29±0.01	4.52±1.14
S-3.4		80	30	16.4±0.5%	74.8±0.2%	8.8±0.4%	8.5	0.27±0.02	4.12±0.59
S-3.5		80	0	36.7±1.7%	46.4±3.5%	16.8±1.8%	2.8	0.35±0.02	4.51±0.50
S-3.6b		80	n/a	37.6±0.0%	43.4±0.0%	19.0±0.0%	2.3	0.36±0.01	4.07±0.75
S-3.7		60	30	14.5±0.5%	72.9±0.3%	12.6±0.3%	5.8	0.28±0.01	4.38±0.61
S-3.8		60	0	44.6±0.8%	34.8±4.9%	20.6±4.6%	1.7	0.40±0.02	n/a
S-3.9		60	n/a	49.4±0.2%	34.0±0.2%	16.7±0.4%	2.0	0.41±0.04	broke

*Carbonized fibers have similar sample ID corresponding to stabilized fibers (i.e., - carbonized fiber of S-3.3 will be C-3.3).

Figure 3.9 shows the trend between the tensile strengths of the stabilized fiber (Figure 3.9a) and carbonized fiber (Figure 3.9b) against the ratio Φ_c/Φ_β. It appears that as Φ_c/Φ_β increases, the tensile strength of the stabilized fiber decreases until an apparent limit at around 0.28 GPa. For the carbon fiber, the results show a possible trend indicating higher Φ_c/Φ_β values will result in high strength carbon fibers. However, this result is far from conclusive as there are two data points contradicting this trend.

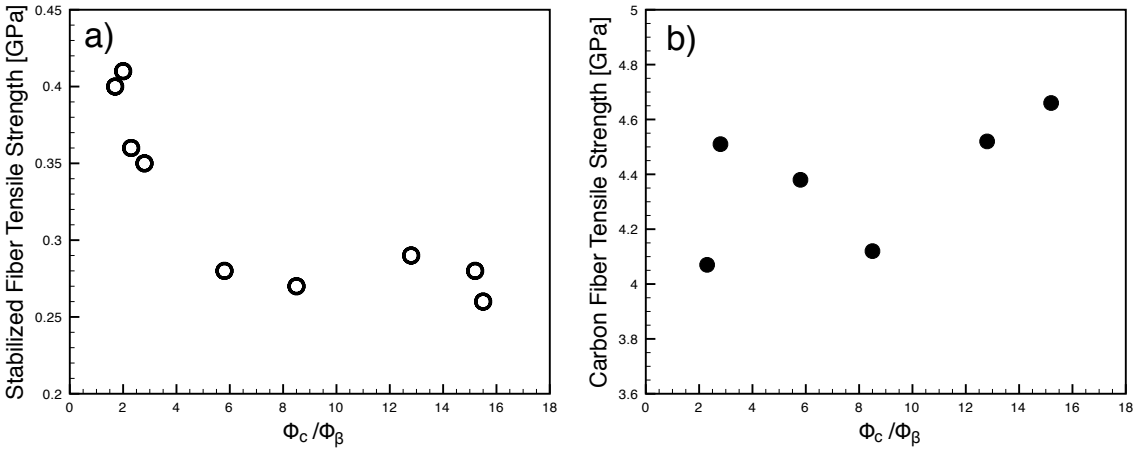

Figure 3.9 Trends of a) stabilized and b) carbonized PAN/CNT sheath-core fiber tensile strengths as a function of Φ_c/Φ_β.

Table 3.8 shows the results from WAXD studies of the stabilized fibers, including a conversion index (AI%)[90], which is defined by Equation 3.3.

$$AI\% = \frac{I_o - I_s}{I_o} \tag{3.3}$$

Where I_o is the normalized intensity of the $2\theta = 17°$ peak in the precursor fiber and I_s is the same in the stabilized fiber. The crystal size and orientation of both PAN and ladder structures are also reported.

The results of M_{cyc} agree well with the experimental data from FTIR (% of unreacted nitrile) as well as WAXD (conversion index; Equation 3.3). Since M_{cyc} is a measure of

the un-cyclized nitrile structure (based on the DSC kinetics data), it should show a linear relationship with the unreacted nitrile results obtained from FTIR. Similarly, the WAXD conversion index should continually increase toward 100% as M_{cyc} tends toward a value of zero. Figure 3.10a confirms the aforementioned trends. Figure 3.10b shows the dependence of carbon fiber tensile strength on unreacted nitrile and extent of reaction (M_{cyc}). Using a 2nd order polynomial fit of the individual data, the maximum tensile strength is predicted to result at an unreacted nitrile level of 24.3% and 31.4% for FTIR and DSC kinetic methods, respectively. The difference in optimal reaction extent can be explained by the definition of each term. The extent of reaction (M_{cyc}) only considers the cyclization reaction that converts unreacted PAN (Φ_u) to its conjugated form (Φ_c). Therefore, it is defined as: $M_{cyc} = 1 - \Phi_c$. Contrary to this, FTIR directly measures the fraction of unreacted PAN present in a sample, which is defined as $\Phi_u = 1 - (\Phi_c + \Phi_\beta)$. As a result, the fraction of unreacted PAN as determined from FTIR analysis will always be less than that obtained by M_{cyc}.

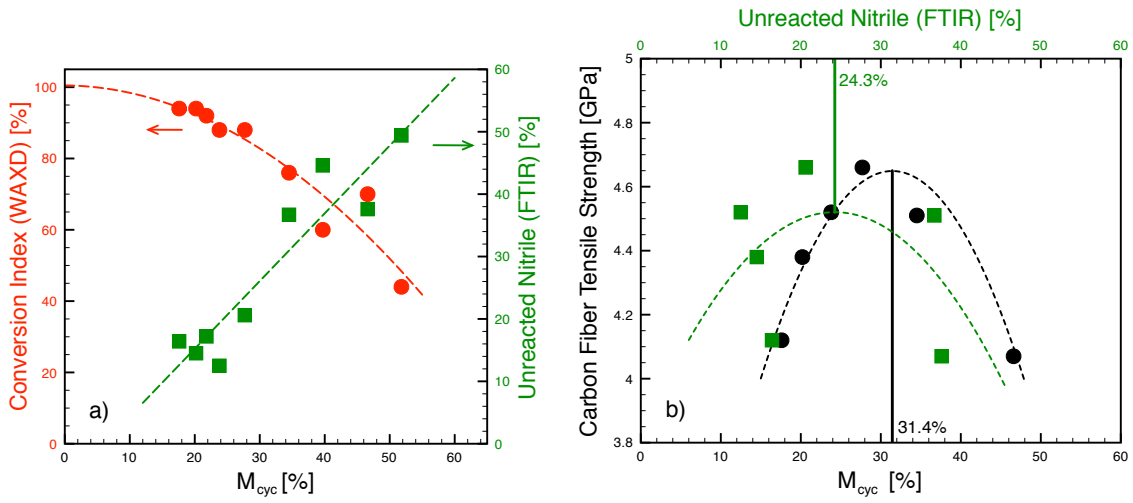

Figure 3.10 The dependence of M_{cyc} on a) the WAXD cyclization index and percentage of unreacted nitrile (FTIR) as well as b) carbon fiber tensile strength.

Table 3.8 Structural parameters from WAXD studies of stabilized PAN fibers.

ID	Pre-stress [MPa]	Stabilization Time [min]		M_{cyc}* [%]	AI%† (XRD)	f_{PAN}‡	f_{ladder}#	$L_{26°}$&	Stab. Fiber Tensile Strength [GPa]	Stab. Fiber Tensile Modulus [GPa]	Carb. Fiber Tensile Strength** [GPa]
		260°C	305°C								
S-3.1	30	140	0	21.8	92%	-	0.655	1.14	0.26±0.01	10.3±0.3	n/a
S-3.2		110	0	27.7	88%	-	0.636	1.03	0.28±0.01	10.4±0.2	4.66±0.73
S-3.3		100	10	23.8	88%	-	0.653	1.11	0.29±0.01	10.6±0.1	4.52±1.14
S-3.4		80	30	17.6	94%	-	0.649	1.16	0.27±0.02	10.3±0.1	4.12±0.59
S-3.5		80	0	34.5	76%	0.603	0.640	1.00	0.35±0.02	11.7±0.1	4.51±0.50
S-3.6b		80	n/a	46.6	70%	0.565	0.667	1.03	0.36±0.01	11.4±0.2	4.07±0.75
S-3.7		60	30	20.2	94%	-	0.655	1.12	0.28±0.01	10.4±0.2	4.38±0.61
S-3.8		60	0	39.7	60%	0.537	0.664	0.97	0.40±0.02	12.0±0.2	n/a
S-3.9		60	n/a	51.8	44%	0.634	0.689	0.94	0.41±0.04	12.3±0.2	broke

*Extent of cyclization as defined in Section 3.2.2.1 and Appendix B. †Conversion index from WAXD data as defined in Equation 3.3 ‡Unreacted PAN orientation in the stabilized fiber from Herman's orientation parameter of 17° peak. #Ladder structure orientation in the stabilized fiber from Herman's orientation parameter of ~26° peak. &Crystal size from Scherrer's equation of ladder structure. **Carbonized fibers have similar sample ID corresponding to stabilized fibers (i.e., - carbonized fiber of S-3.3 will be C-3.3)

Plotting the stabilization index from WAXD and orientation of the ladder structure as a function of stabilization time has been reported as a method for determining the optimal stabilization conditions. The previous study observed a peak in ladder orientation at a specific stabilization time and assigned it to be the optimal. The study attributed the sudden decrease in ladder orientation to degradation occurring due to over-stabilization.[91] If stabilization time is replaced by M_{cyc}, a similar plot is created (Figure 3.11a), but with very different trends. In the current study, no such peak was observed and ladder orientation is confirmed through tensile modulus measurements of the stabilized fiber (Figure 3.11b); as the tensile modulus of the stabilized fiber decreases, so does the orientation for PAN and ladder structure. The stabilization conditions that created the most disoriented ladder structure ($f_{ladder} = 0.636$) resulted in the highest tensile strength carbon fiber (4.66 GPa). This observation was not expected.

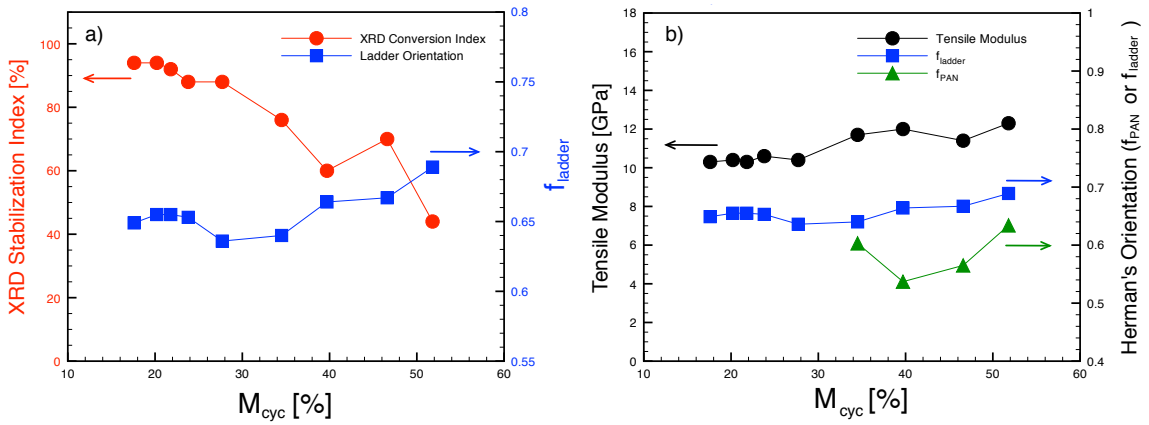

Figure 3.11 a) Stabilization index (AI%) and ladder orientation (Herman's orientation parameter) as a function of M_{cyc} and b) decrease in tensile modulus of stabilized fiber corresponding to a decrease in both PAN and ladder structure orientations.

If the structural properties of the stabilized fiber are investigated further, it can be concluded that the orientation of the ladder structure has a more dramatic impact on the tensile modulus when compared to the PAN orientation (Figure 3.12). This trend is not

only present in the stabilized fibers (Figure 3.12a) but is also maintained in the resulting carbon fiber as well (Figure 3.12b). In Figure 3.12b, there were not sufficient data points to plot the orientation of the PAN against the carbon fiber modulus, yet a similar trend as in Figure 3.12a is expected.

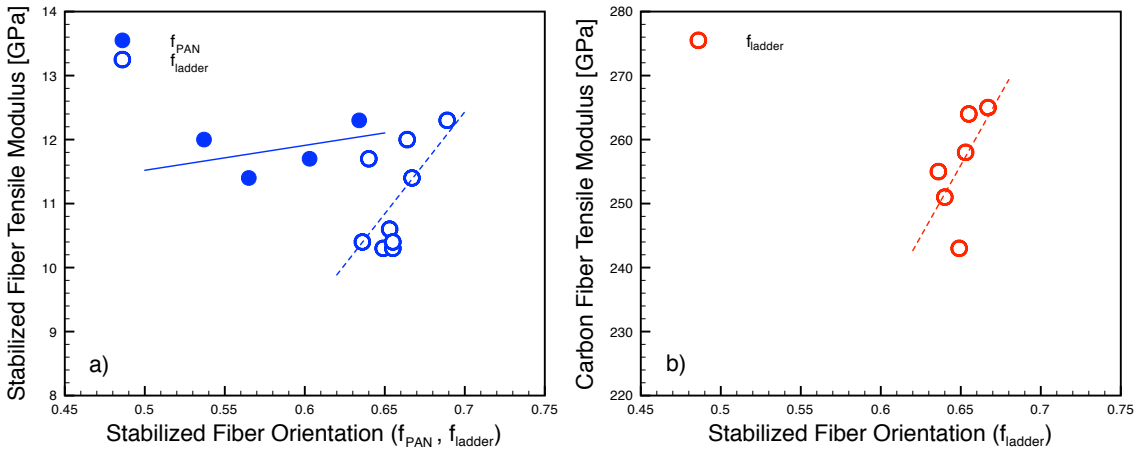

Figure 3.12 The effect of stabilized fiber orientation (PAN and ladder structure) on the a) stabilized fiber tensile modulus and b) carbonized fiber tensile modulus.

3.3.2.3 Stabilized Fiber Surface Morphologies

The surface SEM images of the stabilized fibers exhibited an interesting morphology. Under-stabilized fibers appear to have patchy/grainy regions on their surface, while well-stabilized fibers do not have these signatures. Figure 3.13a shows the surface of a stabilized fiber with, presumably, well-stabilized conditions (resulted in highest tensile strength: 4.66 GPa). Figure 3.13b-d shows the progression of stabilized fiber surface images for the 60 min, 60 min/0 min, and 60 min/30 min samples respectively. It is interesting to note that these grainy regions seem to disappear as stabilization progresses. While these features are not present in the last set of images (Figure 3.13d), the fiber exhibits many surface defects. These defects may have developed as a result of local overheating due to rapid reactions occurring in a fiber that has not been fully stabilized.

Higher magnification images along with energy dispersive X-ray spectroscopy (EDS) results of the grainy regions can be found in Appendix C.

These surface images indicate that there is an optimal structure that is required prior to the cross-linking reaction, which initiates at ~305°C (Figure 3.1). Therefore, the extent of reaction (M_{cyc}) may best be used separately for each stage of stabilization to find the optimal overall conditions. However, further analysis on fibers that have undergone partial stabilization (i.e., - collect fiber after t_1 and before elevating to T_2) needs to be collected before definitive conclusions can be made.

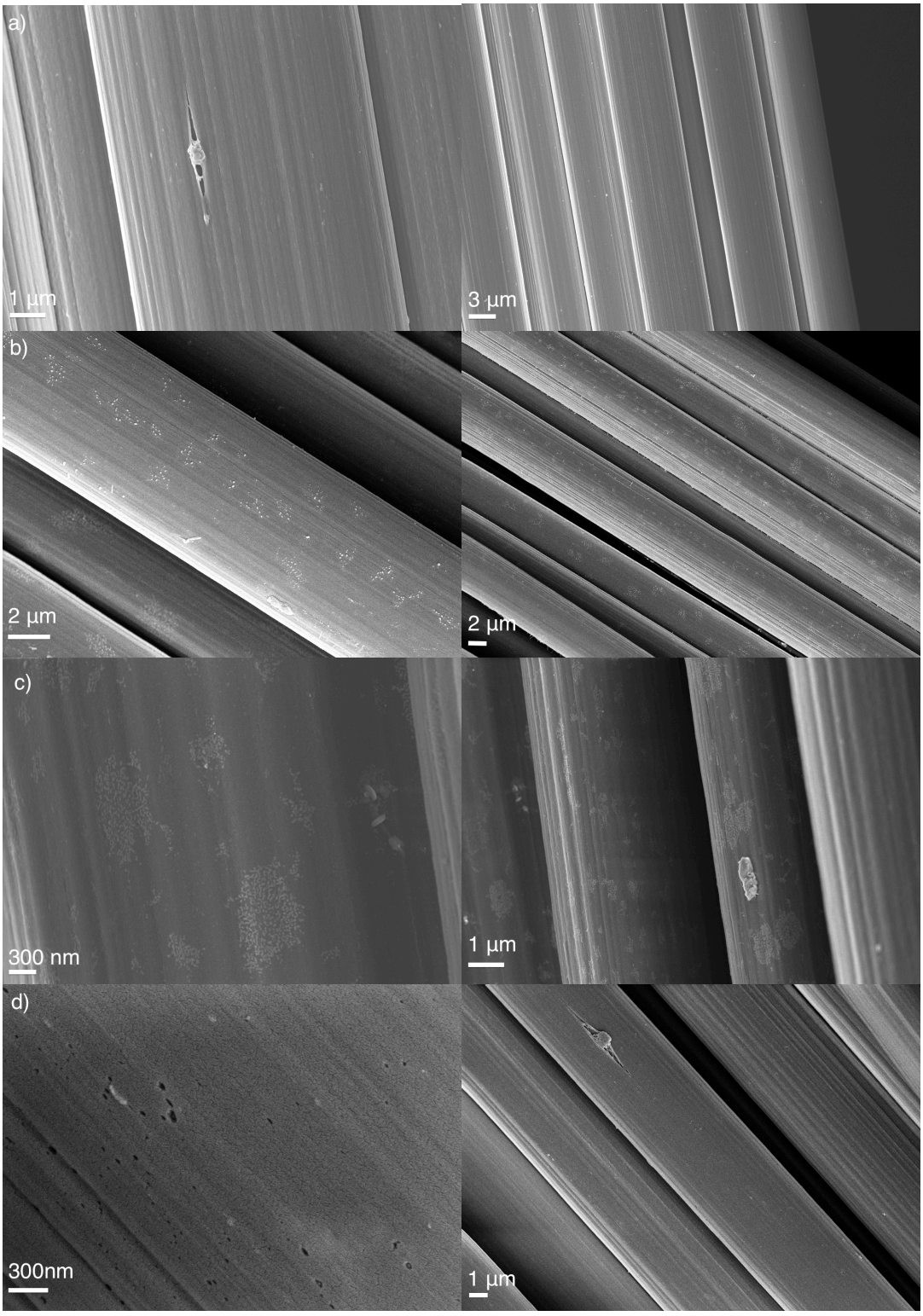

Figure 3.13 Surface morphologies of a) well-stabilized fiber (S-3.2: 110/0min) and under-stabilized fibers b) S-3.9: 60min c) S-3.8: 60/0min and d) S-3.7: 60/30min indicating a possible signature of under-stabilized fibers.

3.3.3 Carbon Fiber Structure and Properties

The carbon fiber properties and structural parameters are presented in Table 3.9 and are compared to two industrial carbon fibers (T300 and IM7). It is well known that as the orientation of the crystallites increase, there will be a corresponding increase in the tensile modulus of the fiber.[92,93,94] It is also intuitive that as the structure becomes more graphitic (as happens with increased carbonization temperature), the modulus will also increase.[95] The behavior of tensile strength is more complicated due to its strong dependence on the defect structure.

The batch carbonized fibers of Fiber A have resulted in tensile strength values that are again lower than the previous trials (Table 3.2 and Table 3.3), but this can be explained by the fact that the pre-stress value for the current fibers has been held constant at 30 MPa (vs. 34.7 MPa and 33.2 MPa for Table 3.2 and 3.3 respectively). The trend between tensile modulus and Herman's orientation parameter remains in the batch carbonized fibers. A clear trend does not exist between the mechanical properties of the batch carbonized fibers and the crystallite size dimensions. However, It is interesting to note that the crystallite dimension perpendicular to the fiber axis ($L_{c,002}$) is the largest in the case of C-2.6a where the fiber may have experienced increased stress during carbonization (see Table 3.9 footnote) resulting in higher orientation. This behavior has been previously suggested.[96]

Table 3.9 Mechanical properties and structural parameters of commercial and PAN/CNT-based* carbon fibers.

ID	Stabilization Time [min]		Tensile Strength† [GPa]	Tensile Modulus† [GPa]	Strain to Failure† [%]	Diameter‡ [μm]	Weibull Mod.	f_c	L_c [nm]	L_a [nm]	d_{002} [nm]
	260°C	305°C									
T300	**-**		**3.81±0.54**	**168±5**	**2.36±0.29**	**6.83±0.18**	**7.2**	**0.779**	**1.44**	**1.91**	**0.348**
IM7	**-**		**6.54±1.09**	**209±27**	**3.38±1.22**	**4.98±0.22**	**6.3**	**0.828**	**1.60**	**2.11**	**0.348**
C-3.2	110	0	4.66±0.73	255±13	1.83±0.33	3.82±0.12	5.2	0.777	1.33	2.34	0.352
C-3.3	100	10	4.52±1.14	258±17	1.86±0.42	3.46±0.10	4.2	0.779	1.32	2.31	0.354
C-3.4	80	30	4.12±0.59	243±14	1.78±0.26	3.58±0.10	7.4	0.770	1.32	2.31	0.354
C-3.5	80	0	4.51±0.50	251±13	1.89±0.20	3.57±0.10	9.7	0.776	1.35	2.16	0.351
C-3.6b	80	n/a	4.07±0.75	265±11	1.58±0.34	3.82±0.17	6.6	0.796	1.34	2.24	0.351
C-3.7	60	30	4.38±0.61	264±20	1.70±0.19	3.42±0.21	7.7	0.780	1.32	2.29	0.354
C-3.6a#	***80***	***n/a***	***5.34±0.73***	***271±20***	***2.13±0.34***	***3.71±0.13***	***8.0***	***0.801***	***1.40***	***2.23***	***0.350***

* The carbonization temperature for PAN/CNT-based carbon fiber was 1300 ^{o}C and pre-stress was held constant at 30 MPa.
† Tensile testing was done using Favimat tensile tester at 6 mm gauge length. For commercial carbon fibers, tensile properties for at 6 mm gauge length are reported from Section 2.3.3.2. Despite low reported modulus values for T300/IM7 (T300: 230 GPa expected; IM7: 276 GPa expected), Section 2.3.3.2 has confirmed accurate modulus determination will be achieved after compliance correction.
‡Diameter of carbon fibers determined from vibroscope linear density measurement at 25.4 mm gauge length assuming 1.7 g/cm^3 for sheath-core fibers and the industrially reported densities for T300 and IM7.
#After batch carbonization, several filaments were found broken, suggesting that the unbroken filaments may experience higher tension

3.4 Conclusions

Sheath/core bi-component spinning was performed to create small diameter PAN/CNT precursor fibers. These precursors have been stabilized under various conditions and subsequently carbonized at 1300 °C. Stabilization kinetics show the activation energy of the cross-linking reaction in the Fiber A precursor is much lower than expected. When the pre-stress values were 34.7 MPa, 33.2 MPa, and 30.0 MPa, the best carbon fibers produced were 5.42 GPa, 4.82 GPa, and 4.66 GPa respectively. The conclusions from FTIR and XRD characterizations validate M_{cyc} from the DSC kinetics study as a method to quantify the extent of reaction through the heat treatment of PAN precursor fibers. The combined results from FTIR and M_{cyc} indicate that the optimal extent of reaction occurs when the percentage of unreacted nitrile groups is between 24% and 34%. The effect of orientation on the tensile modulus in carbon fibers has been confirmed. Preliminary results also indicate that increased stress during carbonization may increase $L_{c,002}$.

CHAPTER 4
CARBONIZATION OF PAN/CNT ISLAND FIBERS

4.1 Introduction

In an effort to achieve improved mechanical properties of polymeric fibers, a number of groups have demonstrated the use of polymer/CNT composite materials as one way to achieve this goal. However, another fundamental improvement that can be targeted is reducing the diameter of the fibers. There have been a number of studies that have shown an increase in tensile strength with a decrease in fiber diameter (e.g., - glass[97], polypropylene[98], poly(ε-caprolactone)[99]). It is generally accepted that smaller diameter fibers have fewer defects/imperfections in a given cross-sectional area, resulting in high tensile strength. In the case where processing conditions are held constant, it has also been shown that tensile properties of the PAN precursor (and as a result, the carbon fiber) are strongly dependent on the fiber diameter.[93,100,101,102] It is well known that solvent/non-solvent exchange occurs during PAN precursor fiber processing, and by-product gases evolve during stabilization and carbonization. The benefit of having small diameter fibers is to reduce the path-length of solvent/non-solvent diffusion and gas removal in these processes, resulting in a structure with fewer defects (e.g., - voids). Therefore, one can expect higher tensile strength in small diameter fibers.

The carbon fiber tensile strength dependence on diameter has been experimentally observed in PAN/CNT composite fibers.[56] The current study continues the small diameter PAN/CNT work by carbonizing islands-in-sea fibers and investigating their mechanical properties through both bundle and single filament testing methods.

4.2 Experimental

4.2.1 Materials

The polymer used in this study for the islands is a 240 kg/mol PAN-co-MAA (4% MAA by weight) obtained from Japan Exlan Company. The carbon nanotubes (CNTs) used were obtained from Continental Carbon Nanotechnologies Inc. (CCNI) (Lot No. XO122UA, catalytic impurity – 1 wt%). A 350 kg/mol poly(methyl methacrylate) (PMMA) polymer was used as the sea component. The solvent was dimethylacetamide (DMAc) for both the PAN and PMMA solutions as well as for CNT dispersion.

4.2.2 Solution Preparation and Fiber Spinning

For island component, a PAN/CNT composite solution was prepared. PAN was dissolved in DMF at a concentration of 14.5 g/100 mL, and CNT/DMF dispersion was prepared separately at a concentration of 15 mg/300 mL by 24 hr bath sonication. The sonicated CNT dispersion was added to the PAN solution and excess DMF was removed by vacuum distillation. For vacuum distillation, the oil bath temperature was maintained at 90 °C. The addition of CNT dispersion was repeated until the CNT concentration reached 1 wt% with respect to the weight of the polymer (i.e. total amount of added CNT was 150 mg). The final solid concentration (polymer+CNT) was 15 g/100 mL. For the sea component, PMMA (350 kg/mol) was prepared at a concentration of 30 g/100 mL DMAc.

Islands-in-a-sea bi-component fiber spinning was done on a single-hole spinning system with a 37-islands geometry. Figure 4.1 shows a schematic of the islands-in-a-sea fiber. The spinneret diameter was 250 μm and the temperature was maintained at 100 °C. During spinning, the linear jetting speed of the solution from the spinneret was ~40

m/min and the solution was spun into a gelation bath (100% methanol) which was maintained at about -50°C. After passing through the gelation bath, the fibers were taken up at a speed of 120 m/min for a spin draw ratio (SDR) of 3. After spinning was completed, the as-spun fiber was subjected to additional drawing in air (cold draw ratio: CDR = 1.42) and in a hot glycerol bath at 170°C (hot draw ratio: HDR = 7.6) for a total draw ratio (TDR) of 32.4. The sea component (PMMA) remained after the drawing process, but will be removed after the thermal treatment steps.

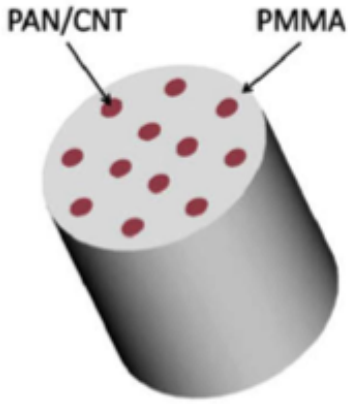

Figure 4.1 Schematic of islands-in-a-sea bi-component fiber (37 islands were used instead of 12 as shown in the figure).[56]

4.2.3 Stabilization and Carbonization

Stabilization and carbonization of PAN precursor fibers were conducted in a tube furnace (MHI Inc.) by hanging the precursor fiber on a graphite platform. A two-stage stabilization was employed for these studies where the dwell times (t_1 and t_2) were varied at the temperature set points (T_1 and T_2). The first stage temperature was held constant at 240ºC and the second was held at 295ºC. Stabilization was performed in an air environment and the flow of air was controlled at 5 L/min. After completion of stabilization, the tube furnace was purged with Argon gas for 30 min, followed by

heating the furnace to 1300 °C at a rate of 5 ºC/min and holding for 5 min while maintaining an inert atmosphere.

4.2.4 Characterization

Structural parameters of the precursor and carbon fibers were determined from WAXD patterns. The patterns were collected by Rigaku micromax-002 (CuK_α radiation) using a Rigaku R-axis IV++ detector. The collected 2D patterns were analyzed using Area Max v2 and peak fitting was performed using JADE 9.1.5. Additionally, the orientation of the CNTs in the precursor fiber was determined from Raman spectra.

The tensile testing for the carbonized islands fibers were conducted using two different testing methods (bundle test and single filament test). For bundle testing, fiber bundles were mounted on paper templates using glue. Tensile tests were conducted on the RSA III solids analyzer (Rheometric Scientific Co.) at a gauge length of 6 mm and a testing speed of 0.006 mm/s (strain rate of 0.1 %/s). Bundle size varied from 222 to 407 island filaments (islands fiber contains 37 filaments) depending on the sample preparation. Mechanical property data was corrected based on the cross-sectional images obtained by scanning electron microscopy (Zeiss Ultra 60 FE-SEM). To ensure accurate measurement, SEM images were collected perpendicular to the fiber axis. The cross-sectional area of the fibers was determined using image analysis software (ImageJ, NIH) for effective fiber diameter calculation. For single filament testing, samples were sent to University of Illinois – Urbana-Champaign (UIUC) for testing on a microelectromechanical system (MEMS) as shown in Figure 4.2. Single filaments were tested at gauge lengths of either 50 μm or 100 μm. Individual filaments were separated

from the bundle using a micro-manipulator and secured on MEMS device by platinum deposition[103]

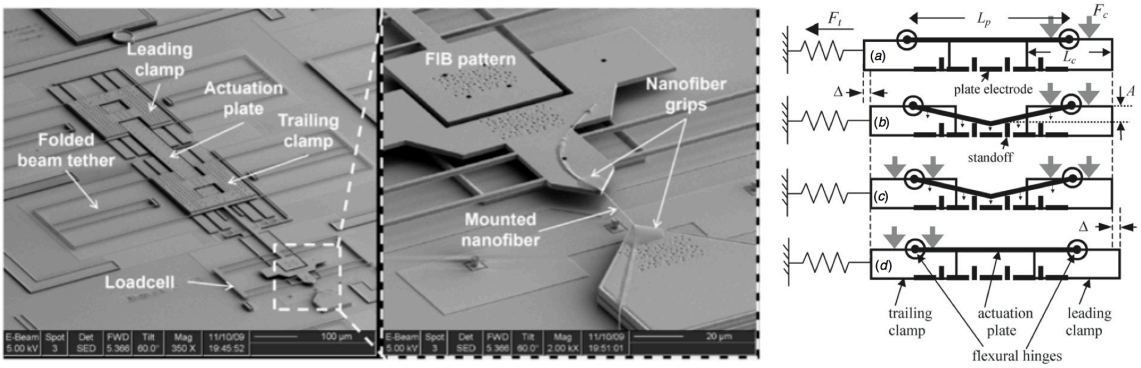

Figure 4.2 SEM image of MEMS device used for small diameter single filament tensile tests with schematic of operation.[104]

4.3 Results and discussion

4.3.1 Island Precursor Fibers: Structural Parameters

The structural parameters of the precursor fiber (Table 4.1) indicate a slightly lower crystallinity than is typically seen in gel spun PAN precursors (~65%) while the crystal size is normal. The orientation of the PAN (0.89) is lower than expected considering it is a small-diameter fiber (smaller capillary induces higher shear forces leading to higher orientation). Single component large diameter fibers routinely exhibit orientation parameters of 0.90 and higher.

Table 4.1 Structural parameters of islands-in-sea precursor fiber from WAXD pattern.

	Islands Precursor Fiber
Crystallinity (%)*	56
$d_{2\theta\sim17^\circ}$ (Å)†	5.279
Crystal Size (nm)‡	13.6
f_{PAN}#	0.89
f_{CNT}**	0.90

*Determined from area fraction of peak fitting result of integrated scan. †Determined from Bragg equation. ‡Scherrer equation (K=0.9) from the (110) plane #Azimuthal scan of 2θ~17°; (110),(200) **Curve fitting of Raman G-band as a function of polarization angle [82,83]

4.3.2 Island Carbon Fibers: Structure and Morphology

The resulting carbon fiber exhibits structural parameters similar to typical carbon fibers. The stacking height of (002) plane (L_c = 1.58 nm) is larger than any of the sheath-core fibers (Chapter 3; Table 3.9).

Table 4.2 Structural parameters of islands-in-sea carbon fiber from WAXD pattern.

	INS 1.5
$d_{(002)}$ (Å)*	3.52
$L_{c_{(002)}}$ (nm)†	1.58
$L_{a_{(10)}}$ (nm)†	2.38
f_{matrix}‡	0.79

*Determined from Bragg equation. † Scherrer equation (K=0.9) for respective crystal plane. For (002) and (10) plane crystal size calculation, equatorial and meridional scans were used, respectively. ‡Azimuthal scan of 2θ~25°; (002)

The cross-sectional SEM images of the island fibers (Figure 4.3) exhibited irregular cross-sectional shapes. Cross sectional area was measured for a number of single filaments and the average effective diameter was determined to be 0.97 μm. The fibrils throughout the cross section appear to have a tight fibril-to-fibril diameter distribution and uniform throughout the cross-section.

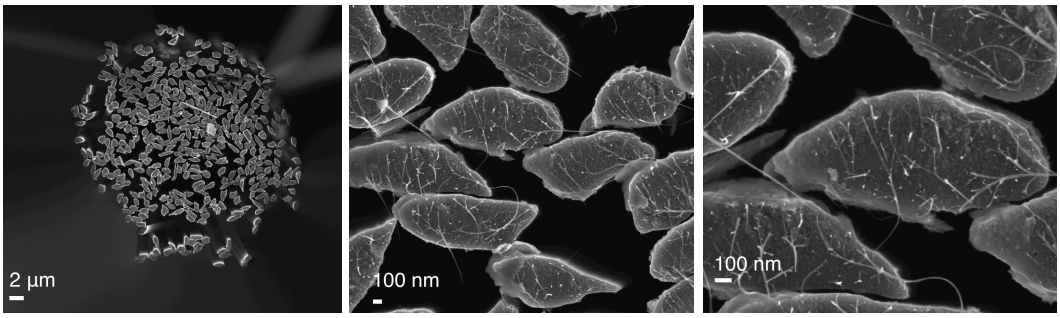

Figure 4.3 SEM images of the carbonized island fiber cross-sections showing irregular shapes with well-dispersed fibrils.

4.3.3 Carbon Fiber Properties

4.3.3.1 Bundle Test (RSA III)

Islands-in-a-sea (INS) fibers were carbonized under the conditions listed in Table 4.3 (page 92). The stabilization temperatures were determined through differential scanning calorimetry (DSC) run in an air atmosphere. The first set of trials (INS 1.x) resulted in a tensile strength as high as 3.2 ± 0.1 GPa. The second set of trials (INS 2.x) was conducted at a different time but under nearly identical processing conditions and yielded a tensile strength value of 2.3 ± 0.1 GPa. Previous studies have shown that the mechanical properties of the PAN precursor fiber significantly changed over a 14-month period due to molecular relaxation. Specifically, the aged fibers showed a 25% and 21% reduction in the tensile strength and modulus respectively; the modulus observations were supported through WAXD results.[84] The two sets of INS trials were separated by 7 months, which may be the reason for the differences in carbon fiber properties.

It should also be noted that the tensile modulus (under identical processing conditions) changes significantly (166 – 214 GPa). This points to the fact that the precursor fiber may not be as uniform as is typically achieved through our spinning process (diameter variation, island discontinuity, etc). The precursor fiber used in INS 2.3

was subjected to a nitromethane treatment, which removed the PMMA prior to stabilization. The stabilization reactions are diffusion limited; therefore, the optimal times for stabilization depend on the fiber diameter.

Table 4.3 Stabilization/carbonization conditions and tensile properties of the carbonized island fiber bundles.

	Pre-stress [MPa]	Stabilization Time [min]		Carbonization		Tensile Strength [GPa]	Tensile Modulus [GPa]	Strain to Failure [%]	UIUC Sample No.
				Temp	Time				
		240°C	295°C	[°C]	[min]				
INS 1.1	20.3	45	10	1500	5	1.3±0.1	175±29	0.80±0.45	
INS 1.2		40	10	1300		2.6±0.1	172±16	1.80±0.97	
INS 1.3		40	7.5			2.5±0.1	178±19	1.53±0.49	
INS 1.4		40	5			3.2±0.1	201±23	1.80±0.65	#3
INS 1.5		40	5			2.7±0.1	181±23	1.83±0.65	
INS 1.6		40	5			3.2±0.3	214±29	1.36±0.65	
INS 2.1	27.4	40	5	1300	5	2.3±0.3	180±28	1.42±0.32	#1
INS 2.2	23.8	40	5			2.1±0.2	166±8	1.36±0.16	
INS 2.3	23.8	40	5			1.2±0.4*	182±11	0.63±0.22	
INS 2.4	20.8	40	5			2.3±0.1	187±8	1.29±0.05	#2

*Sea component (PMMA) was removed by soaking fiber in nitromethane for about 5 min before stabilization and carbonization.

Since the previous trials were optimized based on the complete INS fiber (including sea component – PMMA), these conditions are not suitable when stabilizing the islands component only. As a result, stabilizing the islands fiber only (PMMA removed) under the INS conditions (e.g., - INS 2.3) will result in over-stabilization. This behavior is supported through the observed mechanical properties, which are significantly reduced in the case of INS 2.3.

4.3.3.2 Single Filament Tests (MEMS – UIUC)

The results from bundle tests and single filament tests conducted on the MEMS device at UIUC are listed in Table 4.4.

Table 4.4 Single filament tensile testing results for the carbonized islands fibers by MEMS device and comparison with the bundle testing results using RSA III. The gauge length for MEMS device was 50 or 100 μm and that for RSAIII tensile tester was 6 mm.

	Bundle tests*			MEMS single filament tests†		
ID	Tensile strength [GPa]	Tensile modulus [GPa]	ID	Number of specimens Tested	Tensile strength [GPa]	Tensile modulus [GPa]
INS 2.1	2.32±0.25	180±28	UIUC#1	21	3.41±0.96	224±47
INS 2.4	2.28±0.13	187±8	UIUC#2	3	4.05±0.56	273±60
INS 1.4	3.24±0.10	201±23	UIUC#3	15	4.23±1.28	249±38

*Bundle tests were conducted at 6 mm gauge length. †MEMS single filaments tests were tested at either 50 or 100 μm.

Figure 4.4a shows the relationship between the tensile strength of the single filaments and the filament diameter across all samples. The maximum strength of these single filaments approaches 8 GPa as the diameter is reduced to < 1 μm. There are exceptions to this trend that are usually explained by observing features (e.g., - visible defects, irregular shapes) from the fractured surfaces (Figure 4.4b). The optimal stabilization conditions (Table 4.3) have yet to be thoroughly investigated. As a result, potential improvement in the properties of INS fiber remains a possibility where tensile strength values of

individual filaments can be greater than 10 GPa. Despite this, single filaments with high mechanical properties and desirable morphology (e.g., - no visible defects, long fibril structure) have been observed in the fractured samples (Figure 4.5a-c).

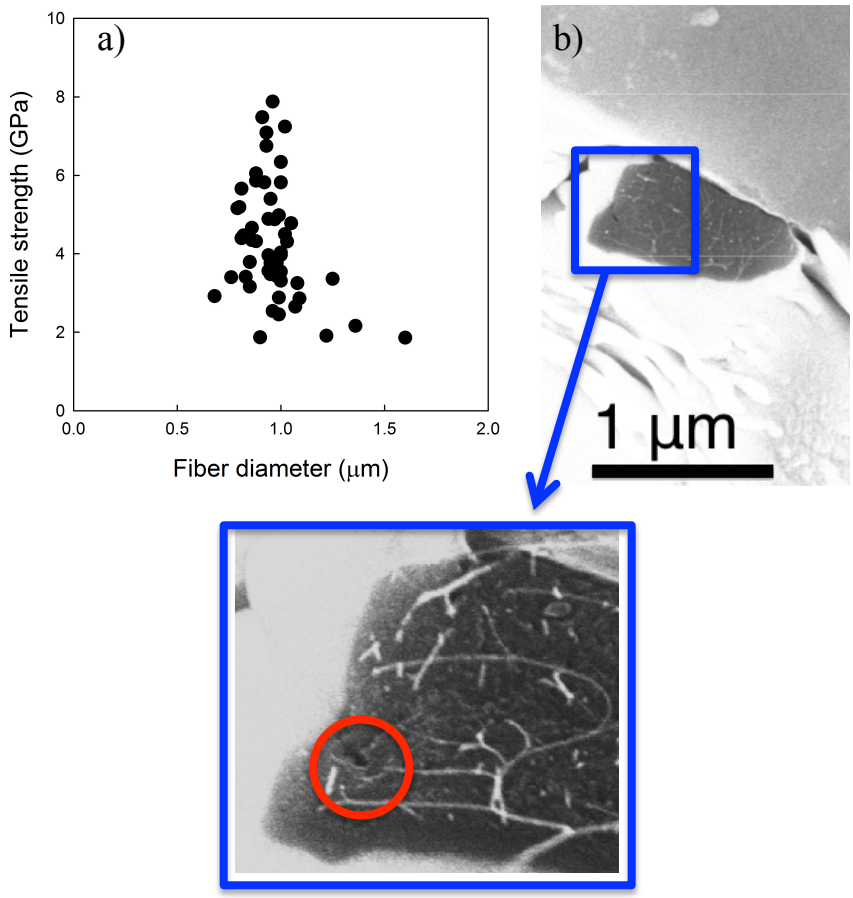

Figure 4.4 a) Single filament tensile strength results as a function of fiber diameter and b) SEM of fractured cross section showing visible defect.[103]

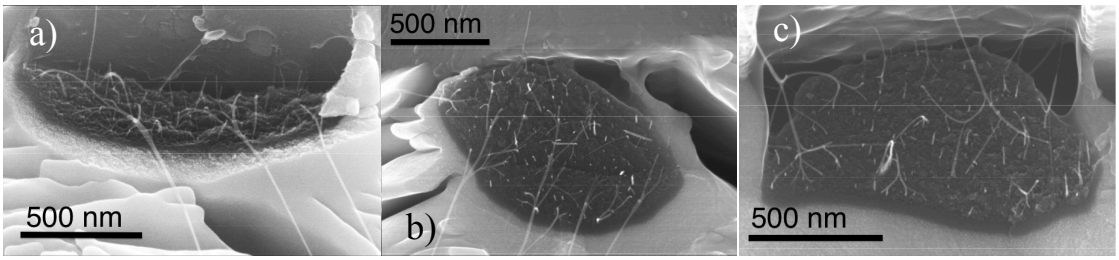

Figure 4.5 Cross-sectional SEM images showing morphology of high strength islands fibers (Tensile Strength / Tensile Modulus): a) 5.16 GPa / 247 GPa b) 5.56 GPa / 285 GPa c) 7.70 GPa / 277 GPa.[103]

The single filament mechanical properties resulted in higher tensile strength and modulus when compared to the bundle-tested samples. Since tensile strength of brittle materials (e.g., - carbon fibers) is highly dependent on the defect structure, there is a strong dependence between the tensile strength of the material and the gauge length at which the tests were performed. At shorter gauge lengths, there is a lower probability for critical defects to be present which results in higher observed tensile strength. Therefore, the difference in tensile strength values can be due to the fact that the MEMS tests were conducted at gauge lengths of 50 or 100 μm and the bundle tests were conducted at 6 mm.

The difference in tensile modulus values can be explained by noting that neither set of tensile modulus values were corrected for compliance; the differences in test procedure likely explains the discrepancy in tensile moduli. In the MEMS tested samples, a single filament was attached directly to the MEMS device through platinum deposition. For bundle tests, the samples were fixed to a paper tab using Loctite super glue, which will have more compliance when compared to the platinum deposition method. Another possible reason would be the non-uniform loading in the case of bundle tests due to insufficient impregnation of glue. Since the area used in the tensile calculations is based on the entire tow, if a small fraction of the tow is not experiencing the force, or has fractured during processing, then the reported modulus values will be lower.

4.4 Conclusions

Islands-in-a-sea bi-component PAN precursor fibers have been processed and subsequently carbonized to make small diameter carbon fibers. The mechanical properties of the fibers were measured using both strand testing and single filament

testing methods. The single filament testing showed tensile strength and modulus as high as 7.7 GPa and 333 GPa, respectively. Further processing optimization may improve the tensile properties.

CHAPTER 5
CONCLUSIONS AND RECOMMENDATIONS

5.1 Conclusions

1. The testing parameters for both precursor and carbon fibers have been investigated. For ensuring an accurate linear density measurement the assumed linear density of the material should be between ~73% and ~170% of the actual linear density. The acceptable pre-stress rage of precursor and carbon fibers was 0.4 – 1.6 cN/tex and 1.30 – 1.35 cN/tex, respectively. The narrow range in the case of carbon fibers implies that accurate determination of filament diameter prior to testing should be a priority. The modulus compliance correction has been verified for different materials (control/composite precursors and carbon fibers) as well as for different testing instruments (Favimat and RSA III).
2. The Weibull modulus has been calculated for three industrial carbon fibers (T300, T650, IM7) at a number of different gauge lengths. The Weibull modulus depends on the analysis method chosen (linear regression (LR) or maximum likelihood estimation (MLE)). For T300, LR showed a decreasing Weibull modulus with decreasing gauge length; this trend was eliminated with the MLE analysis method. For T650, neither LR nor MLE methods yielded a trend with gauge length. The results of IM7 showed an increasing Weibull modulus with decreasing gauge length regardless of analysis method. Further testing should be conducted to confirm this trend.
3. Sheath-core fibers were spun using a geometry that creates a small diameter PAN/CNT fiber surrounded by a PMMA sheath. Precursor fibers were

successfully spun at a diameter of approximately 7 μm. These precursor fibers were batch carbonized to obtain small diameter (~3.5 μm) carbon fibers. The highest average tensile strength and modulus achieved was 5.4 GPa and 365 GPa (uncorrected) respectively; after compliance correction the tensile modulus is expected to exceed 400 GPa. The highest mechanical properties of individual filaments were observed to be 6.5 GPa and 392 GPa (uncorrected) for tensile strength and modulus. The effects of stabilization conditions were monitored by FTIR, DSC, and WAXD. The percent of unreacted nitrile in the stabilized fibers yielded the best trends with the resulting carbon fiber tensile strengths.

4. Islands-in-a-sea (INS) composite precursor fibers were made using a unique spinning geometry that resulted in 37 PAN/CNT islands distributed within a PMMA sea. Stabilization and carbonization of the INS fibers were carried out in a batch process and the resulting carbon fibers had an average diameter of ~1 μm. The PMMA was removed during stabilization and carbonization. The INS carbon fibers were tested using traditional methods (bundle test on RSA III) and as single filaments with the aid of a MEMS device. For the bundle tests, between 222 and 407 individual islands were tested at once (depending on the sample preparation). MEMS-based single filament tests were conducted at gauge lengths of either 50 or 100 μm. Bundle tested samples reached maximum values of 3.24 GPa and 201 GPa for tensile strength and modulus respectively. The MEMS single filament tests yielded much higher average mechanical properties: 4.23 GPa and 249 GPa for tensile strength and modulus respectively. The difference between the two test methods can be accounted for by considering the differences in test setup (e.g., -

test gauge length and compliance). The highest single filament tensile strength from the MEMS-based testes was recorded at 7.7 GPa.

5.2 Recommendations for future works

1. Fundamentally, the Weibull modulus should not exhibit any dependence on gauge length. However, a trend with IM7 carbon fiber was observed. The probability of finding a significant defect in IM7 should be significantly less than T300/T650 due to its superior quality. When conducting 50 tests at 1 mm vs 25.4 mm gauge length, the total sampling length is 50 mm and ~1270 mm respectively. Therefore, in a high quality carbon fiber (e.g., - IM7), it is reasonable to assume that a total sampling length of 50 mm is insufficient to quantify the distribution of defects in the material. Testing IM7 at different gauge lengths while maintaining a constant sampling length will resolve the unexpected dependence of Weibull modulus on gauge length.
2. The extent of cyclization (M_{cyc}) has been shown to agree well with experimental evidence (e.g., - FTIR and XRD). Applying this same method to the other reactions taking place during stabilization (i.e., - oxidation and cross-linking) may reveal new trends in terms of interaction effects and/or optimized stabilization conditions.
3. Investigate (through DSC, FTIR, and XRD) the extent of reaction required prior to the second temperature stage. It is believed that a significant fraction of the cross-linking reaction occurs at the second stabilization temperature (T_2). Therefore, it is reasonable to assume there is an optimal structure that is required

prior to subjecting the material to the cross-linking temperatures. Quantifying this through the extent of reaction may prove to be useful.

APPENDIX A: DSC HEATING RATE SCANS FOR FIBER A PRECURSOR

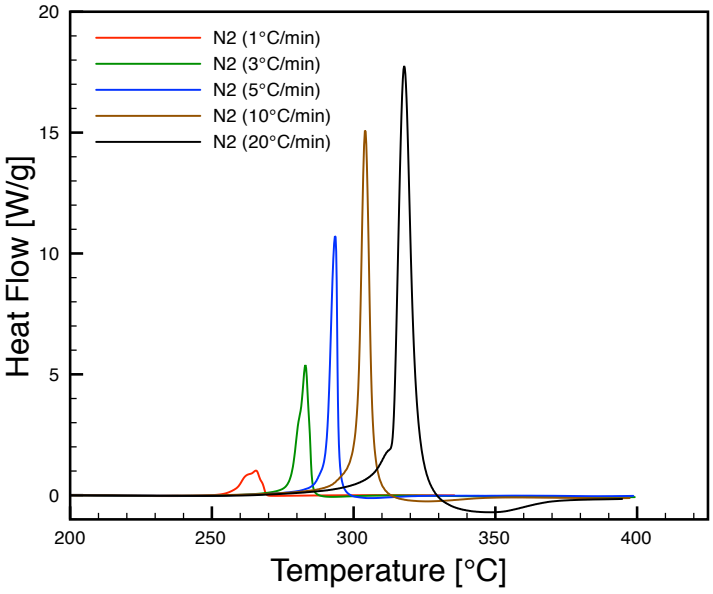

Figure A.1 Fiber A precursor heating rate scans in nitrogen atmosphere.

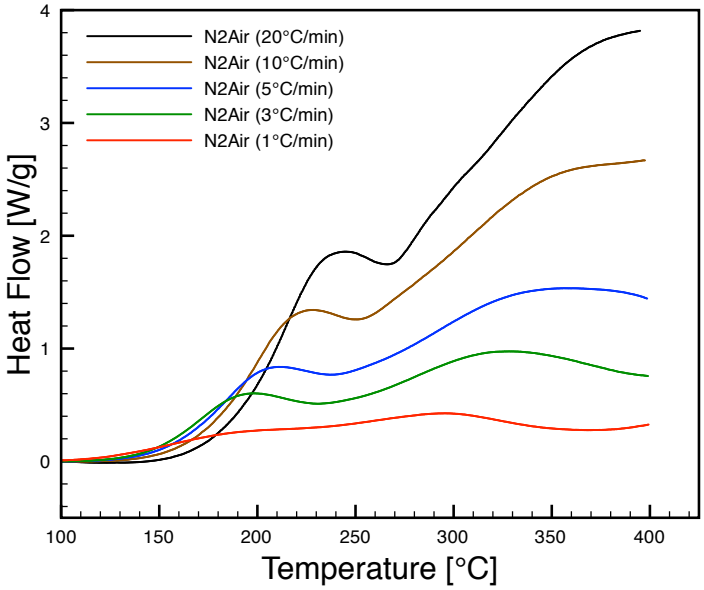

Figure A.2 Fiber A precursor heating rate scans subsequently run in air atmosphere following the scans in nitrogen (Figure A.1).

APPENDIX B: DETAILS OF EXTENT OF REACTION CALCULATION (M_{CYC})

Throughout this section, the variable M refers to the fraction of unreacted nitrile units in a given fiber. Normalizing M to a value of 1at time zero simplifies the analysis (i.e., - $M_{t=0} = 1$). For the case of isothermal kinetics of a first order reaction, the rate of reaction directly proportional to both the remaining reactant (M) and the Arrhenius rate constant (k) (Equation B.1). While M is dependent on time (M(t)) the rate constant remains independent of time in an isothermal process. Solving this simple differential equation yields the result in Equation B.2.

$$\frac{dM}{dt} = -kM(t) \tag{B.1}$$

$$M(t) = e^{-kt} \tag{B.2}$$

Since the processing of polyacrylonitrile (PAN) fibers is not performed under isothermal conditions, this derivation is modified to account for the time-dependent rate constant (Equation B.3); the heating rate (ϕ) is given in units of °C/min.

$$\frac{dM}{dt} = -k(t) \cdot M(t)$$

$$\ln M = -\int k(t)dt = -A\int e^{-\frac{E_a}{R\cdot T(t)}}dt = -A\int e^{-\frac{E_a}{R\cdot\left(\frac{\phi}{60}\cdot t+273.15\right)}}dt$$

$$\ln M = -A\cdot\left(\frac{R(16380+\phi\cdot t)\left(e^{-\frac{60\cdot E_a}{16380\cdot R^2\cdot\phi\cdot t}}\right)+60Ei\left[-\frac{60\cdot E_a}{16380R^2\cdot\phi\cdot t}\right]}{\phi\cdot R}\right) \tag{B.3}$$

Where, Ei is the exponential integral function defined as: $Ei[x] = -\int_{-x}^{\infty}\frac{e^{-t}}{t}dt$

The heating rate (ϕ) was chosen to be 5 °C/min because that is the condition at which stabilization/carbonization trials are conducted. The activation energy (E_a) was taken as the average of the DSC results from the Ozawa and Kissinger methods (Section 3.3.1). The pre-exponential factor (A) is interpreted as the total number of reactant molecular collisions occurring per second in a given system. In principle, this term should also depend on the amount of reactant present in the system and will exhibit exponential decay. For simplicity, the value of A used in the analysis was taken as a constant for each stage of the temperature profile (Figure B.1); where, $A_{Temp} = A_o \cdot e^{-k_{215°C} \cdot t}$. The rate constant ($k_{215°C}$) was chosen based on the initial onset of the DSC exotherm in air at a heating rate of 5 °C/min.

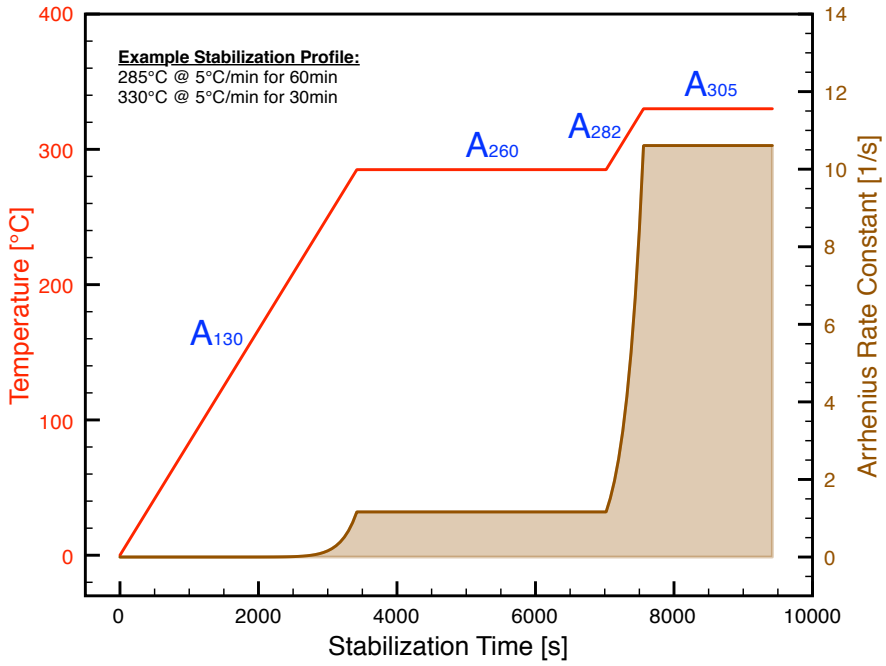

Figure B.1 Schematic of terms used in the derivation of M_{cyc} for a given temperature profile (60min/30min).

APPENDIX C: STABILIZED FIBER MORPHOLOGIES AND CHEMICAL SIGNATURES

Higher magnification images were taken of the patchy/grainy regions of the understabilized sheath-core fibers. These samples were sputter coated with a Gold/Palladium target, which explains the small presence of these elements in the chemical EDS analysis (Table C.1).

The purpose of the EDS analysis was to determine if these particles were a result of the sputter coating process (i.e., - the region results from large Gold/Palladium particles from a malfunctioning sputter coater). The results in Table C.1 indicate this is not the case. The region chosen for the EDS scan has approximately 25% of its area occupied by these particles, yet the quantitative analysis shows just over 3% of Gold and/or Palladium being detected. Furthermore, the chemical mapping did not show strong Au/Pd signals at the location of the particles. These results indicate the particles are a result of the processing and not an artifact of the sputter coating process.

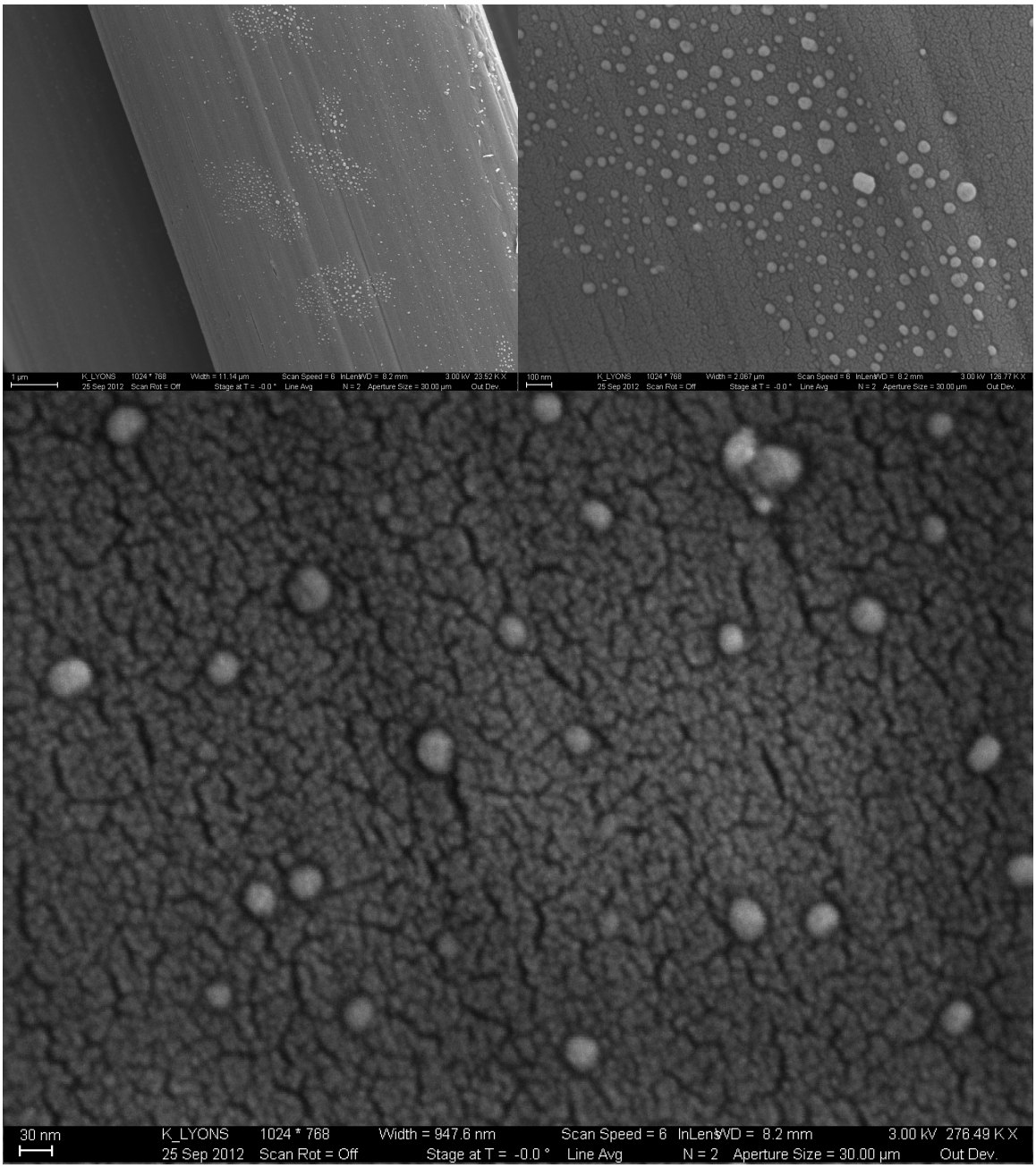

Figure C.1 High magnification images of S-3.9. This particular fiber subjected to 60 min residence time at 260°C without even ramping to the higher temperature (i.e., - 60 min/ na).

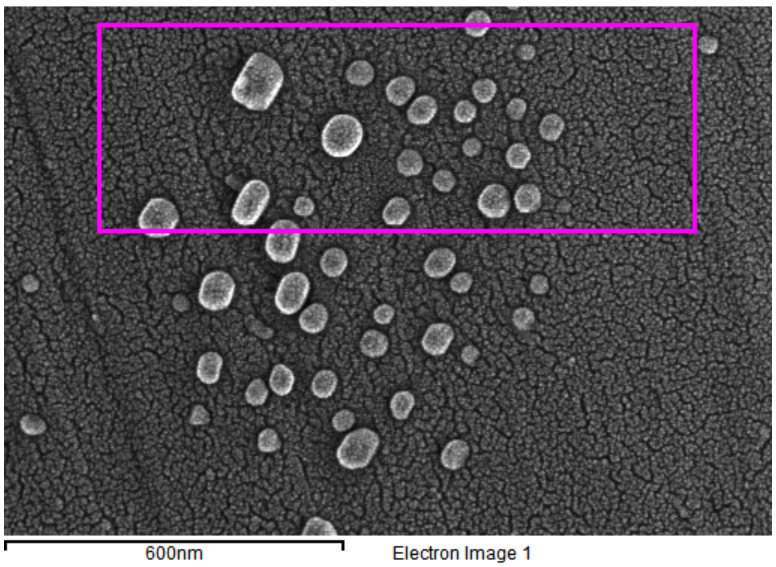

Figure C.2 Scan area of EDS analysis of C-3.9. The element mapping did not show distinct areas corresponding to the observed particles.

Table C.1 Energy dispersive X-ray spectroscopy (EDS) results collected at an accelerating voltage of 15kV.

Element	Weight%
C_K	63.91±1.92
N_K	20.15±2.12
O_K	12.75±0.92
Pd_L	1.49±0.23
Au_M	1.71±0.35
Totals	100.00

APPENDIX D: REACTION KINETIC RESULTS AND PRELIMINARY CARBONIZATIONS OF FIBER B AND FIBER C

Differential scanning calorimetry (DSC) heat rate scans have been performed on three different precursor fibers: 1) Fiber A (250 kg/mol homo-polymer) (Appendix A), 2) Fiber B (470 kg/mol PAN-co-MAA) (Figure D.1), and 3) Fiber C (500 kg/mol homo-polymer) (Figure D.2). Mechanical and structural parameters are shown in Table D.1. DSC was run in nitrogen atmosphere first and then subsequently in air to separate the three main reactions of stabilization (i.e., - cyclization, oxidation, and cross-linking). The following plots show the DSC exotherms that resulted from the aforementioned precursors.

Table D.1 Mechanical and structural parameters of Fiber B and Fiber C precursor fibers.

	Fiber A	**Fiber B – D2**	**Fiber C – D2**
CNT Loading (wt%)	0.75	1.00	1.00
Polymer Description	250K homo-polymer	470K PAN-co-MAA	500K homo-polymer
Draw Ratios (SDR/CDR/ HDR/TDR)*	3.00 / 1.19 / 7.06 / 25.20	3.00 / 1.20 / 6.25 / 22.50	3.00 / 1.23 / 4.92 / 18.10
Diameter [µm]†	6.71 ± 0.2	6.81 ± 0.4	6.57 ± 0.4
Tensile Strength [GPa]	1.06 ± 0.1	0.90 ± 0.09	0.76 ± 0.10
Tensile Modulus [GPa]	19.8 ± 0.7	15.26 ± 0.97	17.66 ± 1.38
Elongation at [%]	9.5 ± 1.2	10.36 ± 0.85	6.98 ± 0.63
d-spacing$_{110}$ [Å]‡	5.247	5.270	5.209
Meridional Peak Pos.	39.05°	38.86°	39.08°
Crystallinity [%]#	66%	61%	61%
Crystal Size [nm]&	10.3	12.0	12.4
f_{PAN}**	0.91	0.90	0.93
f_{CNT}††	0.93	n/a	n/a

*SDR, CDR, HDR, and TDR stand for spin draw ratio, cold draw ratio, hot draw ratio, and total draw ratio, respectively; †Favimat vibroscope linear density measurement (assumed bulk density: 1.18 g/cc) ‡Bragg equation using the (110) peak position of the equatorial scan (XRD); #Peak fitting methods from integrated scan (XRD); &Scherrer equation of (110) peak from equatorial scan; **Herman's orientation parameter from azimuthal scan of ~17° peak; ††Determined from curve fitting methods of Raman data.[82,83]

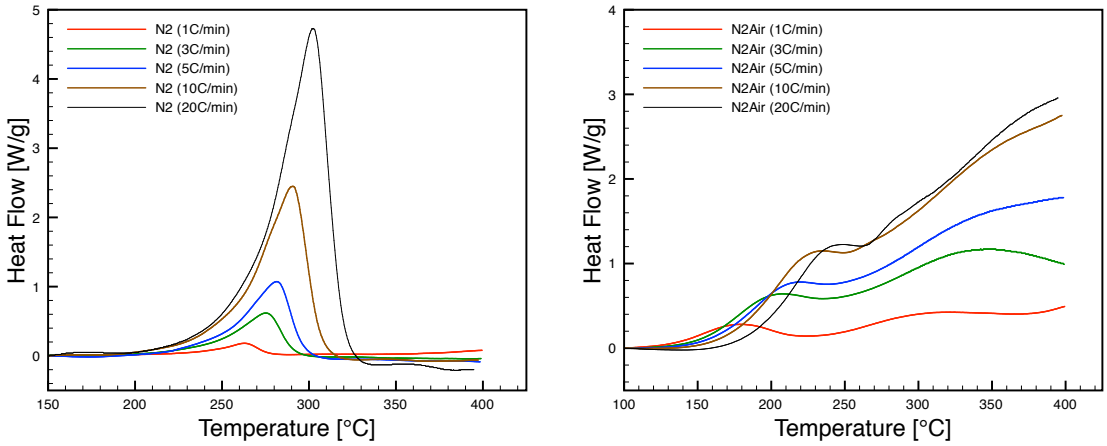

Figure D.1 Fiber B precursor heating rate scans in nitrogen atmosphere (left) and subsequently in air (right).

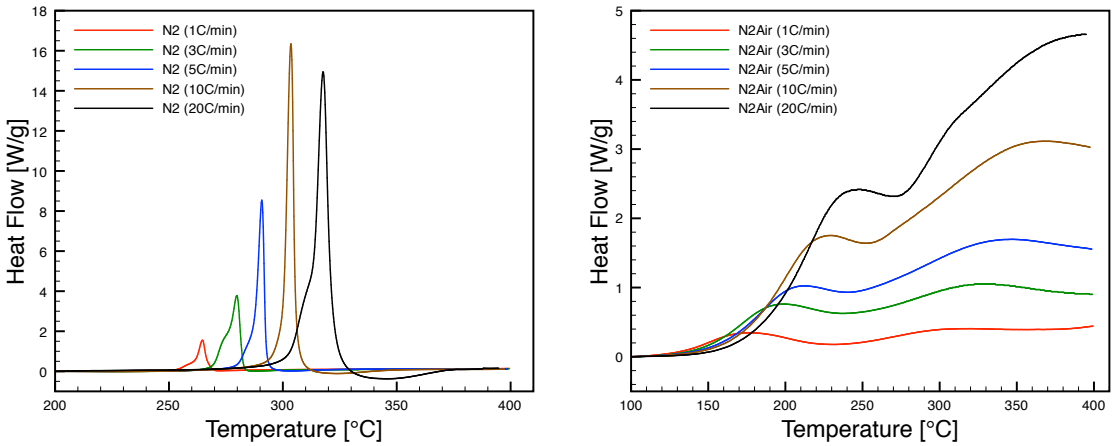

Figure D.2 Fiber C precursor heating rate scans in nitrogen atmosphere (left) and subsequently in air (right).

The observed exotherm peak temperatures of all three sheath-core precursors are recorded in Table D.2. These temperatures were directly used in the kinetic analysis proposed by Ozawa and Kissinger to determine the kinetic parameters (Table D.3) and are displayed graphically in Figure D.3. For Fiber B in Table D.3, the cross-linking kinetic parameters could not be determined due to insufficient exotherm peaks.

Table D.2 Observed peak temperatures of the cyclization exotherm for Fiber B (470 kg/mol PAN-co-MAA) and Fiber C (500 kg/mol homo-polymer).

	Fiber B			Fiber C		
	470K PAN-co-MAA			500K homo-polymer		
Heating Rate [°C/min]	in N2	rerun in Air		in N2	rerun in Air	
	T_p	T_{p1}	T_{p2}	T_p	T_{p1}	T_{p2}
1	263.0	179.7	319.9	264.7	176.4	318.6
3	275.6	207.5	348.2	279.8	199.4	328.7
5	281.4	219.2	-	290.7	212.9	346.7
10	290.9	234.4	-	303.5	228.9	369.7
20	302.5	249.0	-	317.7	247.4	-

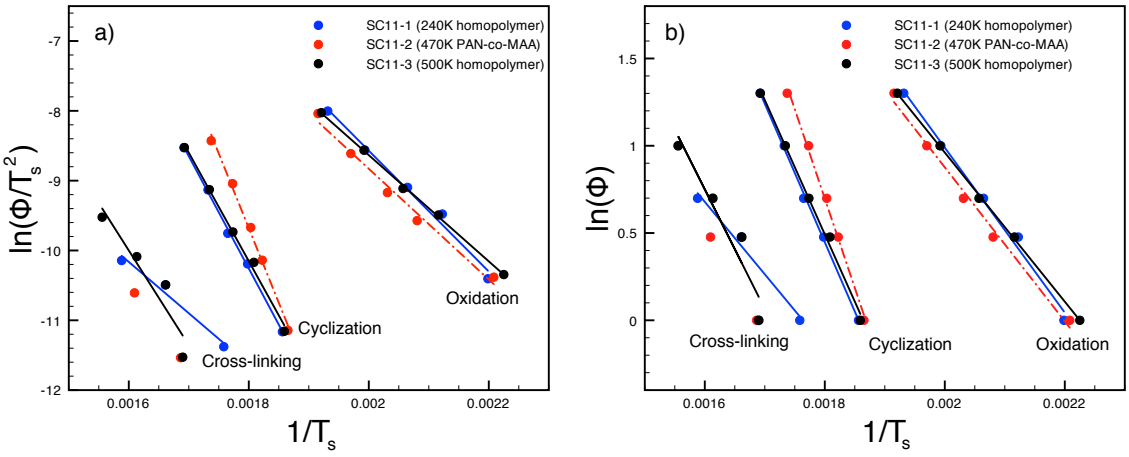

Figure D.3 Reaction kinetics results from a) Kissinger's and b) Ozawa's methods. All three sheath-core precursors are included.

Table D.3 Calculated activation energies and pre-exponential factors for the sheath-core fibers.

		From Ozawa's Equation		From Kissinger's Equation	
		E_a (kJ/mol)	A (s^{-1})	E_a (kJ/mol)	A (s^{-1})
Fiber A (250K homo-polymer)	Cyclization	144.0	5.0×10^{12}	133.6	2.0×10^{12}
	Oxidation	86.1	4.2×10^{8}	72.0	3.5×10^{7}
	Cross-linking	74.8	1.8×10^{5}	61.1	4.3×10^{4}
Fiber B (470K PAN-co-MAA)	Cyclization	189.2	2.4×10^{17}	177.6	7.0×10^{16}
	Oxidation	76.9	2.7×10^{7}	66.0	7.2×10^{6}
	Cross-linking	n/a			
Fiber C (500K homo-polymer)	Cyclization	139.5	2.1×10^{12}	129.1	8.0×10^{8}
	Oxidation	74.3	1.8×10^{7}	63.3	3.9×10^{3}
	Cross-linking	121.6	3.3×10^{9}	112.8	1.6×10^{6}

Looking at the preliminary carbonization results from Fiber B (Table D.4) and Fiber C (Table D.5) it is apparent that Fiber A resulted in much more promising mechanical properties. One possible explanation for this might be the unusually low activation energy observed for the cross-linking reaction in the case of Fiber A.

Table D.4 Preliminary carbonization results of Fiber B (470 kg/mol PAN-co-MAA). Properties collected on Favimat single filament tester at 1-inch gauge length.

ID	Pretension [MPa]	Stabilization Time [min]		Diameter [μm]	Tensile Strength [GPa]	Tensile Modulus [GPa]	Strain to Failure [GPa]	Weibull Mod.
		260°C	305°C					
Fiber B.01	35.6	46	3	3.74±0.16	2.62±0.60	292±12	0.93±0.20	1.48
Fiber B.02	43.5	46	3	3.49±0.12	3.28±0.92	312±10	1.06±0.29	2.93
Fiber B.03#	43.5	46	3	4.21±0.39	2.98±0.73	279±17	1.08±0.28	4.20
Fiber B.04	46.1	35	35	3.60±0.20	3.08±0.64	281±28	1.11±0.19	4.72
Fiber B.05*	46.1	46	17	3.42±0.11	2.42±0.91	292±20	0.86±0.31	2.22
Fiber B.06**	46.1	74	3	3.77±0.24	3.13±1.27	287±17	1.11±0.43	1.77
Fiber B.07	46.1	74	17	3.38±0.14	2.60±0.44	274±17	0.97±0.18	5.27
Fiber B.08†	45.8	40	10	3.68±0.19	3.42±0.70	267±27	1.25±0.23	4.84
Fiber B.09	45.8	80	10	3.50±0.22	3.14±0.86	293±19	1.10±0.27	3.35
Fiber B.10‡	45.8	60	0	3.56±0.18	3.28±0.48	299±13	1.12±0.15	6.95
Fiber B.11	45.8	60	10	3.56±0.24	2.64±0.53	299±12	0.92±0.16	2.62
Fiber B.12	45.8	60	20	3.43±0.11	3.20±0.68	287±12	1.13±0.23	4.77

#Moved down one slot because weight was too close to the rod. *Sample touching base after stabilization. Removed and adjusted for carbonization.**Argon was depleted in the morning. †Weight almost fully touching the base around 650ºC. ‡Fiber broke upon removal from furnace.

Table D.5 Preliminary carbonization results of Fiber C (500 kg/mol homo-polymer). Properties collected on Favimat single filament tester at 1-inch gauge length.

ID	Pretension [MPa]	Stabilization Time [min]		Diameter [μm]	Tensile Strength [GPa]	Tensile Modulus [GPa]	Strain to Failure [GPa]	Weibull Mod.
		260°C	305°C					
Fiber C.01	29.7	76	3	3.45±0.15	2.68±0.63	275±9	0.99±0.22	3.90
Fiber C.02	29.7	76	17	3.36±0.12	2.85±0.43	259±8	1.12±0.15	3.16
Fiber C.03	29.7	70	10	3.73±0.23	2.91±0.40	272±14	1.09±0.13	5.71
Fiber C.04	29.7	104	3	3.75±0.27	2.61±0.43	277±17	0.95±0.16	6.01
Fiber C.05	29.7	104	17	3.34±0.10	2.37±0.50	253±18	0.94±0.21	4.49

Another interesting observation was the change in cyclization enthalpy of reaction as a function of heating rate for the polymer precursors (Table D.6; Figure D.4). For homo-polymer samples, the cyclization reaction occurs very rapidly. Faster heating rates reduce the time in which reactions are allowed to proceed. This may lead to more violent reactions in which the full reaction potential is not realized. This may be an explanation for the reduction in enthalpy for the two homo-polymer samples (Fiber A and Fiber C). The PAN-co-MAA sample experienced a different trend. There seems to be an optimal

heating rate for maximum allowed reaction for copolymer samples. Bajaj et al. recorded 16% and 15% higher enthalpy of reactions (as compared to PAN homo-polymer) for PAN-co-MAA precursors with 3.2% and 3.7% MAA respectively (heating rate of 10 °C/min). Higher co-monomer concentration (5%+) yielded lower enthalpy of reaction.[79]

Table D.6 Enthalpy of cyclization reactions for sheath-core precursors at various heating rates.

	Fiber A (250 kg/mol homo-polymer)	Fiber B (470 kg/mol PAN-co-MAA)	Fiber C (500 kg/mol homo-polymer)
	[J/g]		
1	517.7	310.4	520.2
3	499.5	473.7	524.0
5	447.2	498.6	472.1
10	422.5	561.5	423.9
20	343.0	541.1	367.9

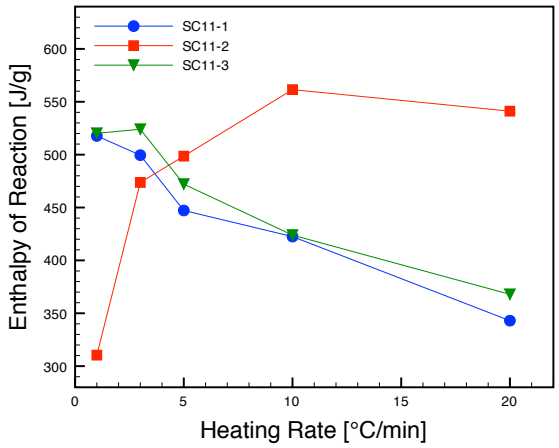

Figure D.4 Enthalpy changes as a function of heating rate during sheath-core DSC trials in a nitrogen atmosphere.

Figure D.5 shows the DSC heating rate scans of Fiber A, Fiber B, and Fiber C for two different heating rates (5 °C/min and 20 °C/min).

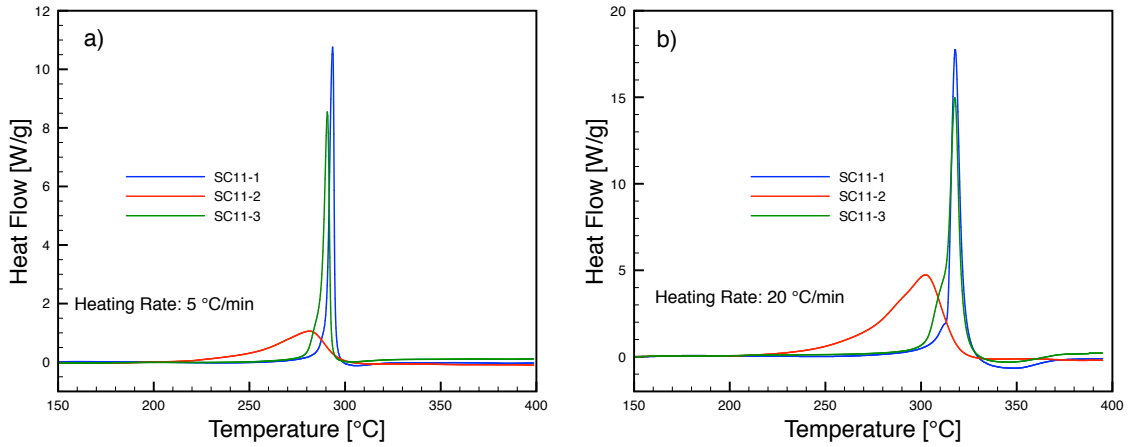

Figure D.5 Individual DSC scans of Fiber A, Fiber B, and Fiber C at heating rates of a) 5 °C/min and b) 20 °C/min.

REFERENCES

1. Edison, T. A. Electric-Lighting Apparatus. 224,329, 1879.

2. Morgan, P., *Carbon Fibers and their Composites*. CRC Press: Taylor and Francis: Boca Raton, 2005.

3. Shindo, A. Japanese Patent 28287, 1959.

4. Shindo, A. Japanese Patent 29270, 1962.

5. Otani, S.; Yamada, K.; Koitabas.T; Yokoyama, A., On Raw Materials of MP Carbon Fiber. *Carbon* **1966,** *4* (3), 425-432.

6. Minus, M. L.; Kumar, S., The processing, properties, and structure of carbon fibers. *Jom* **2005,** *57* (2), 52-58.

7. Sanchez-Soto, P. J.; Aviles, M. A.; del Rio, J. C.; Gines, J. M.; Pascual, J.; Perez-Rodriguez, J. L., Thermal study of the effect of several solvents on polymerization of acrylonitrile and their subsequent pyrolysis. *J. Anal. Appl. Pyrolysis* **2001,** *58*, 155-172.

8. Chae, H. G. Polyacrylonitrile/carbon nanotube composite fibers: reinforcement efficiency and carbonization studies. PhD Dissertation, Georgia Institute of Technology, Atlanta 2008.

9. Gupta, A. K.; Paliwal, D. K.; Bajaj, P., Acrylic precursors for carbon fibers. *Journal of Macromolecular Science-Reviews in Macromolecular Chemistry and Physics* **1991,** *C31* (1), 1-89.

10. Clarke, A. J.; Bailey, J. E., Oxidation of acyrlic fibers for carbon fiber formation. *Nature* **1973,** *243* (5403), 146-150.

11. Goodhew, P. J.; Clarke, A. J.; Bailey, J. E., Review of fabrication and properties of carbon-fibers. *Materials Science and Engineering* **1975,** *17* (1), 3-30.

12. Watt, W.; Johnson, W., Mechanism of oxidization of polyacrylonitrile fibers. *Nature* **1975,** *257* (5523), 210-212.

13. Henriciolive, G.; Olive, S., Inter-versus intramolecular oligomerization of nitrile groups in polyacrylonitrile. *Polymer Bulletin* **1981,** *5* (8), 457-461.

14. Morita, K.; Murata, Y.; Ishitani, A.; Murayama, K.; Ono, T.; Nakajima, A., Characterization of commericially available PAN (polyacrylonitrile)-based carbon-fibers. *Pure and Applied Chemistry* **1986,** *58* (3), 455-468.

15. Usami, T.; Itoh, T.; Ohtani, H.; Tsuge, S., Structural study of polyacrylonitrile fibers during oxidative thermal-degradation by pyrolysis-gas chromatography, solid-state C-13 nuclear-magnetic-resonance, and Fourier-transform infrared spectroscopy. *Macromolecules* **1990,** *23* (9), 2460-2465.

16. Houtz, R. C., Orlon acrylic fiber - chemistry and properties. *Textile Research Journal* **1950,** *20* (11), 786-801.

17. Grassie, N.; Hay, J. N.; McNeill, I. C., Coloration in acrylonitrile and methacrylonitrile polymers. *Journal of Polymer Science* **1958,** *31* (122), 205-206.

18. Burlant, W. J.; Parsons, J. L., Pyrolysis of polyacrylonitrile. *Journal of Polymer Science* **1956,** *22* (101), 249-256.

19. Lacombe, E. M., Color formation in polyacrylonitrile. *Journal of Polymer Science* **1957,** *24* (105), 152-154.

20. Berlin, A. A.; Dubinskaya, A. M.; Moshkovskii, Y. S., Heat treatment of polyacrylonitrile in solution in dimethylformamide. *Polymer Science U.S.S.R.* **1964,** *6* (11), 2145-2151.

21. Fitzer, E.; Muller, D. J., Influence of oxygen on chemical-reactions during stabilization of PAN as carbon-fiber precursor. *Carbon* **1975,** *13* (1), 63-69.

22. Fitzer, E.; Frohs, W.; Heine, M., Optimization of stabilization and carbonization treatment of PAN fibers and structural characterization of the resulting carbon-fibers. *Carbon* **1986,** *24* (4), 387-395.

23. Warner, S. B.; Peebles, L. H.; Uhlmann, D. R., Oxidative stabilization of acrylic fibers: 1. Oxygen-uptake and general model. *Journal of Materials Science* **1979,** *14* (3), 556-564.

24. Peebles, L. H.; Brandrup, J., A chemical means of distiguishing between conjugated -(C=C)- and conjugated -(C=N)- bonds. *Makromolekulare Chemie* **1966,** *98* (NOV), 189-203.

25. Standage, A. E.; Matkowsk.Rd, Thermal oxidation of polyacrylonitrile. *European Polymer Journal* **1971,** *7* (7), 775-783.

26. Schurz, J., Discoloration effects in acrylonitrile polymers. *Journal of Polymer Science* **1958,** *28* (117), 438-439.

27. Takata, T.; Hiroi, I.; Taniyama, M., Coloration in acrylonitrile polymers. *Journal of Polymer Science Part a-General Papers* **1964,** *2* (4PA), 1567-1585.

28. Brandrup, J.; Peebles, L. H., On the Chromophore of Polyacrylonitrile. IV. Thermal Oxidation of Polyacrylonitrile and Other Nitrile-Containing Compounds. *Macromolecules* **1968,** *1* (1), 64-72.

29. Friedlander, H. N.; Peebles, L. H.; Brandrup, J.; Kirby, J. R., On the Chromophore of Polyacrylonitrile. VI. Mechanism of Color Formation in Polyacrylonitrile. *Macromolecules* **1968,** *1* (1), 79-86.

30. Grassie, N.; McGuchan, R., Pyrolysis of polyacrylonitrile and related polymers 2. Effect of sample preparation on thermal behavior of polyacrylonitrile. *European Polymer Journal* **1971,** *7* (8), 1091-1104.

31. Olive, S.; Olive, G., Molecular Interactions and Macroscopic Properties of Polyacrylonitrile and Model Substances. *Advances in Polymer Science* **1979,** *32*.

32. Hoffman, W. P.; Hurley, W. C.; Liu, P. M.; Owens, T. W., The surface-topography of non-shear treated pitch and PAN carbon-fibers as viewed by the STM. *Journal of Materials Research* **1991,** *6* (8), 1685-1694.

33. Johnson, D. J., Structure property relationships in carbon-fibers. *Journal of Physics D-Applied Physics* **1987,** *20* (3), 286-291.

34. Minagawa, M.; Onuma, H.; Ogita, T.; Uchida, H., Pyrolysis gas chromatographic analysis of polyacrylonitrile. *J. Appl. Polym. Sci.* **2001,** *79* (3), 473-478.

35. Nielsen, M.; Jurasek, P.; Hayashi, J.; Furimsky, E., Formation of toxic gases during pyrolysis of polyacrylonitrile and nylons. *J. Anal. Appl. Pyrolysis* **1995,** *35* (1), 43-51.

36. Jain, M. K.; Abhiraman, A. S., Conversion of acrylonitrile-based precursor fibers to carbon-fibers .1. a review of the physical and morphological aspects. *Journal of Materials Science* **1987,** *22* (1), 278-300.

37. Guigon, M.; Oberlin, A.; Desarmot, G., Microtexture and structure of some high-modulus, PAN-base carbon fibres. *Fibre Science and Technology* **1984,** *20* (1), 55-72.

38. Fischer, L.; Ruland, W., The influence of graphitization on the mechanical-properties of carbon-fibers. *Colloid and Polymer Science* **1980,** *258* (8), 917-922.

39. Johnson, D. J., Recent advances in studies of carbon-fiber structure. *Philosophical Transactions of the Royal Society of London Series a-Mathematical Physical and Engineering Sciences* **1980,** *294* (1411), 443-449.

40. Takaku, A.; Shioya, M., X-Ray Measurements and the Structure of Polyacrylonitrile- and Pitch-Based Carbon Fibres. *Journal of Materials Science* **1990,** *25* (11), 4873-4879.

41. Kumar, S.; Anderson, D. P.; Crasto, A. S., Carbon-fiber compressive strength and its dependence on structure and morphology. *Journal of Materials Science* **1993,** *28* (2), 423-439.

42. Guigon, M.; Oberlin, A., Heat-treatment of high-tensile strength PAN-based carbon-fibers - microtexture, structure and mechanical-properties. *Composites Science and Technology* **1986,** *27* (1), 1-23.

43. Rennhofer, H.; Loidl, D.; Puchegger, S.; Peterlik, H., Structural development of PAN-based carbon fibers studied by in situ X-ray scattering at high temperatures under load. *Carbon* **2010,** *48* (4), 964-971.

44. Ruland, W., X-ray studies on preferred orientation in carbon fibers. *J. Appl. Phys.* **1967,** *38* (9), 3585-3589.

45. Yu, M. F.; Files, B. S.; Arepalli, S.; Ruoff, R. S., Tensile loading of ropes of single wall carbon nanotubes and their mechanical properties. *Physical Review Letters* **2000,** *84* (24), 5552-5555.

46. Yu, M. F.; Lourie, O.; Dyer, M. J.; Moloni, K.; Kelly, T. F.; Ruoff, R. S., Strength and breaking mechanism of multiwalled carbon nanotubes under tensile load. *Science* **2000,** *287* (5453), 637-640.

47. Demczyk, B. G.; Wang, Y. M.; Cumings, J.; Hetman, M.; Han, W.; Zettl, A.; Ritchie, R. O., Direct mechanical measurement of the tensile strength and elastic modulus of multiwalled carbon nanotubes. *Materials Science and Engineering a-Structural Materials Properties Microstructure and Processing* **2002,** *334* (1-2), 173-178.

48. Sreekumar, T. V.; Liu, T.; Min, B. G.; Guo, H.; Kumar, S.; Hauge, R. H.; Smalley, R. E., Polyacrylonitrile single-walled carbon nanotube composite fibers. *Advanced Materials* **2004,** *16* (1), 58-61.

49. Chae, H. G.; Sreekumar, T. V.; Uchida, T.; Kumar, S., A comparison of reinforcement efficiency of various types of carbon nanotubes in poly acrylonitrile fiber. *Polymer* **2005,** *46* (24), 10925-10935.

50. Guo, H.; Sreekumar, T. V.; Liu, T.; Minus, M.; Kumar, S., Structure and properties of polyacrylonitrile/single wall carbon nanotube composite films. *Polymer* **2005,** *46* (9), 3001-3005.

51. Jain, R.; Minus, M. L.; Chae, H. G.; Kumar, S., Processing, Structure, and Properties of PAN/MWNT Composite Fibers. *Macromolecular Materials and Engineering* **2010,** *295* (8), 742-749.

52. Chae, H. G.; Minus, M. L.; Kumar, S., Oriented and exfoliated single wall carbon nanotubes in polyacrylonitrile. *Polymer* **2006,** *47* (10), 3494-3504.

53. Sawai, D.; Yamane, A.; Kameda, T.; Kanamoto, T.; Ito, M.; Yamazaki, H.; Hisatani, K., Uniaxial drawing of isotactic poly(acrylonitrile): Development of oriented structure and tensile properties. *Macromolecules* **1999,** *32* (17), 5622-5630.

54. Chae, H. G.; Minus, M. L.; Rasheed, A.; Kumar, S., Stabilization and carbonization of gel spun polyacrylonitrile/single wall carbon nanotube composite fibers. *Polymer* **2007,** *48* (13), 3781-3789.

55. Niyogi, S.; Hamon, M. A.; Hu, H.; Zhao, B.; Bhowmik, P.; Sen, R.; Itkis, M. E.; Haddon, R. C., Chemistry of single-walled carbon nanotubes. *Accounts of Chemical Research* **2002,** *35* (12), 1105-1113.

56. Chae, H. G.; Choi, Y. H.; Minus, M. L.; Kumar, S., Carbon nanotube reinforced small diameter polyacrylonitrile based carbon fiber. *Composites Science and Technology* **2009,** *69* (3-4), 406-413.

57. Quinn, J. B.; Quinn, G. D., A practical and systematic review of Weibull statistics for reporting strengths of dental materials. *Dental Materials* **2010,** *26* (2), 135-147.

58. Tiryakioglu, M., On estimating Weibull modulus by moments and maximum likelihood methods. *Journal of Materials Science* **2008,** *43* (2), 793-798.

59. (a) Dowling, N. E., *Mechanical Behavior of Materials: Engineering Methods for Deformation, Fracture, and Fatigue*. 3rd ed.; Pearson Prentice Hall: Upper Saddle River, 2007; (b) Lee, C.; Wei, X. D.; Kysar, J. W.; Hone, J., Measurement of the elastic properties and intrinsic strength of monolayer graphene. *Science* **2008,** *321* (5887), 385-388.

60. Warren, C. D.; Paulauskas, F. L.; Baker, F. S.; Eberle, C. C.; Naskar, A., Development of Commodity Grade, Lower Cost Carbon Fiber-Commercial Applications. *Sampe Journal* **2009,** *45* (2), 24-36.

61. Terry L. White, F. L. P., Timothy S. Bigelow System to Continuously Produce Carbon Fiber via Microwave Assisted Plasma Processing. US Patent 7824495, 2010.

62. Naito, K.; Tanaka, Y.; Yang, J. M.; Kayawa, Y., Tensile properties of ultrahigh strength PAN-based, ultrahigh modulus pitch-based and high ductility pitch-based carbon fibers (Toray Cleanroom). *Carbon* **2008,** *46* (2), 189-195.

63. Thomas, A. D.; Tang, L. G., Test method effects on the reported tensile strength of carbon fiber. In *Advanced Materials & Processes Preparing for the New Millennium*, Green, J.; Howell, D. D., Eds. Soc Advancement Material & Process Engineering: Covina, 1999; Vol. 31, pp 319-328.

64. Weibull, W., A statistical distribution function of wide applicability. *Journal of Applied Mechanics-Transactions of the ASME* **1951,** *18* (3), 293-297.

65. Vanderzwaag, S., The concept of filament strength and the weibull modulus. *Journal of Testing and Evaluation* **1989,** *17* (5), 292-298.

66. Stoner, E. G.; Edie, D. D.; Durham, S. D., An end-effect model for the single-filament tensile test. *Journal of Materials Science* **1994,** *29* (24), 6561-6574.

67. Bergman, B., On the estimation of the weibull modulus. *Journal of Materials Science Letters* **1984,** *3* (8), 689-692.

68. Asloun, E. M.; Donnet, J. B.; Guilpain, G.; Nardin, M.; Schultz, J., On the estimation of the tensile-strength of carbon-fibers at short lengths. *Journal of Materials Science* **1989,** *24* (10), 3504-3510.

69. Padgett, W. J.; Durham, S. D.; Mason, A. M., Weibull analysis of the strength of carbon-fibers using linear and power-law models for the length effect. *Journal of Composite Materials* **1995,** *29* (14), 1873-1884.

70. Naito, K.; Yang, J. M.; Tanaka, Y.; Kagawa, Y., The effect of gauge length on tensile strength and Weibull modulus of polyacrylonitrile (PAN)- and pitch-based carbon fibers. *Journal of Materials Science* **2012,** *47* (2), 632-642.

71. Torayca T300 Data Sheet. http://www.toraycfa.com/pdfs/T300DataSheet.pdf (accessed February 2012).

72. T650/35 PAN-based Fiber. http://www.cemselectorguide.com/pdf/THORNEL_T650-35_052112.pdf (accessed February 2012).

73. HexTow IM7 Carbon Fiber Product Data. http://www.hexcel.com/Resources/DataSheets/Carbon-Fiber-Data-Sheets/IM7.pdf (accessed February 2012).

74. Yu, M. J.; Bai, Y. J.; Wang, C. G.; Xu, Y.; Guo, P. Z., A new method for the evaluation of stabilization index of polyacrylonitrile fibers. *Materials Letters* **2007,** *61* (11-12), 2292-2294.

75. Tsai, J. S.; Hsu, H. N., Determination of the aromatization index for oxidized polyacrylonitrile fiber by the differential scanning calorimetry method. *Journal of Materials Science Letters* **1992,** *11* (21), 1403-1405.

76. Zhu, Y.; Wilding, M. A.; Mukhopadhyay, S. K., Estimation, using infrared spectroscopy, of the cyclization of poly(acrylonitrile) during the stabilization stage of carbon fibre production. *Journal of Materials Science* **1996,** *31* (14), 3831-3837.

77. Collins, G. L.; Thomas, N. W.; Williams, G. E., Formulation of an empirical kinetic-model to describe heat evolution from poly(acrylonitrile) co-polymer in air at 265°C. *Fibre Science & Technology* **1984,** *20* (1), 37-53.

78. Ouyang, Q.; Cheng, L.; Wang, H. J.; Li, K. X., Mechanism and kinetics of the stabilization reactions of itaconic acid-modified polyacrylonitrile. *Polym. Degrad. Stabil.* **2008,** *93* (8), 1415-1421.

79. Bajaj, P.; Sreekumar, T. V.; Sen, K., Thermal behaviour of acrylonitrile copolymers having methacrylic and itaconic acid comonomers. *Polymer* **2001,** *42* (4), 1707-1718.

80. Bahrami, S. H.; Bajaj, P.; Sen, K., Thermal behavior of acrylonitrile carboxylic acid copolymers. *J. Appl. Polym. Sci.* **2003,** *88* (3), 685-698.

81. Liu, Y. D.; Chae, H. G.; Kumar, S., Gel-spun carbon nanotubes/polyacrylonitrile composite fibers. Part II: Stabilization reaction kinetics and effect of gas environment. *Carbon* **2011,** *49* (13), 4477-4486.

82. Park, M. S.; Wong, Y. S.; Park, J. O.; Venkatraman, S. S.; Srinivasarao, M., A Simple Method for Obtaining the Information of Orientation Distribution Using Polarized Raman Spectroscopy: Orientation Study of Structural Units in Poly(lactic acid). *Macromolecules* **2011,** *44* (7), 2120-2131.

83. Liu, T.; Kumar, S., Quantitative characterization of SWNT orientation by polarized Raman spectroscopy. *Chemical Physics Letters* **2003,** *378* (3-4), 257-262.

84. Liu, Y. Stabilization and carbonization studies of polyacrylonitrile/carbon nanotube composite fibers. PhD Dissertation, Georgia Institute of Technology, Atlanta, 2010.

85. Ozawa, T., A new method of analyzing thermogravimetric data. *Bulletin of the Chemical Society of Japan* **1965,** *38* (11), 1881-1886.

86. Kissinger, H. E., Reaction kinetics in differential thermal analysis. *Analytical Chemistry* **1957,** *29* (11), 1702-1706.

87. Nair, C. P. R.; Krishnan, K.; Ninan, K. N., Differential scanning calorimetric study on the Claisen rearrangement and thermal polymerisation of diallyl ether of bisphenols. *Thermochimica Acta* **2000,** *359* (1), 61-67.

88. Choi, Y. H. Polyacrylonitrile / carbon nanotube composite fibers: effect of various processing parameters on fiber structure and properties. PhD Dissertation, Georgia Institute of Technology, Atlanta, 2010.

89. Liu, Y. D.; Chae, H. G.; Kumar, S., Gel-spun carbon nanotubes/polyacrylonitrile composite fibers. Part I: Effect of carbon nanotubes on stabilization. *Carbon* **2011,** *49* (13), 4466-4476.

90. T. Uchida, I. S., Y. Ito and K. Nukuda, Proceedings of the 10th Biennial Conference on Carbon,. 31.

91. Liu, Y. D.; Chae, H. G.; Kumar, S., Gel-spun carbon nanotubes/polyacrylonitrile composite fibers. Part III: Effect of stabilization conditions on carbon fiber properties. *Carbon* **2011,** *49* (13), 4487-4496.

92. Northolt, M. G.; Veldhuizen, L. H.; Jansen, H., Tensile deformation of carbon-fibers and the relationship with the modulus for shear between the basal planes. *Carbon* **1991,** *29* (8), 1267-1279.

93. Fitzer, E., PAN-based carbon-fibers present state and trend of the technology from the viewpoint of possibilities and limits to influence and to control the fiber properties by the process parameters. *Carbon* **1989,** *27* (5), 621-645.

94. Manocha, L. M.; Bahl, O. P., On the relation between young modulus and orientation in carbon-fibers. *Fibre Science & Technology* **1982,** *17* (3), 221-226.

95. Guigon, M.; Oberlin, A.; Desarmot, G., Microtexture and structure of some high-modulus, PAN-base carbon fibres. *Fibre Science and Technology* **1984,** *20* (3), 177-198.

96. Peebles, L. H., *Carbon Fibers: Formation, Structure, and Properties*. CRC Press Inc.: Boca Raton, 1995.

97. Griffith, A. A., The phenomena of rupture and flow in solids. *Royal Society of London -- Philosophical Transactions* **1920,** *221* (A 587), 163-198.

98. Kusy, R. P.; Whitley, J. Q., Influence of the suture diameter on the tensile strength of polypropylene monofilaments and its relationship to the USP specification. *Journal of Biomedical Materials Research* **1984,** *18* (7), 781-787.

99. Wong, S.-C.; Baji, A.; Leng, S., Effect of fiber diameter on tensile properties of electrospun poly(-caprolactone). *Polymer* **2008,** *49* (21), 4713-4722.

100. Naraghi, M.; Arshad, S. N.; Chasiotis, I., Molecular orientation and mechanical property size effects in electrospun polyacrylonitrile nanofibers. *Polymer* **2011,** *52* (7), 1612-1618.

101. Arshad, S. N.; Naraghi, M.; Chasiotis, I., Strong carbon nanofibers from electrospun polyacrylonitrile. *Carbon* **2011,** *49* (5), 1710-1719.

102. Young, K.; Blighe, F. M.; Vilatela, J. J.; Windle, A. H.; Kinloch, I. A.; Deng, L.; Young, R. J.; Coleman, J. N., Strong Dependence of Mechanical Properties on Fiber Diameter for Polymer-Nanotube Composite Fibers: Differentiating Defect from Orientation Effects. *Acs Nano* **2010,** *4* (11), 6989-6997.

103. Fansanella, N. Mechanical characterization of advanced polyacrylonitrile derived carbon fibers reinforced with carbon nanotubes. M.S. Thesis, University of Illinois at Urbana-Champaign, 2012.

104. Naraghi, M.; Ozkan, T.; Chasiotis, I.; Hazra, S. S.; de Boer, M. P., MEMS platform for on-chip nanomechanical experiments with strong and highly ductile nanofibers. *Journal of Micromechanics and Microengineering* **2010,** *20* (12).